

SOFT CLASSIFICATION OF HYPERPECTRAL IMAGERY BASED ON LINEAR MIXING MODEL AND SUPERVISED FUZZY LOGIC ALGORITHMS

by

Wilma Nydia Pabón Ramírez

A thesis submitted in partial fulfillment of the requirements for the degree of

MASTER OF SCIENCE
in
ELECTRICAL ENGINEERING

UNIVERSITY OF PUERTO RICO
MAYAGÜEZ CAMPUS
2008

Approved by:

Shawn Hunt, Ph.D.
Member, Graduate Committee

Date

Vidya Manian, Ph.D.
Member, Graduate Committee

Date

Miguel Vélez-Reyes, Ph.D.
President, Graduate Committee

Date

Fernando Gilbes, Ph.D.
Representative of Graduate Studies

Date

Isidoro Couvertier Reyes, Ph.D.
Chairperson of the Department

Date

ABSTRACT

SOFT CLASSIFICATION OF HYPERSPECTRAL IMAGERY BASED ON LINEAR MIXING MODEL AND SUPERVISED FUZZY LOGIC ALGORITHMS

By

Wilma Nydia Pabón Ramírez

August 2008

Chair: Miguel Vélez Reyes, Ph.D.

Major Department: Electrical and Computer Engineering

Hyperspectral Imagery (HSI) is an important technology used in remote sensing and plays an important role in environmental remote sensing because it provides valuable spectral information of the objects in the scene. Using the measured spectral signatures, it is possible to discriminate between materials in the scene for object detection, recognition or identification. Hyperspectral technologies are of great value for environmental applications where it is possible to take advantage of spectral, spatial, and radiometric resolutions. A problem for current and proposed spaceborne hyperspectral platforms is their low spatial resolution which ranges from 20 to 30m. The key problem with low spatial resolution is mixed pixels where the measured spectral signature is a combination of the contributions of the spectral signatures of the materials in the field of view in the sensor. In such cases, the high spectral resolution can be used to extract information about objects at the subpixel level by their contribution to the measured spectral signature. A common technique in HSI analysis is hard classification where each pixel is assigned to one and only one specific class. In this research work, we investigated soft classification algorithms which can consider the mixed pixel problem for image classification. Soft classifiers assign multiple classes to a single pixel using membership functions which weight the membership of the pixel into the available classes. As a result, soft classification could be used to develop models and thematic maps that are more appropriate for low resolution remote sensing imagery. This thesis presents a comparative study of soft classification algorithms based on Linear Mixing Model and supervised Fuzzy Logic classification systems as an alternative for hard classification of low spatial resolution HSI. As part of the research, we developed a Spectral Soft Classification Tool (SSCT), which should be valuable resource for image analysts because it provides soft classification outputs, visualization tools, and accuracy assessment to analyze multi/hyperspectral imagery. Remotely sensed data from HYPERION and ETM+ (LANDSAT 7) collected over Puerto Rico were used in this study.

CLASIFICACIÓN SUAVE DE IMÁGENES HIPERESPECTRALES BASADO EN EL MODELO DE MEZCLADO LINEAL Y EN ALGORITMOS SUPERVISADOS DE LÓGICA DIFUSA

Por

Wilma Nydia Pabón Ramírez

Agosto 2008

Consejero: Miguel Vélez Reyes, Ph.D.

Departamento: Ingeniería Eléctrica y Computadoras

Las imágenes y sensores hiperespectrales (HSI por sus siglas en inglés) son una tecnología de gran valor para la percepción remota ambiental porque proveen valiosa información espectral de los objetos en la escena. Utilizando las firmas espectrales medidas, es posible discriminar entre los materiales presentes en una escena para aplicaciones de detección, reconocimiento e identificación de objetos. La tecnología hiperespectral es relevante para aplicaciones ambientales cuando es posible tomar ventaja de la resolución espacial, espectral y radiométrica del sensor. Sin embargo, un problema actual de los sensores en plataformas espaciales propuestos y existentes, es su pobre resolución espacial cuyo rango está entre 20 – 30 metros. El principal inconveniente de los sensores con una pobre resolución espacial es la presencia de píxeles mixtos en la escena donde la firma espectral de estos píxeles es una combinación de la contribución de las firmas espectrales de los materiales en el campo de visión del sensor. En estos casos, la alta resolución espectral puede ser utilizada para extraer información de los materiales a nivel de sub-píxel por su contribución a la firma espectral medida. Una de las técnicas más comunes para el análisis de imágenes hiperespectrales es clasificación dura en donde cada píxel en la escena es asignado a una y solo una clase. En este trabajo, nosotros investigamos algoritmos de clasificación suave, los cuales pueden considerar el problema de píxeles mixtos en la escena como parte del proceso de clasificación. Los clasificadores suaves asignan múltiples clases a un píxel utilizando funciones de membresía las cuales determinan el grado de pertenencia que tiene ese píxel asociado a las clases disponibles. Como resultado, la clasificación suave puede ser utilizada para desarrollar modelos y mapas temáticos que sean más apropiados para imágenes de pobre resolución espacial. Ésta tesis presenta un estudio comparativo de algoritmos de clasificación suave basados en el Modelo de Mezclado Lineal (LMM por sus siglas en inglés) y sistemas de clasificación supervisada utilizando lógica difusa como alternativa a la clasificación dura de imágenes hiperespectrales de pobre resolución espacial. Como parte de la investigación, desarrollamos una herramienta de clasificación suave para el análisis de imágenes multi/hiperespectrales (“Spectral Soft Classification Tool” (SSCT)), el cual debe ser un valioso recurso para los analistas de imágenes al proveer algoritmos de clasificación suave, herramientas de visualización, y funciones para la evaluación del rendimiento de los clasificadores. Datos de percepción remota adquiridos sobre regiones de Puerto Rico con los sensores HYPERION y ETM+ (LANDSAT 7) fueron utilizados en este estudio.

DEDICATION

To the Lord for give me the support and energy to overcome obstacles ...

To the memory of my loving parents Ing. Orlando Pabón Torres and Mrs. Margeline Ramírez Montalvo. I love you with all of my heart.

To the people who believe in me ...

ACKNOWLEDGMENTS

I would like to give special thanks to my advisor Dr. Miguel Vélez Reyes for his guidance and patience during my Graduates Studies. I really respect him and admire his professionalism. It was an honor and privilege to work with him. I would also like to thanks my Graduate Committee: Dr. Shawn D. Hunt and Dra. Vidya Manian for their suggestions and help during the research work.

Also, I would like to give special thanks to LARSIP and IRISE staff especially Mr. Samuel Rosario, Ms. Marie Ayala, Ms. Maribel Feliciano, and Mrs. Vanessa Gutierrez. Marie and Samuel thank for always offering your technical support and friendship. Maribel and Vanessa thank for your time, compromise and effort.

A special thanks to Dr. Nasser M. Nasrabadi from US Army Research Laboratory who provided valuable ideas and suggestions after our participation in the 2008 International Symposium on Spectral Sensing Research.

This research work reported herein was funded primarily by the Bernard M. Gordon Center for Subsurface Sensing and Imaging Systems, under the Engineering Research Centers Program of the National Science Foundation (Award Number EEC-9986821). Ms. Wilma N. Pabón was also supported by a Fellowship from the Puerto Rico Space Grant Consortium (PRSGC) sponsored by NASA.

TABLE OF CONTENTS

ABSTRACT.....	ii
DEDICATION	iv
ACKNOWLEDGMENTS	v
LIST OF TABLES.....	ix
LIST OF FIGURES	xi
LIST OF ACRONYMS	xvi
1 CHAPTER 1	1
Introduction.....	1
1.1 Justification.....	1
1.2 Research Objectives.....	2
1.3 Contribution of this Research Work	2
1.4 Thesis Overview	3
2 CHAPTER 2	4
Background and Literature Review	4
2.1 Image Classification System.....	4
2.1.1 Hyperspectral Image Classification	5
2.2 Spatial Resolution of Hyperspectral Sensors – Satellite Platforms	7
2.3 Soft Classification.....	11
2.3.1 Fuzzy Logic	12
2.3.2 Linear Mixing Model.....	15
2.3.3 Evaluation of Soft Classifiers Performance	18
2.3.3.1 Degree of Mixing.....	20
2.3.3.1.1 Entropy.....	20
2.3.3.1.2 Euclidean Distance	22
2.3.3.2 Fuzzy Error Matrix.....	24
2.3.3.3 Correlation Coefficients.....	27
2.4 Existing Remote Sensing and Image Processing Tools.....	28
2.5 Summary	29
3 CHAPTER 3	30
Supervised Soft-Classification Algorithms.....	30

3.1	Supervised Soft Classification	30
3.1.1	Fuzzy Supervised Classification System (FSCS)	32
3.1.1.1	Softening or Fuzzyfication Process.....	33
3.1.1.2	Soft Classification.....	34
3.1.1.3	Hardening or Defuzzyfication Process.....	35
3.1.2	Fuzzy Maximum Likelihood (FML).....	35
3.1.3	Supervised Fuzzy C- Means (SFCM)	38
3.1.4	Linear Mixing Model (LMM).....	40
3.1.5	Maximum Likelihood (ML) Algorithm	40
3.2	Summary	41
4	CHAPTER 4	42
	The Spectral Soft Classification Tool	42
4.1	Hyperspectral Image Analysis Toolbox (HIAT)	42
4.2	The Spectral Soft Classification Tool (SSCT).....	43
4.3	Using the SSCT: Enrique Reef, La Parguera, Puerto Rico scene	46
4.3.1	Experimental Set-up.....	46
4.3.2	Land Cover References	47
4.3.3	Pre-Processing.....	51
4.3.4	Feature Extraction / Band Selection.....	54
4.3.4.1	Singular Value Decomposition – Subset Selection (SVDSS).....	54
4.3.4.2	Feature Extraction/Band Selection for Enrique Reef scene	54
4.3.5	Soft Classification.....	55
4.3.5.1	Hardening of Membership Map Outputs	58
4.3.6	Visualization Techniques	65
4.3.6.1	Fractional Maps.....	65
4.3.6.2	Binary Maps.....	65
4.3.6.3	Thematic Map Derived by a User-Defined Threshold.....	66
4.3.7	Accuracy Assessment	67
4.3.7.1	Measures of the Degree of Mixing.....	67
4.3.7.2	Fuzzy Error Matrix (FEM).....	75
4.3.7.3	Linear Relationship among Membership Outputs and Soft Reference Data	79
4.3.7.4	Conventional Hard Assessment	80
4.4	Summary	86
5	CHAPTER 5	87

Experimental Results using Real Data.....	87
5.1 Multispectral Case Study	87
5.1.1 Ground Truth Reference: USDA Puerto Rico Land Cover 1991.....	88
5.1.2 Soft Classification Results	91
5.2 Summary	100
6 CHAPTER	106
6.1 Conclusions.....	106
6.2 Future Work	108
BIBLIOGRAPHY	110
APPENDICES	115

LIST OF TABLES

Table 1: Fuzzy Error Matrix derived from LMM membership values (C) and True Abundances (R) of synthetic image shown in Figure 14.....	25
Table 2: Three classes – one pixel instance of the fuzzy error matrix for three possible cases: (a) perfect matching, (b) underestimation, and (c) overestimation (Binaghi et al., 1999) (Binaghi 2001).....	26
Table 3: SSCT – Description of .M files functions.....	45
Table 4: Specifications of HYPERION (EO-1) (Folkman et al., 2001) Hyperspectral sensor.....	47
Table 5: Description of bands selected by SVDSS in terms of wavelengths and original band number in a HYPERION dataset.....	56
Table 6: Measures Degree of Mixing for SFCM, FSCS, FML, and LMM	75
Table 7: Fuzzy Error Matrix reference derived by a Perfect Matching of testing samples (ideal case)	76
Table 8: Fuzzy Error Matrix derived from SFCM membership values (C) and LMM abundances used as Soft Reference (R).....	77
Table 9: Fuzzy Error Matrix derived from FML membership values (C) and LMM abundances used as Soft Reference (R).....	77
Table 10: Fuzzy Error Matrix derived from FML-LMM (LMM abundances used to initialize the FML algorithm) membership values (C) and LMM abundances used as Soft Reference (R)	78
Table 11: Fuzzy Error Matrix derived from FSCS membership values (C) and LMM abundances used as Soft Reference (R).....	78
Table 12: Correlation coefficient (ρ_{XY}) and RMS error of SFCM, FML, and FSCS using LMM abundances as soft reference data	80
Table 13: Confusion Error Matrix of a LMM thematic map derived by a hardening LMM abundance maps	82
Table 14: Confusion Error Matrix of a SFCM thematic map derived by a hardening SFCM membership maps	83
Table 15: Confusion Error Matrix of a FML thematic map derived by a hardening FML membership maps	83
Table 16: Confusion Error Matrix of a FML-LMM (LMM abundances used to initialized the FML algorithm) thematic map derived by a hardening FML-LMM membership maps.....	84

Table 17: Confusion Error Matrix of a FSCS thematic map derived by a hardening FSCS membership maps	84
Table 18: Confusion Error Matrix of a ML thematic map.....	85
Table 19: Specifications of ETM+ sensor on – board Landsat 7	87
Table 20: Distribution of original and modified land cover types of the USDA PR Land Cover 1991 (Helmer et al., 2002) for classification purposes.....	90
Table 21: Confusion Error Matrix of a LMM-1 thematic map derived by a hardening LMM-1 abundance maps	101
Table 22: Confusion Error Matrix of a LMM-2 thematic map derived by a hardening LMM-2 abundance maps	101
Table 23: Confusion Error Matrix of a SFCM thematic map derived by a hardening SFCM membership maps	102
Table 24: Confusion Error Matrix of a FSCS thematic map derived by a hardening FSCS membership maps	102
Table 25: Confusion Error Matrix of a FML (initialized using LMM) thematic map derived by a hardening FML membership maps.....	103
Table 26: Confusion Error Matrix of a ML thematic map.....	103

LIST OF FIGURES

Figure 1: A basic classification system for multi/hyperspectral imagery	4
Figure 2: Concept of hyperspectral imaging spectroscopy	6
Figure 3: Methodology for the Analysis of High Dimensional Data [Adapted from (Landgrebe 2002)]	7
Figure 4: Mixed Pixel constituent by three object spectra.	8
Figure 5: HYPERION (Folkman et al., 2001) and IKONOS (Dial et al., 2003) True Color Composites of Enrique Reef at La Parguera, Lajas PR.....	9
Figure 6: Spatial PSF response larger than GIFOV [Figure adapted from (Van Der Meer and Jong 2006)]	10
Figure 7: Mixed pixels caused by boundaries among informational classes in the scene [From Dr. Nicholas Short's Remote Sensing Tutorial].....	10
Figure 8: Hard and Soft Classification approaches applied to instance of 4 pixels mosaic.....	12
Figure 9: Fuzzyfication process using a triangular function.....	13
Figure 10: Different types of membership functions	15
Figure 11: Conceptual diagram of spectral unmixing [Adapted from (Keshava and Mustard 2002)]	18
Figure 12: Layout of a confusion error matrix and computation of user's and producer's accuracy (Landgrebe 2003).....	19
Figure 13: (a) Entropy image generated by a mixture of two endmembers (corners were comprised by pure pixels and 50% of mixture can be appreciated at the center) (b) Entropy values for along-track transect	22
Figure 14: Synthetic image, true abundance maps (soft ground truth data), and LMM membership maps. Synthetic Image courtesy of Dr. Ronald Lockwood and Lt. Angela Puetz from AFRL.....	23
Figure 15: Testing samples (red rectangles) used to compute the Fuzzy Error Matrix of the synthetic image shown in Figure 14	25
Figure 16: Scatterplot of soft reference data ($y(i)$) and estimated degree of membership values ($x(i)$) of synthetic image example shown in Figure14	27
Figure 17: A general soft classification scheme for multi/hyperspectral imagery.....	31
Figure 18: Block diagram of Fuzzy Supervised Classification System (FSCS) methodology (Melgani, Al Hashemy and Taha 2000).....	32

Figure 19: HIAT Processing Methodology including the proposed Spectral Soft Classification Tool	43
Figure 20: SSCT as an end-to-end soft classification system	44
Figure 21: IKONOS true color image of Enrique Reef, La Parguera that shows informational classes selected for SSCT experiments	48
Figure 22: HYPERON true color image (bands 31-21-11) of Enrique Reef used as Hyperspectral data for SSCT experiments	48
Figure 23: (a) IKONOS classification map, (b) Co-registration of IKONOS and HYPERION imagery used as Land Cover Reference for Enrique Reef scene (Rivera-Borrero and Hunt 2007).....	49
Figure 24: Benthic Habitat Map of La Parguera, PR generated in 1999 by CCMA, NOAA (Kendall et al., 2001)	50
Figure 25: Distribution of 200 ground truth point across the study area of La Parguera, PR (Kendall et al., 2001)	50
Figure 26: Abundances estimates derived from co-registration of IKONOS and HYPERION Imagery (Rivera-Borrero and Hunt 2007)	51
Figure 27: HYPERION (a) Band 9 raw image, (b) Band 9 - 96% PCA filter image, and (c) Line 25 of a first Enrique Reef, PR subset of 41 x 67 scene	53
Figure 28: Mean training samples spectral response of bands selected by SVDSS	55
Figure 29: Training samples used for (a) SFCM, and FSCS, (b) FML, and ML.....	57
Figure 30: Sea Grass membership map using a 0-1 scale (left side) and ranges scale on the right side (0-20%, 21-40%, 41- 60%, 61-80%, 81-100%) obtained with (a) LMM, (b) SFCM, (c) FML, (d) FSCS, and (e) soft reference derived by co-registration of IKONOS and HYPERION imagery (Rivera-Borrero and Hunt 2007)	59
Figure 31: Sand membership map using a 0-1 scale (left side) and ranges scale on the right side (0-20%, 21-40%, 41- 60%, 61-80%, 81-100%) obtained with (a) LMM, (b) SFCM, (c) FML, (d) FSCS, and (e) soft reference derived by co-registration of IKONOS and HYPERION imagery (Rivera-Borrero and Hunt 2007).....	60
Figure 32: Reef Flat membership map using a 0-1 scale (left side) and ranges scale on the right side (0-20%, 21-40%, 41- 60%, 61-80%, 81-100%) obtained with (a) LMM, (b) SFCM, (c) FML, (d) FSCS, and (e) soft reference derived by co-registration of IKONOS and HYPERION imagery (Rivera-Borrero and Hunt 2007)	61
Figure 33: Mangrove membership map using a 0-1 scale (left side) and ranges scale on the right side (0-20%, 21-40%, 41- 60%, 61-80%, 81-100%) obtained with (a) LMM, (b) SFCM, (c) FML, (d) FSCS, and (e) soft reference derived by co-registration of IKONOS and HYPERION imagery (Rivera-Borrero and Hunt 2007)	62

Figure 34: Deep Water membership map using a 0-1 scale (left side) and ranges scale on the right side (0-20%, 21-40%, 41- 60%, 61-80%, 81-100%) obtained with (a) LMM, (b) SFCM, (c) FML, (d) FSCS, and (e) soft reference derived by co-registration of IKONOS and HYPERION imagery (Rivera-Borrero and Hunt 2007)	63
Figure 35: Classification maps obtained with (a) LMM, (b) SFCM, (c) FSCS, (d) FML, (e) FML-LMM to initialized, (f) ML, (g) hardening of soft references, and (h) threshold of 0.55 was applied to the classification map obtained in (g).	64
Figure 36: Fraction color maps derived by a combination of Reef Flat, Sea Grass, and Sand membership maps in the RGB channels	66
Figure 37: Binary maps of sand LMM abundances derived by user-defined thresholds of 0.85, 0.7, 0.5, and 0.2	68
Figure 38: Binary maps of reef-flat LMM abundances derived by user-defined thresholds of 0.85, 0.7, 0.5, and 0.2	69
Figure 39: Binary maps of sea-grass LMM abundances derived by user-defined thresholds of 0.85, 0.7, 0.5, and 0.2	70
Figure 40: (a) Hardening LMM abundances, (b) with threshold of 0.5 (unclassified class), and (c) with threshold of 0.5 and specified by class label which obtained higher degree of membership	71
Figure 41: Thematic map with threshold (T=0.5). (a) Pixels with $T < 0.5$ are in red, (b) pixels with $T < 0.5$ are labeled by the class which obtained higher weight.	72
Figure 42: Entropy values derived from estimated LMM abundances	73
Figure 43: Entropy values derived from estimated SFCM membership outputs	73
Figure 44: Entropy values derived from estimated FSCS membership outputs	74
Figure 45: Entropy values derived from estimated FML membership outputs	74
Figure 46: Fuzzy Error Matrix overall accuracy of SFCM, FML, FML-LMM, and FSCS approaches.....	79
Figure 47: Relationships between SFCM and LMM for deep water, mangrove, sand, sea grass, and reef flat informational classes.....	81
Figure 48: (a) Enrique Reef Testing Samples selected for a hard assessment, (b) Number of samples per informational class	82
Figure 49: Confusion error matrix overall accuracy percentage of testing samples of LMM, SFCM, FML, FML-LMM, ML, and FSCS approaches.....	85
Figure 50: A true color (bands 3-2-1) and color infrared images (bands 4-3-2) of Lajas, PR scene acquired with an ETM+ sensor.	88

Figure 51: USDA Puerto Rico Land Cover Reference 1991 (Helmer et al., 2002) (a) Original Thematic Map, and (b) Modified thematic map after perform a merge of classes, (c) NDVI of a scene, (d) legend of USDA Land Cover showed in (a)	89
Figure 52: Spectral response of informational classes used to compute LMM-1	91
Figure 53: Membership maps obtained using a LMM-1 (endmembers selected manually from the image) of (a) Water, (b) Urban and Barren Land, (c) Forest, (d) Pasture, and (e) Agriculture. A scale based on ranges were used (0-20%, 21-40%, 41-60%, 61-80%, and 81-100%).....	92
Figure 54: (a) Classification map derived from LMM-1 hardening process, (b) threshold of 0.5 was applied, (c) USDA PR Land Cover Reference 1991 (Helmer et al., 2002), and (d) LMM-1 Fractional Map, R-Pasture, G-Forest, B-Agriculture	92
Figure 55: Spectral response of informational classes used to compute LMM-2 (derived from PMF algorithm (Masalmah and Vélez-Reyes 2007)).....	93
Figure 56: Membership maps obtained using a LMM-2 (PMF initialized with endmembers selected manually from the image) of (a) Water, (b) Urban and Barren Land, (c) Forest, (d) Pasture, and (e) Agriculture. A scale based on ranges were used (0-20%, 21-40%, 41-60%, 61-80%, and 81-100%)	94
Figure 57: (a) Classification map derived from LMM-2 hardening process (b) threshold of 0.5 was applied, (c) USDA PR Land Cover Reference 1991 (Helmer et al., 2002), and (d) LMM-2 Fractional Map, R-Pasture, G-Forest, B-Agriculture	94
Figure 58: Training samples of (a) SFCM, and FSCS, (b) FML, and (c) testing samples	96
Figure 59: Membership maps obtained using a SFCM-Euclidean Norm of (a) Water, (b) Urban and Barren Land, (c) Forest, (d) Pasture, and (e) Agriculture. A scale based on ranges were used (0-20%, 21-40%, 41-60%, 61-80%, and 81-100%)	97
Figure 60: (a) Classification map derived from SFCM-Euclidean Norm hardening process (b) threshold of 0.5 was applied (c) USDA PR Land Cover Reference 1991 (Helmer et al., 2002) , and (d) SFCM Fractional Map, R-Pasture, G-Forest, B-Agriculture	97
Figure 61: Membership maps obtained using a FSCS of (a) Water, (b) Urban and Barren Land, (c) Forest, (d) Pasture, and (e) Agriculture. A scale based on (0-20%, 21-40%, 41-60%, 61-80%, and 81-100%) ranges were used.	98
Figure 62: (a) Classification map derived from FSCS hardening process, and (b) USDA PR Land Cover Reference 1991 (Helmer et al., 2002), and (c) FSCS Fractional Map, R-Pasture, G-Forest, B-Agriculture	98
Figure 63: Membership maps obtained using a FML-initialized with LMM of (a) Water, (b) Urban and Barren Land, (c) Forest, (d) Pasture, and (e) Agriculture. A scale based on (0-20%, 21-40%, 41-60%, 61-80%, and 81-100%) ranges were used.....	99

Figure 64: (a) Classification map derived from FML-initialized LMM hardening process (b) USDA PR Land Cover Reference 1991 (Helmer et al., 2002), (c) Maximum Likelihood, (d) FML Fractional Map, R-Pasture, G-Forest, B-Agriculture 99

Figure 65: LMM-1, LMM-2, SFCM, FSCS, FML, and ML overall accuracy percentage of testing samples 104

LIST OF ACRONYMS

ARTEMIS	Advanced Responsive Tactically Effective Military Imaging Spectrometer
AFRL	Air Force Research Laboratory
ED	Euclidean Distance
EnMAP	Environmental Mapping and Analysis Program
ETM+	Enhanced Thematic Mapper
FCM	Fuzzy C – Means
FEM	Fuzzy Error Matrix
FML	Fuzzy Maximum Likelihood
FSCS	Fuzzy Supervised Classification System
GIFOV	Ground Instantaneous Field of View
HERO	Hyperspectral Environment and Resource Observer
HIAT	Hyperspectral Image Analysis Toolbox
HSI	Hyperspectral Imagery
LARSIP	Laboratory for Applied Remote Sensing and Image Processing
LMM	Linear Mixing Model
LMM-1	Linear Mixing Model – (1) Endmembers selected manually from image
LMM-2	Linear Mixing Model – (2) Endmembers from PMF algorithm
LWIR	Long Wave Infrared
MAP	Maximum A Posteriori
MODIS	Moderate Resolution Imaging Spectroradiometer
MWIR	Middle Wave Infrared
NIR	Near Infrared
PDF	Probability Density Function
PMF	Positive Matrix Factorization
PPI	Pixel Purity Index
PSF	Point Spread Function
RGB	Red, Green, Blue channels
SFCM	Supervised Fuzzy C-Means
SSCT	Spectral Soft Classification Tool
SVM	Support Vector Machine
SWIR	Short Wave Infrared

CHAPTER 1

Introduction

1.1 Justification

Hyperspectral imagery (HSI) is a significant technology used in remote sensing and play an important role in the success of image classification because provides valuable spectral information of the materials of interest in the scene. Hyperspectral sensors consists of hundred of narrow bands that collects electromagnetic energy through the visible, near infrared (NIR), middle wave infrared (MWIR), and long wave infrared (LWIR) regions of the electromagnetic spectrum. Using the spectral signatures, it is possible to discriminate between materials or identifying objects. Hyperspectral technologies are useful for environmental applications when it is possible to take advantage of spectral, spatial, and radiometric resolutions. Mixed pixels are a major problem of remote sensed data which is a common scenario when spatial resolution of a sensor is low and a combination of materials occupy a single pixel. Existing and proposed hyperspectral sensors on-board satellite platforms such as HYPERION, Environmental Mapping and Analysis Program (EnMAP) (Kaufmann et al., 2006), Hyperspectral Environment and Resource Observer (HERO) (Hollinger et al., 2006), and Advanced Responsive Tactically Effective Military Imaging Spectrometer (ARTEMIS) (Lockwood et al., 2002) have a spatial resolution ranging between 20 – 30 m. In addition, the impact of the point spread function (PSF) is an inherent source of uncertainty in satellite images because a portion of the signal acquired by the HSI sensors in a single pixel comes from surrounding pixels caused by many factors such as the optics of the instruments, the detectors, electronics, and atmospheric effects (Huang et al., 2002) (Van Der Meer and Jong 2006). In such cases, the high spectral resolution can be used to identify objects at the subpixel level by their contribution to the measured spectral signature. A common technique in HSI analysis is hard classification where each pixel is assigned to one specific class (Richards 1995) (Landgrebe 2002)(Landgrebe 2003)(Lu and Weng 2007). The most popular supervised multispectral hard classification algorithm is Maximum Likelihood due its robustness and good performance. We think that it is necessary to study alternatives to hard classification algorithms which can consider the mixing

problem in the image classification because it could be more descriptive of real variation of landscape images.

Soft classification works with the idea of assigning multiple classes to a single pixel. As a result, soft-classification could be used to develop models that are more representative of remote sensing imagery. This research project was focus on studying soft classification algorithms and in developing an end to end soft-classification system which provides to image analysts and decision makers a useful tool that combines state of the art soft classification algorithms, visualization tools, accuracy assessment to evaluate the performance of soft classifiers, and metrics to measure the strength of the membership partition.

1.2 Research Objectives

The main objective of the research work was to study potential soft-classification algorithms for hyperspectral imagery in order to generate an end to end soft classification system. More specific objectives of the investigation were:

- Study and implement two soft classification approaches based on fuzzy logic, and linear mixing model.
- Study methods to evaluate the performance of soft classification algorithms and visualization techniques which can provide alternatives to image analysts in the process of analyzing a particular scene.
- Comparison of soft classification algorithms developed on imagery of different landscapes, spectral resolutions, and with conventional hard classifiers such as Maximum Likelihood.
- Develop a Spectral Soft Classification Tool which will be incorporated into the UPRM Hyperspectral Image Analysis Toolbox (HIAT).

1.3 Contribution of this Research Work

The main contributions of this work are the integration of different soft-classification methodologies, visualization, and assessment tools in the Spectral Soft Classification Tool (SSCT) which is an end to end classification system. In the literature review, we have found that existing HSI analysis

tools such as ENVI® (ITT Visual Information Solutions 2007), Multispec (Biehl and Landgrebe 2002) (Landgrebe and Biehl, Purdue/LARS Multispec 1994-2008), and HIAT (Arzuaga-Cruz et al., 2004) (Rosario-Torres et al., 2005) do not provide capability for soft classification of HSI, accuracy assessment and visualization techniques as required for remote sensing image analysis. SSCT provides a complete and a useful resource that can be used by many image analysts and decision makers for the analysis of different landscapes imagery at the subpixel level.

1.4 Thesis Overview

The thesis is organized as follow. In Chapter 2, background and previous work are discussed. State of the arts soft classification algorithms proposed to be used in the SSCT such as Supervised Fuzzy C-Means (SFCM) (Zhang and Foody 2001) (Bezdek et al., 1984), Fuzzy Supervised Classification System (FSCS) (Melgani et al., 2000), Fuzzy Maximum Likelihood (FML) (Wang 1990), and Linear Mixing Model (LMM) (Keshava and Mustard 2002) are discussed in Chapter 3. Chapter 4 presents the proposed Spectral Soft Classification Tool (SSCT) which is an end to end classification system which provides visualization tools to analyze soft classification outputs and accuracy assessment to evaluate the performance of soft classifiers. Real multi/hyperspectral imagery collected with sensors onboard satellite platforms for land remote sensing applications were used for experimental results described in Chapter 5. Chapter 6 presents the conclusions of this research and suggestions for further work.

CHAPTER 2

Background and Literature Review

This chapter presents the general concepts of HSI classification, challenges in terms of spatial resolution of current and proposed HSI satellite sensors, and accuracy assessment to evaluate the performance of soft classifiers. The soft classification algorithms studied in this research work, Linear Mixing Model and Supervised Fuzzy Logic Algorithms, are presented.

2.1 Image Classification System

In past years and decades, researchers have been working in develop image classification algorithms such as supervised and unsupervised methods, parametric and non parametric statistics algorithms, per pixel or object oriented classification, hard and soft classifiers in order to improve classification accuracy (Richards 1995)(Landgrebe 2003)(Lu and Weng 2007)(Schowengerdt 2007). Image classification outputs or thematic maps are the basis for many environmental and socioeconomic applications. The success of image classification could be affected by many factors, such as type of remotely sensed data (type of sensors and multi/hyperspectral imagery), complexity of landscapes, and classification algorithm approaches. Figure 1 shows a simple scheme of classification where the sensor acquires electromagnetic energy in form of multispectral and/or hyperspectral imagery, a feature extraction is used for dimensionality reduction while keeping class separability in the lowest dimensional space, and finally an image classification algorithm is applied which produces a thematic map in the case of hard classification.

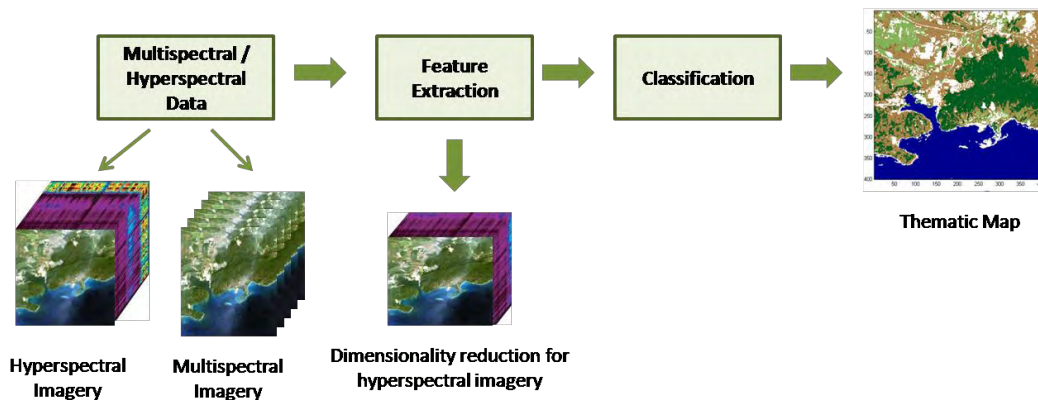


Figure 1: A basic classification system for multi/hyperspectral imagery

Hard, per-pixel or crisp classification of HSI is the process of producing thematic or classification maps which are informational description of a given area where each pixel in the scene is assigned to one and only one specific class (Schowengerdt 2007). The image analyst has prior knowledge of the area to be analyzed in the supervised hard classification. It allows defining information classes corresponding to specific regions of the image and select representative training samples to train the classifier to be used. The most popular hard classifier is the Maximum Likelihood (Richards 1995) due its good performance, robustness and its availability in almost any image processing and remote sensing software such as ENVI®¹ (ITT Visual Information Solutions 2007), Multispec² (Biehl and Landgrebe 2002)(Landgrebe and Biehl 1994-2008), HIAT³ (Arzuaga-Cruz et al., 2004)(Rosario-Torres et al., 2005), and others. The partial membership of the pixel to multiple classes is not allowed under hard classification algorithms. In other words, a pixel is a full member or not of a class. This kind of processing is not the best way to work with data acquired at low spatial resolution where a single pixel includes multiple objects from different classes.

2.1.1 Hyperspectral Image Classification

Hyperspectral Imagery consists of hundreds of narrow bands acquired by satellite or airborne sensors at different wavelengths of the electromagnetic spectrum typically from VIS to SWIR as shown in Figure 2. One would expect that the increment in the number of bands would result in an increase in the classification accuracy in comparison with multispectral sensors. Conversely, it is possible that classification accuracy decrease as the number of features increased. Previous works (Landgrebe 2002)(Landgrebe 2003) demonstrates that the number of training samples and data dimensionality are related. The uses of high dimensional data sets require a large number of training samples which is a limitation of remote sensed data. Feature extraction methods reduce high dimensional data without a

¹ Environment for Visualizing Images (ENVI) developed by ITT Visual Information Solutions, formerly Research Systems Inc. (RSI) is widely used software for remote sensing and image processing which provides code extensibility through Interactive Data Language (IDL). <http://www.itvis.com/envi>

² Multispec developed at Purdue University by Dr. David Landgrebe and the Remote Sensing research group in Purdue's Laboratory for Applications of Remote Sensing (LARS) is non commercial software for image processing. Multispec provides similar features to ENVI but does not provide feature extensibility. <http://cobweb.ecn.purdue.edu/~biehl/MultiSpec>

³ Hyperspectral Image Analysis Toolbox (HIAT) was developed over the past 8 years by UPRM researchers at the Laboratory for Applied Remote Sensing and Image Processing (LARSIP) to analyze multi/hyperspectral imagery. This toolbox runs over MATLAB® environment and incorporates the algorithms developed at LARSIP along with standard algorithms for image classification similar to those included in other remote sensing tools such as ENVI and Multispec. <http://www.censsis.neu.edu/software/hyperspectral/hyperspectral.html>

significant loss of information and in some manner can mitigate the Hughes phenomenon (Landgrebe 2002) (Landgrebe 2003).

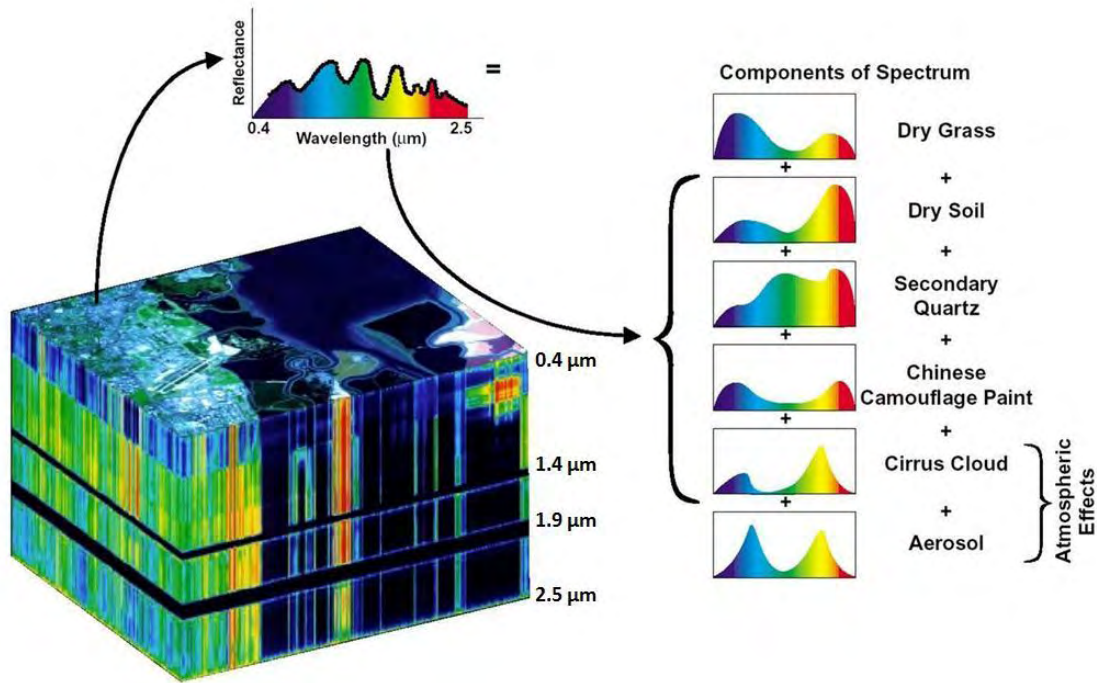


Figure 2: Concept of hyperspectral imaging spectroscopy

Figure 3 shows nominal sequences of steps for the analysis of HSI in a supervised case which consists of a pre-processing of raw data using algorithms to remove atmospheric effects and denoise images, selection of informative and spectral classes, feature extraction methods such as Principal Components (PCA) (Schowengerdt 2007), Minimum Noise Fraction (MNF) (Schowengerdt 2007), Discriminant Analysis (Landgrebe 2003), Band Subset Selection by Singular Value Decomposition (Vélez-Reyes and Jiménez-Rodríguez 1998), and others. Classification algorithms are applied to HSI when several tests of training samples are done to assure the best representation of informational classes. Finally a hard thematic map is obtained and accuracy assessment methods are used to evaluate the performance of hard classifiers. A broad outline of the HSI data analysis process is given in (Landgrebe 2002)(Landgrebe 2003)(Varshney and Arora 2004)(Jiménez-Rodríguez et al., 2007)(Schowengerdt 2007).

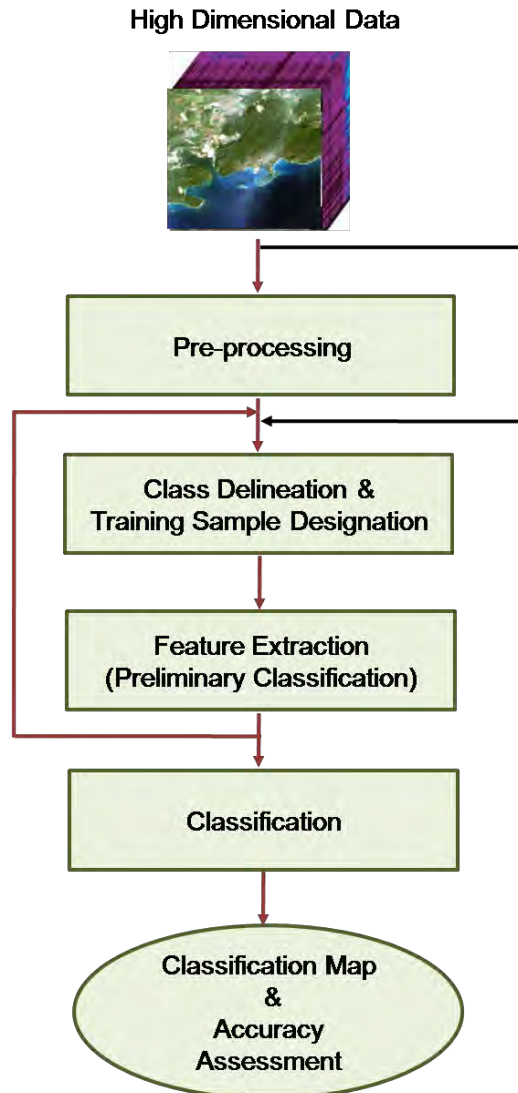


Figure 3: Methodology for the Analysis of High Dimensional Data [Adapted from (Landgrebe 2002)]

2.2 Spatial Resolution of Hyperspectral Sensors – Satellite Platforms

Current and proposed hyperspectral sensors such as HYPERION (Folkman et al., 2001), EnMAP (Kaufmann et al., 2006), HERO (Hollinger et al., 2006), and ARTEMIS (Lockwood et al., 2007) have a medium or coarse spatial resolution between 20 – 30 m. For instance, HYPERION (Folkman et al., 2001) which is an existing satellite hyperspectral sensor, collects 220 unique spectral channels ranging from visible portion (0.357 μm) to the short wave infrared (SWIR) portion (2.576 μm) of the electromagnetic (EM) spectrum with a 10 nm bandwidth and 30m of spatial resolution for all bands. On the other hand,

EnMAP (Kaufmann et al., 2006), which is a proposed hyperspectral instrument and schedule for launch in 2011, will collect 218 spectral channels ranging from visible region (0.420 μm) to the SWIR region (2.450 μm) of the EM spectrum at a spatial resolution of 30 m. The EnMAP hyperspectral mission will focus on current issues related to the land use / land cover, environment, agriculture, water systems, geology, and further associated science problems. A medium spatial resolution of imagery acquired by satellite platforms generally introduces the major problem of mixing pixels in the scene because frequently a pixel is occupied by a collection of materials or constituent spectra commonly known as endmembers as shown in Figure 4.

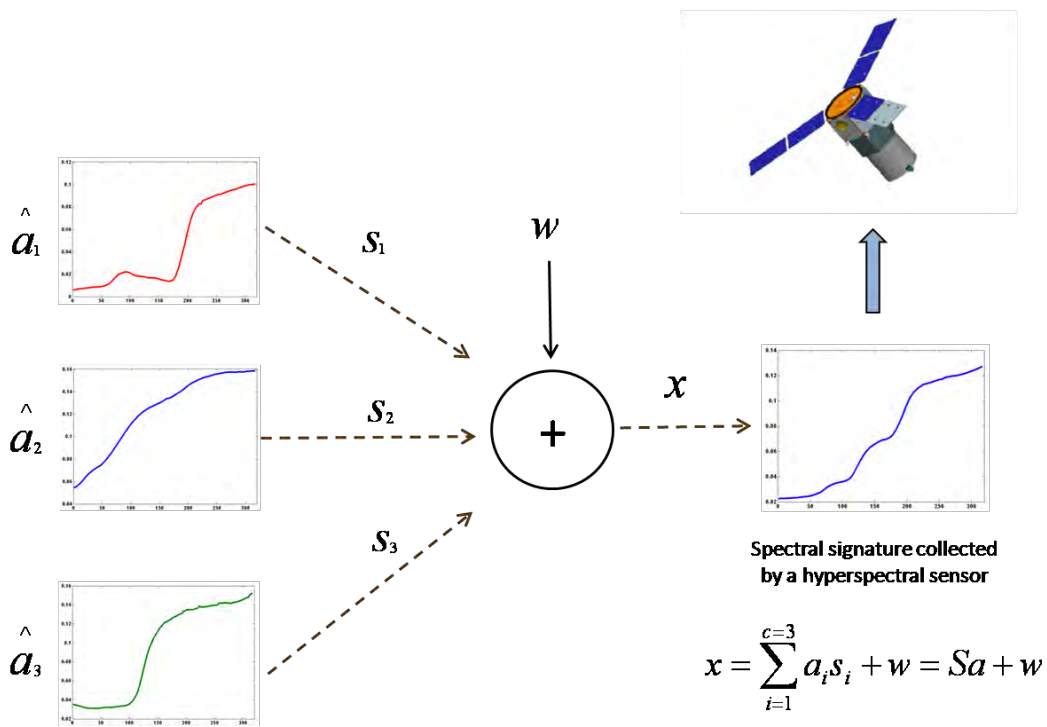
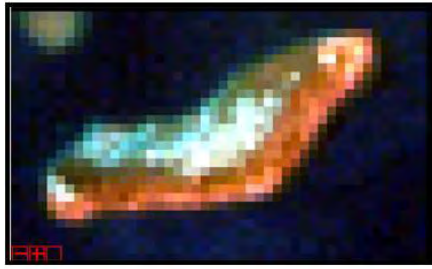


Figure 4: Mixed pixel constituent by three object spectra.

Figure 5 illustrates a spatial degradation caused by a low spatial resolution by comparing true color composites of the same region acquired with HYPERION (Folkman et al., 2001), a hyperspectral sensor with 30m of spatial resolution and IKONOS (Dial et al., 2003), a multispectral sensor with high spatial resolution of 1m PAN sharpened.



**Hyperion Image
30m Spatial Resolution**



**IKONOS PAN Sharpened
1m Spatial Resolution**

Figure 5: HYPERION (Folkman et al., 2001) and IKONOS (Dial et al., 2003) True Color Composites of Enrique Reef at La Parguera, Lajas PR

There are other factors such as Point Spread Function (PSF) which introduce an inherent source of uncertainty to low spatial resolution satellite imagery (Van Der Meer and Jong 2006)(Huang, et al. 2002). Measured and modeled PSF indicates that spectral response acquired by MSI/HSI sensors for a pixel have a significant portion which comes from surrounding pixels as can be seen in Figure 6. For instance, it has been estimated, for a given pixel, that less than half of the spectral response recorded at the Multispectral Scanner (MSS) sensor (first multispectral sensor onboard Landsat satellite) which has spatial resolution of 79 m was originated by the materials in the pixel itself (Huang et al., 2002) resulting in a spectral response which has contributions from neighbors pixels. Another example is presented in (Townshend et al., 2000), where a study based on the estimation of land cover proportions using a linear mixing analysis was conducted. In that study, pure pixels which come from data acquired with multispectral Thematic Mapper (TM) sensor were degraded to 250 m of spatial resolution in order to obtain data comparable with coarse spatial resolution of bands 1-2 of the Moderate Resolution Imaging Spectroradiometer (MODIS). The study revealed an increment of approximately 7% in the standard error of estimation of the land cover proportions when PSF effects are present (Townshend et al., 2000) (Huang et al., 2002).

The net sensor PSF (1) (Schowengerdt 2007) is a convolution of individual responses from instrument optics, image motion, detector which defines the geometrical GIFOV, and electronics. Generally, PSF darkens bright objects and brightens dark objects (Huang et al., 2002).

$$PSF_{net}(x, y) = PSF_{opt}(x, y) \otimes PSF_{IM}(x, y) \otimes PSF_{det}(x, y) \otimes PSF_{el}(x, y) \quad (1)$$

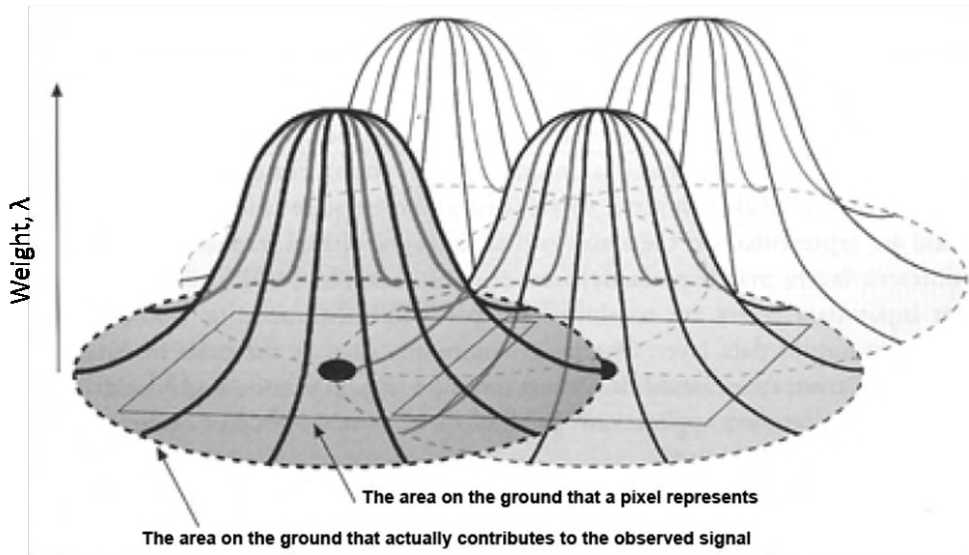


Figure 6: Spatial PSF response larger than GIFOV [Figure adapted from (Van Der Meer and Jong 2006)]

Mixed pixels also can be generated when Ground-projected Instantaneous Field of View (GIFOV) of a given pixel is comprised by boundaries among informational classes as can be seen in Figure 7.

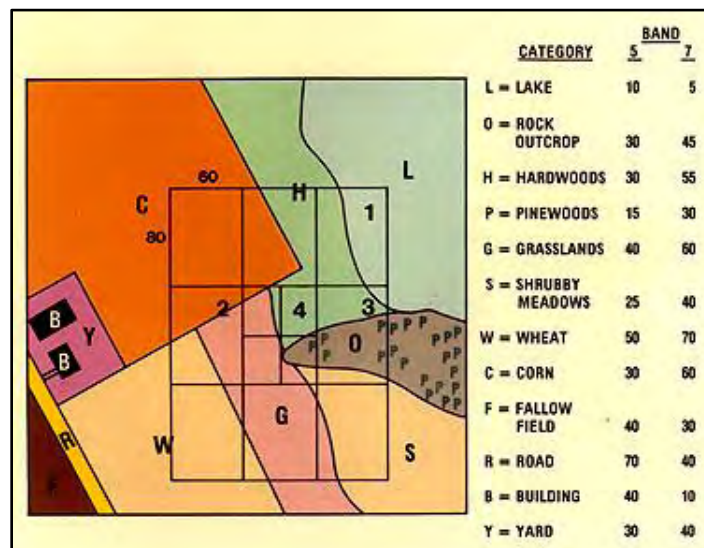


Figure 7: Mixed pixels caused by boundaries among informational classes in the scene [From Dr. Nicholas Short's Remote Sensing Tutorial]

Conventional image classification algorithms ignore the impact of mixed pixels in the classification process resulting in thematic maps which may not be representative of real variation of landscape.

2.3 Soft Classification

Due to the need to find potential subpixel classification algorithms and models to provide a more appropriate representation of remote sensing imagery, researchers have been working on the development of algorithms that could be capable of managing mixed pixels in a scene, especially when images from satellite multi/hyperspectral sensors are used. A class of classification algorithms which deal with the mixed pixel problem are Soft Classification algorithms (Foody 1998)(Lu and Weng 2007) (Schowengerdt 2007) (Varshney and Arora 2004)(Van Der Meer and Jong 2006). Soft Classification allows the assignment of one pixel to multiple classes or a partial membership of that pixel using membership functions to generate weight fractions or degree of membership in a range from 0 to 1. The membership functions of the soft input variables could be obtained from statistical values of band training samples or using band indexes such as vegetation indexes, or band ratios to seek separate certain features. Soft classifiers estimate the contribution of each class in the pixel. The pixel has no requirement to have contribution from all classes. Soft classification algorithms produce membership maps sometimes called fraction images as outputs, one for each class, in which pixel value represents the degree of membership for that class. Figure 8 shows an instance of 4 pixels mosaic comprised of three land cover classes, urban, forest, and grass and how soft and hard classification approaches assign each pixel into the mosaic. As can be seen in Figure 8, hard classification ignores the mixing between land cover types assigning each pixel to one and only one specific class. On the other hand, soft classification produces for each pixel a degree of membership in a range from 0 to 1 associated to urban, forest, and grass informational classes per pixel as shown in Figure 8. For instance, the right corner pixel at the bottom of Figure 8 (mosaic) is comprised of forest and grass land-cover types. As can be seen in Figure 8, soft classification assigned this pixel to forest and grass classes with degree of membership of 0.7 and 0.3, respectively.

The research was focused on the study of soft classifiers based on Linear Mixing Model (Foody and Cox 1994)(Adams 2006) (Keshava 2003)(Keshava and Mustard 2002) and Supervised Fuzzy Logic algorithms (Zhang and Foody 2001) (Mendel 1995) (Varshney and Arora 2004)(Wang 1990)(Foody and Cox 1994)(Melgani et al., 2000). However, other possibilities based on neural networks and neuro-fuzzy approaches available in the literature are (Foody 1996) (Tsoukalas 1997)(Nauck and Kruse 1997)(Schouten 1999). A soft classification algorithm based on spectral-spatial kernels and Support Vector Machine (SVM) to generate the degree of membership associated to each class was proposed in

(Gu et al., 2007). An unsupervised soft classification algorithm based on blind source separation using an Independent Component Analysis (ICA) was proposed by Du and Chakravarthy (Du and Chakravarthy 2003).

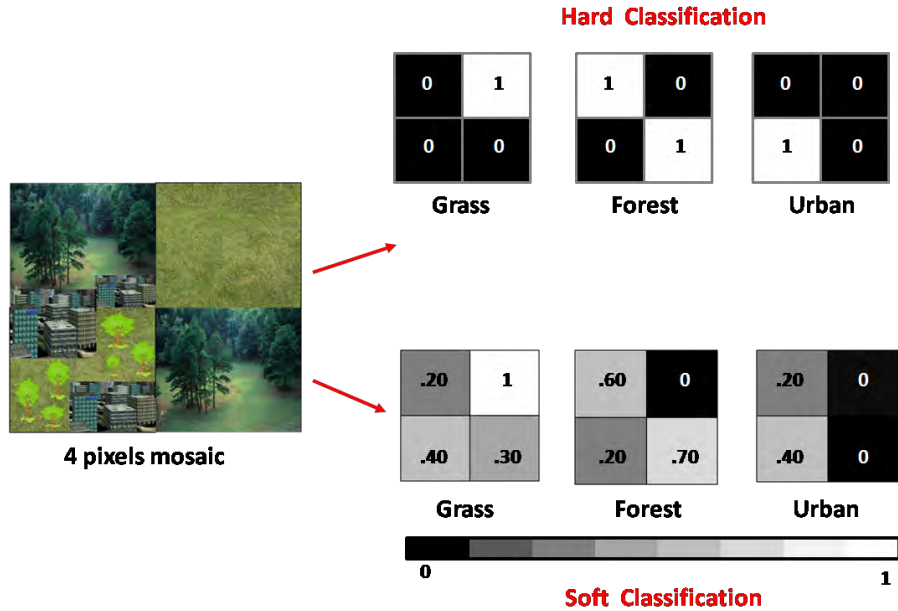


Figure 8: Hard and soft classification approaches applied to instance of 4 pixels mosaic.

2.3.1 Fuzzy Logic

A popular approach to derive soft classifiers is Fuzzy Logic (FL). FL extends the conventional Boolean logic using the concept of partial truth for those values falling between “0” and “1”, which corresponds to a “totally true” and “totally false”, respectively. This method consists of mathematical tools, to model approximate reasoning when data is imprecise, uncertain, vague, and incomplete, using fuzzy sets. In crisp logic, an element in the universe is defined as a member or not of a given set (Tsoukalas 1997). For instance, the membership of a crisp set H can be defined through a membership function defined for every element y of the universe as

$$\mu_H(y) = \begin{cases} 1 & y \in H \\ 0 & y \notin H \end{cases} \quad (2)$$

On the other hand, in fuzzy sets members have degree of membership in the set. The membership in a set is represented by a number in the range from 0 to 1 (3) (Tsoukalas 1997).

$$\mu_H(y): Y \rightarrow [0,1] \quad (3)$$

where y is an element of the universe. A sample membership function is shown in Figure 9.

A fuzzyfication process is conducted in order to generate a membership values in a range from 0 to 1 deduced by a membership functions, which define how each pixel (bands) is mapped to a class. Membership functions can be determine on the basis of statistical data or through the aid of neural networks sometime called neuro-fuzzy classifiers (Tsoukalas 1997)(Nauck and Kruse 1997). Membership functions commonly used in engineering applications are presented next and shown in Figure 10.

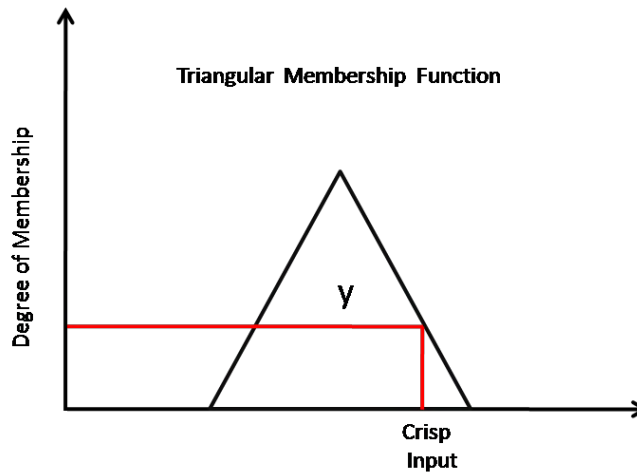


Figure 9: Fuzzyfication process using a triangular function

Triangular

A triangular membership function $G(x)$ with end points in $(a,0)$ and $(c,0)$ and high points in $(b,1)$, it can be defined as follow

$$G(x) = \begin{cases} \left(\frac{x-a}{b-a}\right) & \text{if } a \leq x \leq b \\ \left(\frac{c-x}{c-b}\right) & \text{if } b \leq x \leq c \\ 0 & \text{otherwise} \end{cases} \quad (4)$$

Trapezoidal

The trapezoidal membership function $T(x)$ with end points in $(a,0)$ and $(d,0)$ and high points in $(b,1)$ and $(c,1)$, it can be defined as follow

$$T(x) = \begin{cases} \left(\frac{x-a}{b-a}\right) & \text{if } a \leq x \leq b \\ 1 & \text{if } b \leq x \leq c \\ \left(\frac{d-x}{d-c}\right) & \text{if } c \leq x \leq d \\ 0 & \text{otherwise} \end{cases} \quad (5)$$

Sigmoid –Type S

Sigmoid membership function $S(x)$ is given by the following equation

$$S(x) = \frac{1}{1+e^{-x+1}} \quad (6)$$

Gaussian

Gaussian is a widely used membership function on image classification. It can be written as follows

$$B(x) = \exp\left(-\frac{(x-\mu)^2}{2\sigma^2}\right) \quad (7)$$

where μ and σ corresponds to mean and standard deviation, respectively.

Typically, these membership functions (for instance $G(x)$, $T(x)$, $S(x)$, and $B(x)$) are combined with mathematical operators such as minimum, maximum, negation which are given by

Minimum

$$K(x) \wedge L(x) = \min(K(x), L(x))$$

Maximum

$$K(x) \vee L(x) = \max(K(x), L(x)) \quad (8)$$

Negation

$$NOT: (-L)(x) = 1 - L(x)$$

where $K(x)$ and $L(x)$ are membership functions (Tsoukalas 1997).

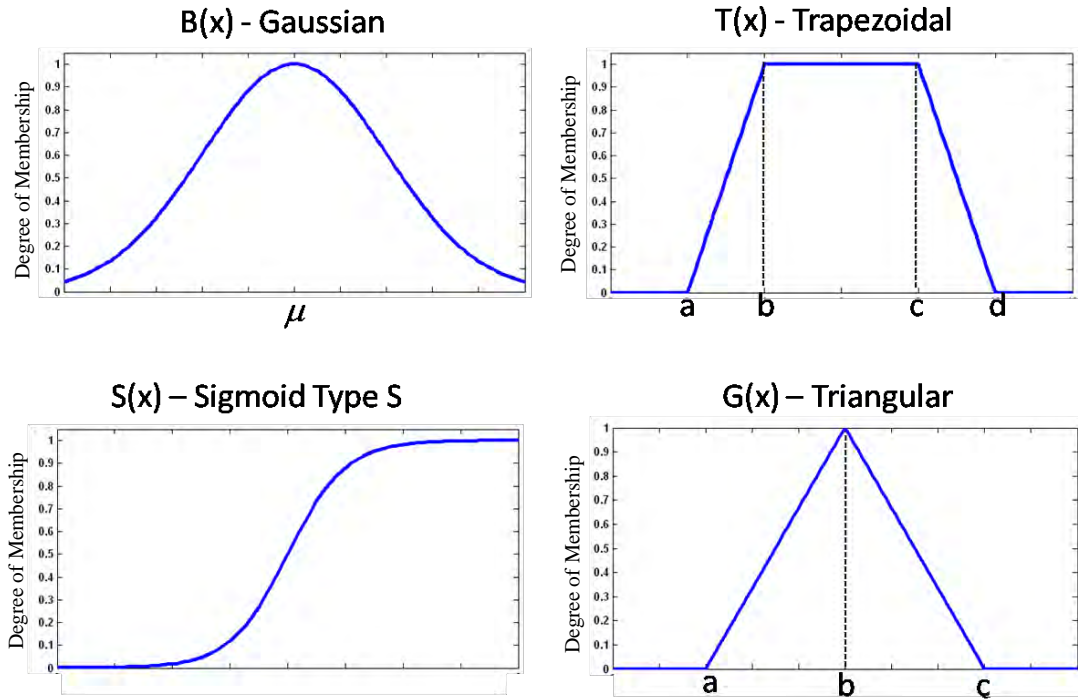


Figure 10: Different types of membership functions

2.3.2 Linear Mixing Model

Linear Mixing Model (LMM) (Keshava and Mustard 2002)(Keshava 2003)(Adams 2006) is the simplest model and most widely used to conduct spectral unmixing. Unmixing is the process of decomposing the measured spectrum of a pixel into a collection of constituent spectra or endmembers, and a set of corresponding fractions or abundances, that indicate the proportion of each endmembers in a pixel. Endmembers are spectra but normally corresponds to objects or classes in the scene such as water, urban, vegetation, etc (Foody and Cox 1994). As we know, when incident solar radiation strikes the surface it can intimate with materials that produce multiple bounces like soil, which is a mixture of inorganic minerals and organic matter. In those cases, a nonlinear spectral mixing approach would produce better results than linear mixing approach.

Accordingly with LMM (Keshava and Mustard 2002), the measured radiance of a pixel is a linear combination of the individual spectra presents in the scene weighted by fractional area coverage, known as abundances. LMM can be expressed as follow:

$$x = a_1s_1 + a_2s_2 + \dots + a_cs_c + w \tag{9}$$

$$\mathbf{x} = \sum_{i=1}^C a_i \mathbf{s}_i + \mathbf{w} = \mathbf{S}\mathbf{a} + \mathbf{w}$$

where \mathbf{x} corresponds to the observed pixel, \mathbf{S} is $N \times C$ matrix of endmembers or materials in the scene, \mathbf{a} is a $C \times 1$ fractional abundance vector, and \mathbf{w} is the $N \times 1$ additive noise vector. C is the number of endmembers and N is the number of pixels in the image. The LMM has to satisfy the following two constraints:

$$a_i \geq 0, \quad i = 1, 2, \dots, C \quad \text{and} \quad \sum_{i=1}^C a_i = 1$$

For hyperspectral or multispectral image, Equation 9 can be written in matrix form as follows

$$\mathbf{X} = \mathbf{S}\mathbf{A} + \mathbf{W} \tag{10}$$

where $\mathbf{X} = [\mathbf{x}_1, \mathbf{x}_2, \dots, \mathbf{x}_N]$, $\mathbf{S} = [\mathbf{s}_1, \mathbf{s}_2, \dots, \mathbf{s}_C]$, $\mathbf{A} = [\mathbf{a}_1, \mathbf{a}_2, \dots, \mathbf{a}_N]$, $\mathbf{W} = [\mathbf{w}_1, \mathbf{w}_2, \dots, \mathbf{w}_N]$, N is the number of pixels, and C the number of endmembers. If the endmember matrix, \mathbf{S} , is known, the unmixing problems reduces to the abundance estimation problem.

Figure 11 shows a conceptual diagram of spectral unmixing in order to determine the appropriate numbers of endmembers and estimate weights. The first step consists of applying an algorithm to reduce the data dimensionality. This is an optional step but it is useful to eliminate redundant data and reduce the computational load to subsequent steps. Principal Component Analysis (PCA) (Schowengerdt 2007) and Maximum Noise Fraction (MNF) (Schowengerdt 2007) are two widely used methods to reduce hyperspectral data. Next, endmember determination consists of finding out which are the distinct spectra that constitute the mixed pixel in the scene. Theoretically (Keshava and Mustard 2002) the limit of endmembers in a scene is equal to the number of bands plus one, $C \leq M + 1$ (where C are the endmembers and M the number of bands) but in practice the number of endmembers ranges from three to seven depending of the number of bands and spectral variability of scene components (Plaza et al., 2004). For supervised soft classification (Foody and Cox 1994), the endmember determination consists of finding out nearly pure pixels from the image itself which are representative of information classes. We

can compute the root mean square (RMS) error to evaluate the selection of endmembers (Keshava 2003)(Keshava and Mustard 2002) .

$$RMS = \left[\frac{1}{M} \sum_{k=1}^M w_k^2 \right]^{1/2} \quad (11)$$

where M is the number of bands, and w_k is the estimation residual. When we have chosen constituent spectra appropriately, the value of the RMS error will be small. Conversely, if we obtain a high RMS value, a different set of endmember spectra is needed for the mixing model. The next stage in the LMM subpixel classification process is the inversion phase which consists in the estimation of weights or fractional abundances of each pixel from its measured spectrum and endmember spectra. The abundance estimation (Keshava and Mustard 2002) can be view as a distance minimization problem, where the distance between measured spectral and its estimate is minimized as follows:

$$\hat{a} = \arg \min_a D(x, Sa) \quad (12)$$

$$\text{Subject to } a \geq 0 \text{ and } \sum_{i=1}^C a_i = 1 \text{ or } \sum_{i=1}^C a_i \leq 1$$

where $D(x, Sa)$ is a distance function, x is the observed pixel, S is the endmember matrix, and a is the fractional abundance vector. The most common distance function used in literature is the least square (LS) (Keshava and Mustard 2002) :

$$LS(x, Sa) = \|Sa - x\|_2^2 \quad (13)$$

There are software applications such as N-FINDR⁴ (Winter 1999) (Winter 2004), ENVI/IDL® (ITT Visual Information Solutions 2007), and others to use for endmember determination and fractional abundance estimation. N-FINDR (Winter 1999)(Winter 2004) is a widely used algorithm to find, in an automated way, the purest pixels in the image, which corresponds to the endmembers in a particular scene without apriori information.

⁴ N-FINDR is software which provides an automated endmember determination and spectral unmixing [33].

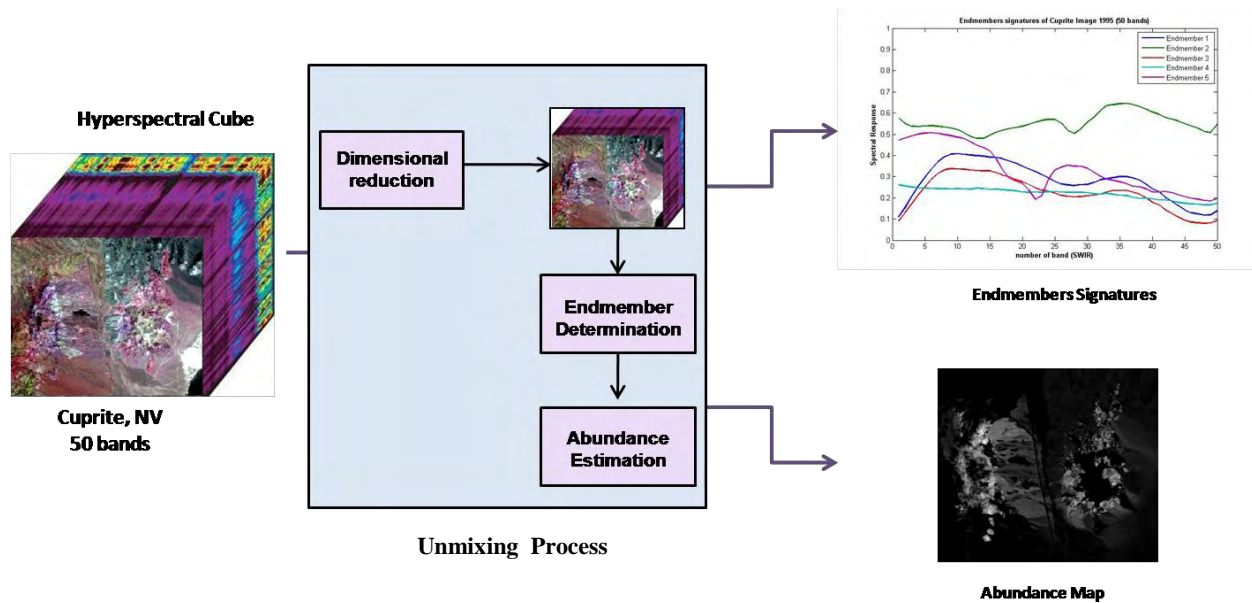


Figure 11: Conceptual diagram of spectral unmixing [Adapted from (Keshava and Mustard 2002)]

2.3.3 Evaluation of Soft Classifiers Performance

Accuracy assessment is a critical component of any image classification process to provide a quantitative measure of classifier performance. The confusion or contingency matrix (Landgrebe 2003) shown in Figure 12 is used as a common assessment method to evaluate conventional hard classifiers. Testing samples selected for the assessment are summarized in the form of a contingency table. The rows in the matrix list the classes and indicate how the pixels labeled for each class were assigned by the classifier. For an ideal classification, the matrix will only have values on the diagonal and off-diagonal values will be zero. Off-diagonal elements represent errors by omission or commission in the confusion matrix methodology. Omission errors refer to pixels that belong to a particular class and were erroneously assigned to other informational class. Conversely, the commission errors refer to pixels which not belong to a particular class and were erroneously assigned to it. The “Producer’s Accuracy” which is equal to 100% minus the percent of omission error can be found along the right side of the matrix in Figure 12. On the other hand, the “User’s Accuracy” or “Reliability Accuracy” which is equal to 100% minus the percent of commission error can be found along the bottom of the matrix in Figure 12. The Overall Accuracy, which is calculated by the sum of the samples on the diagonal (pixels correctly classified) divided by the total of samples, could be a simple way to assessing the classification output with a single number.

		Predicted Class				Producer's Accuracy	
		C ₁	C ₂	...	C _m		
Actual Class	Number of Samples						
	C ₁	n _{c1}	n _{c1c1}	n _{c1c2}	...	n _{c1c4}	%n _{c1}
	C ₂	n _{c2}	n _{c2c1}	n _{c2c2}	...	n _{c2c4}	%n _{c2}

	C _m	n _{c4}	n _{cmc1}	n _{cmc2}	...	n _{cmcm}	%n _{cm}
TOTAL	$\sum_{i=1}^m n_{c_i}$	$\sum_{i=1}^m n_{c_i c_1}$	$\sum_{i=1}^m n_{c_i c_2}$...	$\sum_{i=1}^m n_{c_i c_m}$	$\sum_{i=1}^m n_{c_i c_i}$	
User's Accuracy or Reliability Accuracy		%n _{c1}	%n _{c2}	...	%n _{cm}		

m=number of classes

k= class for which is calculated the user's or producer's accuracy

$$\text{User's Accuracy } (\%n_{c_k}) = \frac{n_{kk}}{\sum_{i=1}^m n_{c_i c_k}} \times 100\%$$

$$\text{Overall Accuracy} = \frac{\sum_{i=1}^m n_{c_i c_i}}{\sum_{i=1}^m n_{c_i}} \times 100\%$$

$$\text{Producer's Accuracy } (\%n_{c_k}) = \frac{n_{kk}}{n_k} \times 100\%$$

Figure 12: Layout of a confusion error matrix and computation of user's and producer's accuracy (Landgrebe 2003)

The confusion matrix is not the best way to evaluate the performance of soft classifiers because it assumes that classes are mutually exclusive and each observation belongs to a single class. However, many researchers evaluate the thematic map produced by a hardening or defuzzification process using a hard classifier assessment such as confusion error matrix. Other research works propose the use of entropy (Foody 1995)(Foody 1996)(Van Der Meer and Jong 2006) to show how is the strength of class memberships, a Euclidean Distance (Foody 1996) to estimate the separation of two data sets based on the proportion of each class in the pixel, and/or the fuzzy error matrix, which is an extension of the confusion matrix using the principles of fuzzy set theory (Binaghi et al., 1999) (Binaghi 2001)(Foody 2002)(Lu and Weng 2007)(Varshney and Arora 2004). All those approaches are discussed next.

2.3.3.1 Degree of Mixing

The accuracy assessment of soft classification is really difficult because involve the use of a soft reference data as Ground Truth which in many cases is not available. The scene complexity also affects the performance of soft classifiers. Entropy (Foody 1995)(Foody 1996)(Van Der Meer and Jong 2006), and Euclidean Distance (Foody 1996) are described next to describe how strong is the partition of membership.

2.3.3.1.1 Entropy

Entropy is a measure of information and uncertainty widely used in information theory and communications and it is defined as follows (Haykin, 2001, p.568).

"Suppose that a probabilistic experiment involves the observation of the output emitted by a discrete source during every unit of time (signaling interval). The source output is modeled as a discrete random variable, S

$$S = \{s_0, s_1, \dots, s_{K-1}\} \quad (14)$$

with probabilities

$$P(S = s_k) = p_k \quad k = 0, 1, \dots, K - 1$$

We assume that the symbols emitted by the source are statistically independent. This is called a discrete memoryless source, memoryless in terms that the symbol emitted in any time is independent of the previous choices.

We define the amount of information gained after observing the event $S = s_k$, which occurs with probability p_k , as the logarithmic function,

$$\begin{aligned} I(s_k) &= \log\left(\frac{1}{p_k}\right) \\ &= -\log(p_k) \quad \text{for } k = 0, 1, \dots, K - 1 \end{aligned} \quad (15)$$

The amount of information $I(s_k)$ produced by the source during an arbitrary signaling interval depends on the symbol s_k emitted by the source at that time. Certainly, $I(s_k)$ is a discrete random variable that takes on the values $I(s_0), I(s_1), \dots, I(s_{k-1})$ with

probabilities p_0, p_1, \dots, p_{k-1} respectively. The mean of $I(s_k)$ over the source S is given by

$$\begin{aligned}
 H(S) &= E[I(s_k)] & (16) \\
 &= \sum_{k=0}^{K-1} p_k I(s_k) \\
 &= \sum_{k=0}^{K-1} p_k \log\left(\frac{1}{p_k}\right) = -\sum_{k=0}^{K-1} p_k \log(p_k)
 \end{aligned}$$

$H(S)$ is called the entropy of a discrete memoryless source with source S . $H(S)$ is a measure of the average information content per source symbol". (Haykin 2001, p.568-569)

The degrees of membership produced by soft classifiers are not probabilities but are numbers in a range from 0 to 1. We found in the literature that previous works has been trying to related it with entropy concept as a measure of the degree of mixing in a particular scene (Van Der Meer and Jong 2006)(Foody 1996)(Foody 1995). It could be useful when soft ground truth data is not available. The entropy of a pixel in a particular scene is given by

$$H(X) = -\sum_{i=1}^m x(i) \log x(i) \quad (17)$$

where $x(i)$ refers to the degree of membership derived by a soft classifier associated with class i and m is the number of informational classes in a scene.

Entropy is maximized when the membership space is partitioned evenly between informational classes (mixed pixels) and minimized when is allocate to one specific class (pure pixels). An entropy image can be useful to show the degree of softness of the classification output. It would expect that highly mixed pixels in the scene have high entropy values (Foody 1996) (Foody 1995). Figure⁵ 13 shows an instance of a synthetic image generated using a gradual mixture of two endmembers which began as pure pixels in the corner and continue to reach a mixture of 50% of proportion coverage of the pixel in the center. Entropy (17) was computed for this instance and as can be seen in Figure 13b, entropy is higher when mixed pixel is present and lower when pure or almost pure pixel is present.

⁵ Axes of images (figures) in whole document correspond to discrete spatial coordinates.

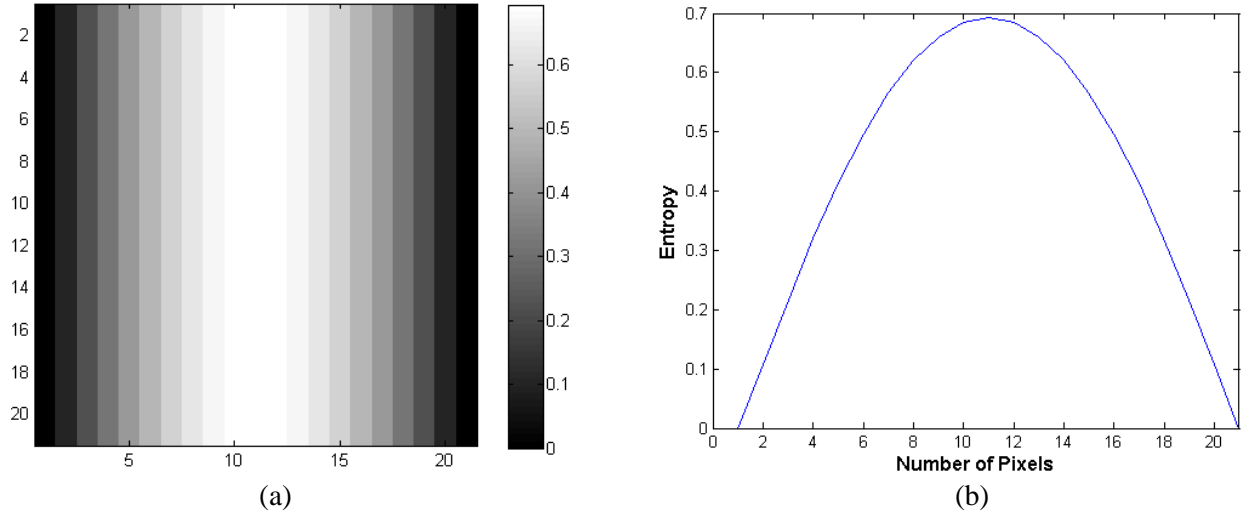


Figure 13: (a) Entropy image generated by a mixture of two endmembers (corners were comprised by pure pixels and 50% of mixture can be appreciated at the center) (b) Entropy values for along-track transect

2.3.3.1.2 *Euclidean Distance*

One approach to evaluate the performance of a soft classifier when soft ground truth data is available is to measure the distance between the degree of membership obtained by a soft classification and the soft reference ground truth. There are several ways to determine this distance where Euclidean Distance (ED) (Foody 1996) a simple way to do this. ED can estimates the separation of two data sets (soft classification and soft reference data) based on the proportion coverage associate to each class in the pixel. Lower values of ED can be interpreted as an accurate estimate of degree of membership for all defined informational classes. The ED derived for each pixel can be expressed as follow,

$$D_{ED}(X) = \frac{1}{m} \sqrt{\left(\sum_{i=1}^m (y(i) - x(i))^2 \right)} \quad (18)$$

where $y(i)$ refers to the proportion coverage of class i into the soft ground truth data data, $x(i)$ is the degree of membership derived by a soft classification for class i , and m is the number of informational classes. Figure 14 shows the LMM membership maps obtained using a synthetic image without adding noise (Masalmah and Vélez-Reyes 2007) provided by Ronald Lockwood from AFRL. The spectral responses

shown in Figure 14 were used to mix along the diagonals with different fraction values based on its position with respect to the cube corners (pure spectra). Equation 18 (Euclidean Distance) was computed for the synthetic image shown in Figure 14 obtaining an average distance value of 0.00021. The minimum ED value was 0 and the maximum ED value for this image was 0.0013. This lower average ED value (0.00021) can be interpreted as an accurate degree of membership obtained from a soft classification for this image shown in Figure 14. As can be seen in Figure 14, the LMM membership values have a good correlation with true abundance maps.

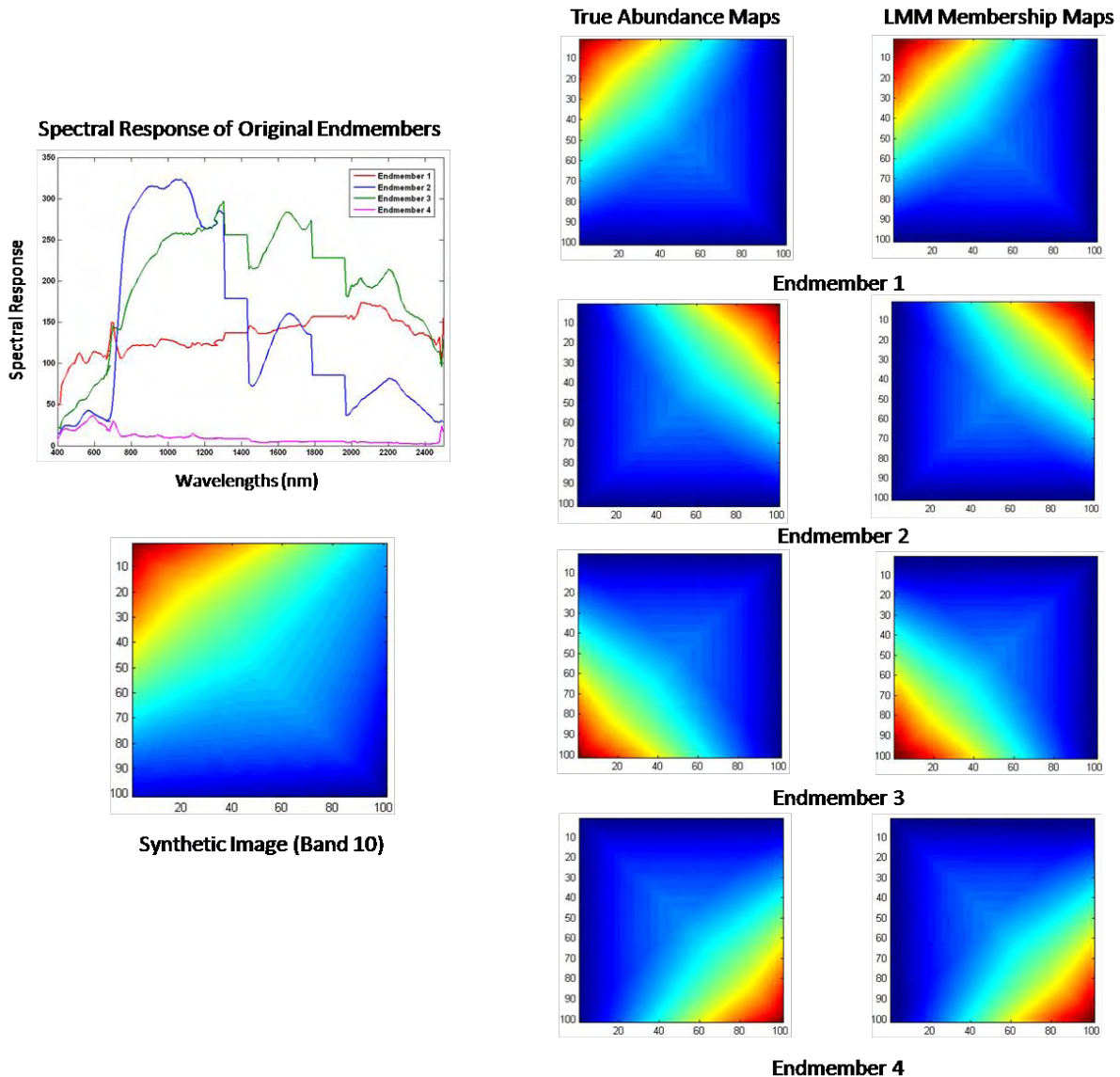


Figure 14: Synthetic image, true abundance maps (soft ground truth data), and LMM membership maps. Synthetic Image courtesy of Dr. Ronald Lockwood and Lt. Angela Puetz from AFRL

2.3.3.2 Fuzzy Error Matrix

Fuzzy error matrix (Binaghi et al., 1999) (Binaghi 2001) which is an extension of the confusion error matrix using the principles of fuzzy set theory could be a better alternative to assess the performance of soft classifiers when soft ground truth data is available. The reliability of soft reference data is essential to avoid under or over estimation of accuracy assessment.

Table 2 shows a three class one pixel instance of the fuzzy error matrix for the cases of perfect matching, underestimation, and overestimation between soft ground truth data and degree of membership derived by soft classification. Let R_i and C_i be the soft ground truth data and soft classification output for class i , respectively. R_i and C_i can be considered a fuzzy sets in the soft classification context having a membership function as follow

$$x_{R_i}: Y \rightarrow [0,1] \quad (19)$$

$$x_{C_i}: Y \rightarrow [0,1]$$

where $[0,1]$ denotes the interval of real numbers from 0 to 1. $x_{R_i}(y)$ and $x_{C_i}(y)$ are the degree of memberships of the sample element y in class i for the soft ground truth data and classification data. The fuzzy error matrix diagonal and off-diagonal values are determined using *min operator*

$$x_{C_i} \cap x_{R_i}(x) = \min(x_{C_i}(x), x_{R_i}(x)) \quad (20)$$

The “Total Grades” row at the bottom of the matrix corresponds to the sum of the soft ground truth data for each informational class samples available (see Table 1-2). On the other hand, “Total Grades” column at the right side of the matrix corresponds to the sum of the degree of membership for each informational class samples available (see Table 1-2). Similar to confusion error matrix method, we can obtain the “Producer’s Accuracy” related to omission errors, and the “User Accuracy’s” related to errors of commission with computation of fuzzy error matrix. Overall Accuracy can be interpreted as a measure of the total match between soft ground truth data and soft classification output and could be a simple way to assess soft classifier in a single number. Accurate soft ground truth data is not available in much of the cases; as a result computation of fuzzy error matrix is not possible with a hard ground truth data where each pixel is allocated to one specific class. For that reason some researchers used hard thematic map produced by a hardening process (defuzzyfication) to compute the confusion error matrix.

This approach does not allow partial membership resulting in a loss of information and errors in accuracy estimation.

Table 1 shows the Fuzzy Error Matrix derived from the LMM membership values (soft classification outputs (C)) and True Abundances (soft ground truth data (R)) for the testing samples shown in Figure 15 of the synthetic image example shown in Figure 14 (Masalmah and Vélez-Reyes 2007). As can be seen, the overall accuracy of the fuzzy error matrix for this example is 98%. In addition, the Producer's and User's Accuracy for all classes are above 97%. Accordingly with the fuzzy error matrix analysis, this result can be interpreted as an accurate estimation of degree of memberships in terms of the soft ground truth data.

Table 1: Fuzzy Error Matrix derived from LMM membership values (C) and True Abundances (R) of synthetic image shown in Figure 14

	$R_{\text{Endmember1}}$	$R_{\text{Endmember2}}$	$R_{\text{Endmember3}}$	$R_{\text{Endmember4}}$	Total grades (C)	User's Accuracy
$C_{\text{Endmember1}}$	504.0955	334.3208	342.2735	259.9587	512.6795	98.33%
$C_{\text{Endmember2}}$	330.4055	460.3736	262.6564	310.9814	466.6507	98.65%
$C_{\text{Endmember3}}$	342.0213	263.8119	467.8989	316.1223	476.1373	98.27%
$C_{\text{Endmember4}}$	262.1251	315.1205	320.2766	443.0229	454.5996	97.45%
Total grades (R)	512.6418	472.7633	476.3437	448.251		
Producer's Accuracy	98.33%	97.38%	98.23%	98.83%		
Overall Accuracy	98.19%					

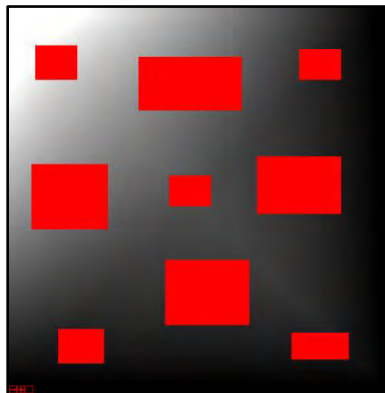


Figure 15: Testing samples (red rectangles) used to compute the Fuzzy Error Matrix of the synthetic image shown in Figure 14

Table 2: Three classes – one pixel instance of the fuzzy error matrix for three possible cases: (a) perfect matching, (b) underestimation, and (c) overestimation (Binaghi et al., 1999) (Binaghi 2001)

(a) Fuzzy Error Matrix - Perfect Matching (1 pixel instance)

	R ₁	R ₂	R ₃	Total grades	User's Accuracy	Soft Reference Data	Degree of Membership	
C ₁	0.5	0.5	0.5	0.5	100%	x _{R1} (y)=0.5	x _{C1} (y)=0.5	
C ₂	0.5	0.5	0.5					
C ₃	0.5	0.5	0.5					
Total grades	0.5	0.5	0.5				x _{R2} (y)=0.5	x _{C2} (y)=0.5
Producer's Accuracy	100%	100%	100%				x _{R3} (y)=0.5	x _{C3} (y)=0.5
Overall Accuracy	100%							

(b) Fuzzy Error Matrix - Underestimation (1 pixel instance)

	R ₁	R ₂	R ₃	Total grades	User's Accuracy	Soft Reference Data	Degree of Membership	
C ₁	0.4	0.4	0.4	0.4	100%	x _{R1} (y)=0.5	x _{C1} (y)=0.4	
C ₂	0.5	0.5	0.5					
C ₃	0.3	0.3	0.3					
Total grades	0.5	0.5	0.5				x _{R2} (y)=0.5	x _{C2} (y)=0.5
Producer's Accuracy	80%	100%	60%				x _{R3} (y)=0.5	x _{C3} (y)=0.3
Overall Accuracy	80%							

(c) Fuzzy Error Matrix - Overestimation (1 pixel instance)

	R ₁	R ₂	R ₃	Total grades	User's Accuracy	Soft Reference Data	Degree of Membership	
C ₁	0.5	0.5	0.5	0.7	71%	x _{R1} (y)=0.5	x _{C1} (y)=0.7	
C ₂	0.5	0.5	0.5					
C ₃	0.5	0.5	0.5					
Total grades	0.5	0.5	0.5				x _{R2} (y)=0.5	x _{C2} (y)=0.5
Producer's Accuracy	100%	100%	100%				x _{R3} (y)=0.5	x _{C3} (y)=0.6
Overall Accuracy	100%							

2.3.3.3 Correlation Coefficients

Many researchers measure the linear relation among soft reference data and degree of membership derived by a soft classifier using calculation of correlation coefficient (ρ_{XY}) which is defined as follow,

$$\rho_{XY} = \frac{\sigma_{XY}}{\sigma_X \sigma_Y} \quad (21)$$

where σ_{XY} is the covariance between two datasets (soft ground truth data and soft classification output) and σ_X and σ_Y are standard deviation of each dataset, respectively (Foody 1996). Figure 16 shows a scatter plot between degree of membership ($x(i)$) derived by a LMM soft classifier and soft ground truth data ($y(i)$) of synthetic image example shown in Figure 14.

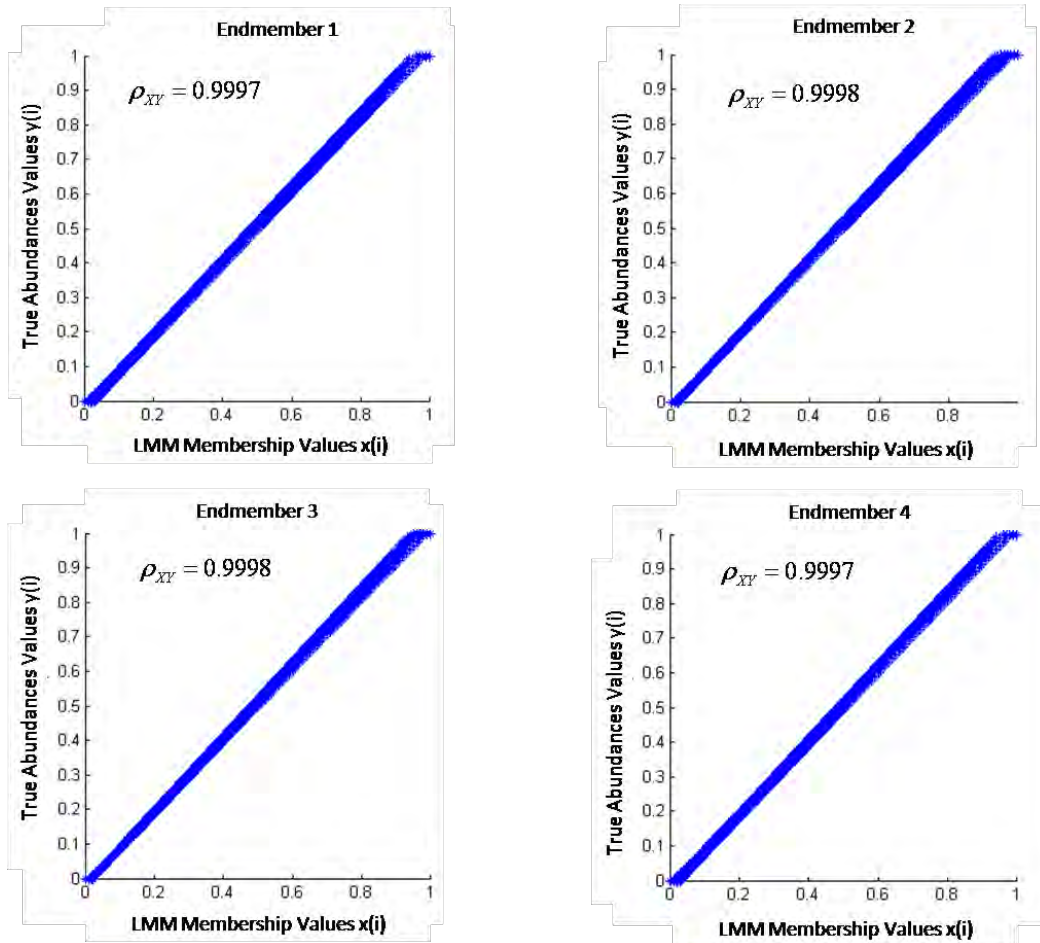


Figure 16: Scatterplot of soft reference data ($y(i)$) and estimated degree of membership values ($x(i)$) of synthetic image example shown in Figure14

2.4 Existing Remote Sensing and Image Processing Tools

There are commercial and non-commercial image processing and remote sensing software such as ENVI®(ITT Visual Information Solutions 2007), Multispec©(Biehl and Landgrebe 2002)(Landgrebe and Biehl 1994-2008), HIAT (Arzuaga-Cruz et al., 2004)(Rosario-Torres, Arzuaga-Cruz and Vélez-Reyes 2005), and others which provide valuable tools to image analysts. ENVI® (ITT Visual Information Solutions 2007) is user-friendly commercial software to extract information from geospatial imagery developed by ITT Visual Information Solutions, which provides code extensibility through Interactive Data Language (IDL). Multispec© (Landgrebe and Biehl 1994-2008) (Biehl and Landgrebe 2002) developed by Dr. Landgrebe and the Remote Sensing research group in Purdue's Laboratory for Applied Remote Sensing (LARS) is the most known non-commercial tool used for hard image classification of multi/hyperspectral images. The Hyperspectral Image Analysis Tool (HIAT) (Arzuaga-Cruz et al., 2004) (Rosario-Torres et al., 2005) is a MATLAB® toolbox developed by the UPRM researchers at the Laboratory for Applied Remote Sensing and Image Processing (LARSIP) over the past 10 years. HIAT provides functions to analyze multi/hyperspectral images in terms of hard classification, supervised and unsupervised spectral unmixing, feature extraction/band selection and other functionalities. The proposed Spectral Soft Classification Tool (SSCT) it will be incorporated to the HIAT.

We found in the literature non-commercial tools such as PARBAT (Lucieer 2004) and VTBeans⁶ (Bastin, Fisher and Wood 2002) which were primarily developed to deal with the problem of visualize uncertainty of results obtained from soft classification of remote sensed imagery. However, we found that existing remote sensing tools do not provide capability for soft classification of HSI, visualization tools, and accuracy assessment as an end to end classification system. The proposed SSCT developed as part of this research intend to group many efforts of researchers in the area of Soft Classification integrating soft-classification methodologies based on linear mixing model and fuzzy logic, visualizations tools, and accuracy assessment to evaluate the performance of soft classifiers.

⁶ VTBeans toolkit is not available to download at the website mentioned in (Bastin, Fisher and Wood 2002). Accessed June 2008. For that reason, it was not possible to use and explore the VTBeans tool.

2.5 Summary

This chapter presented background and literature review about conventional and soft classification techniques. The accuracy assessment for both hard and soft classification was also introduced. In addition, the challenge to extract and process data from current and proposed satellite sensors was discussed and how it affects the performance of conventional hard classifiers.

CHAPTER 3

Supervised Soft-Classification Algorithms

This chapter presents the soft-classification algorithms used in the Spectral Soft Classification Tool (SSCT). The algorithms were based on Supervised Fuzzy Logic algorithms and Linear Mixing Model such as Supervised Fuzzy C-Means (SFCM) (Zhang and Foody 2001) (Bezdek et al., 1984), Fuzzy Supervised Classification System (FSCS)(Melgani et al., 2000), Fuzzy Maximum Likelihood (FML) (Wang 1990), and Linear Mixing Model (LMM)(Keshava and Mustard 2002) (Keshava and Mustard 2002)(Rosario-Torres 2004).

3.1 Supervised Soft Classification

Figure 17 shows a block diagram of the soft classification scheme for multi/hyperspectral data. The best known soft-classification algorithms found in literature are based in fuzzy sets theory such as FML, and FCM or SFCM (supervised version of Fuzzy C-Means). FML and FCM are an extension of Maximum Likelihood and C-Means hard classification algorithms respectively. In addition, there are a variety of soft classifiers based in fuzzy rules such as SFCS. Soft classifiers are basically comprised of three steps: (1) *softening process* (fuzzyfication) which involves the division of the feature space into fuzzy subspaces specified by a membership function either Gaussian, Triangular, or Trapezoidal (the most commonly used), (2) *inference step* (classification) which apply fuzzy rules to data and calculate the strength or membership proportions of each land cover type per pixel, and, finally, (3) a *hardening process* (defuzzyfication) which produces a hard outcome in the form of a single thematic map (Tso and Mather 2001).

The softening process divides the spectral space into fuzzy subspaces and generates fuzzy rules for each fuzzy subspace. The degree of membership for each input pixel is calculated using membership functions (see Section 2.3.1). The selection of a membership function and the width of each subspace are case dependent (Tso and Mather 2001). For instance, FSCS uses a Gaussian membership function to obtain the degree of membership but they introduce a modulated Gaussian distribution for the case of classes that have a large extent where it is difficult to decide the degree of membership by spectral regions

overlapping (Melgani et al., 2000). A pixel that fall within the overlap regions of membership functions necessitates the uses of fuzzy rules. Hence, a final solution requires the use of inference and defuzzyfication stages.

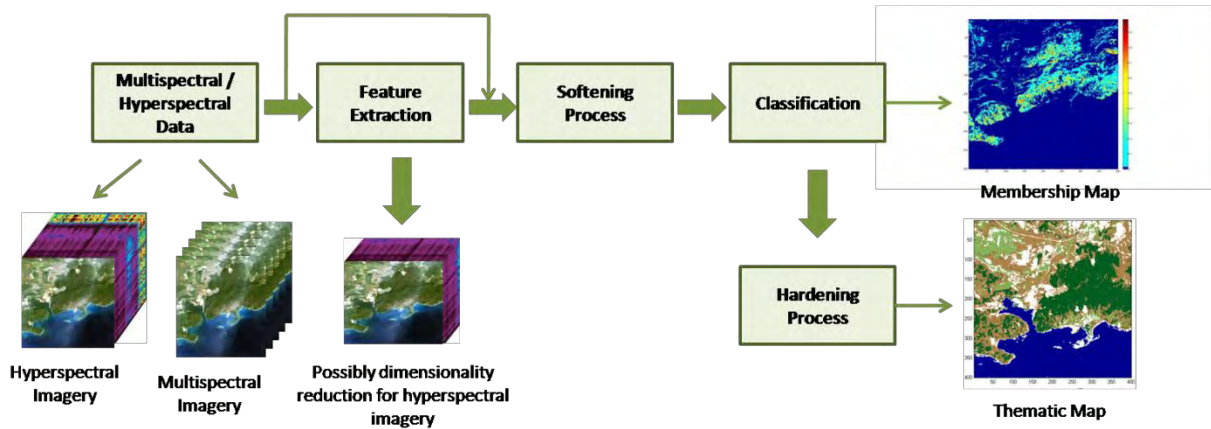


Figure 17: A general soft classification scheme for multi/hyperspectral imagery

The inference stage computes the degree of membership contributed by fuzzy rules and generates the fraction maps for each pre-defined informational class where each pixel value corresponds to the weight value of that class associated to the pixel. Finally, a defuzzyfication process is performed to convert fuzzy outputs into crisp values. Centroid and Maximum are two commonly techniques used for it (Tso and Mather 2001). The Centroid method calculates the crisp values finding the center of gravity of the membership function. On the other hand, in the maximum method, the crisp value is chosen as the value where each fuzzy subset has its maximum degree of membership (“truth value”). In image classification, the hardening process is performed to produce a single thematic map which sometimes can be preferred by image analysts instead of the fraction maps.

FSCS (Melgani et al., 2000), FML(Wang 1990), SFCM with Mahalanobis and Euclidean norms (Bezdek et al., 1984) (Zhang and Foody 2001), and ML (Duda et al., 2001) are discussed next. All these algorithms are implemented in a supervised mode which requires prior knowledge by the image analyst in order to determine the best representation of land cover types in the scene as informational classes. Supervised algorithms require an adequate selection of training data which, in some way, could result in good or poor performance of the classifier. The training data can be soft or non-soft which is the case of FML, and SFCS, respectively.

3.1.1 Fuzzy Supervised Classification System (FSCS)

(Melgani et al., 2000) proposed an explicit fuzzy supervised classification system using statistical values comprised of three step: (1) fuzzyfication process where each pixel per band is transformed into a matrix of membership degrees corresponding to the fuzzy inputs of the process using a Gaussian membership function, (2) fuzzy classification using a MIN reasoning rule to deduce fuzzy outputs, and finally, (3) a defuzzyfication process to generate a single thematic map which can be used to conduct a conventional hard accuracy assessment when soft ground truth data is not available. One of the advantages of the proposed method of (Melgani et al., 2000) is its simplicity and flexibility in terms of inserting and removing bands without further changing modules of the classifier. Figure 18 shows a block diagram describing the FSCS method proposed by (Melgani et al., 2000). Each module of FSCS (Melgani et al., 2000) is explained next.

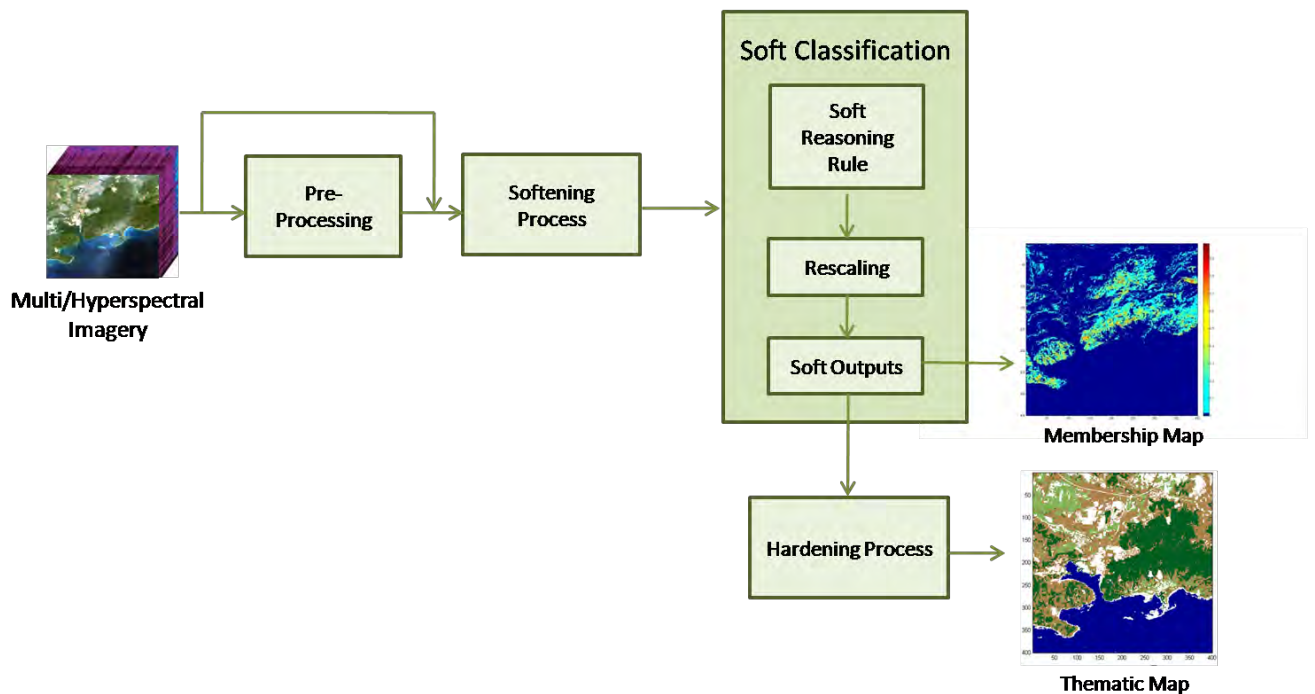


Figure 18: Block diagram of Fuzzy Supervised Classification System (FSCS) methodology (Melgani et al., 2000)

3.1.1.1 Softening or Fuzzyfication Process

After the selection of training samples, a softening process is performed in order to transform each pixel per band into a matrix of membership degrees representing the soft inputs of the process. Bands and land cover classes are represented by fuzzy sets and fuzzy subsets, respectively. Each fuzzy subset (*class j*), in a given fuzzy set (*band i*), is defined by a Gaussian function, $f_{i,j}(x_i)$. The vector pixel \mathbf{Y} in the N-dimensional space is defined by

$$\mathbf{Y} = [x_1, x_2, \dots, x_i, \dots, x_N]^T \quad (22)$$

The membership function of *class j* in *band i* is defined by

$$f_{i,j}(x_i) = \exp\left(-\frac{(x_i - \mu_{i,j})^2}{2\sigma_{i,j}^2}\right) \quad (23)$$

where $\mu_{i,j}$ and $\sigma_{i,j}$ are the mean and standard deviation values of class *j* in band *i*, respectively.

The mean μ_j is the point without any uncertainty about its membership degree and the standard deviation, σ_j , indicates the width of a fuzzy subset (*class j*). FSCS (Melgani et al., 2000) approach introduces a modulated Gaussian distribution if a priori knowledge of class extent is available. The modulation factor calculation takes into consideration the number of pixels in the histogram which corresponds to class mean in order to avoid the problem of the a priori knowledge of class extent. The modulation principle is useful over large extent classes where membership degree decision is difficult because of spectral regions overlapping (Melgani et al., 2000).

The modulated standard deviation can be calculated as follow (Melgani et al., 2000):

$$\sigma_{i,j}^* = \alpha_{i,j}\sigma_{i,j} \quad (24)$$

where $\sigma_{i,j}$ is the standard deviation of class *j* in band *i* and $\alpha_{i,j}$ is the modulation factor.

The modulation factor can be calculated as follows (Melgani et al., 2000):

$$\alpha_{i,j} = \log(CE_{i,j} + \beta_o) \quad (25)$$

where $CE_{i,j}$ is the extent of class j in band i . β_o is a constant (Melgani et al., 2000) defined by empirical observation as the value which satisfies the condition of not reinforce strong classes or weaken the weak classes. The $CE_{i,j}$ can be calculated as follow by inspection the histogram to find out the number of pixels which corresponds to mean of class j , defined as $H_{i,j}$ (Melgani et al., 2000)

$$CE_{i,j} = \frac{H_{i,j}}{\sum_{k=1}^M H_{i,k}} \quad (26)$$

where M is the number of classes.

As a result, we get a $N \times M$ soft input matrix, \mathbf{S} , where N and M are the number of bands and classes, respectively. For a pixel \mathbf{Y} , the soft input matrix can be written as follow:

$$\mathbf{S} = \begin{bmatrix} f_{1,1}(x_1) & f_{1,2}(x_1) & \dots & f_{1,M}(x_1) \\ f_{2,1}(x_2) & f_{2,2}(x_2) & \dots & f_{2,M}(x_2) \\ \dots & \dots & \dots & \dots \\ f_{N,1}(x_N) & f_{N,2}(x_N) & \dots & f_{N,M}(x_N) \end{bmatrix} \quad (27)$$

3.1.1.2 Soft Classification

Soft classification (Melgani et al., 2000) consists of analyzing the soft input matrix, \mathbf{S} , using a MIN reasoning rule which finds out the minimum degree of membership provided by different fuzzy sets (bands) for each fuzzy subset (class) per pixel. As a result, we get a primitive fuzzy output vector defined as follows (Melgani et al., 2000):

$$\mathbf{F}' = [F'_1(Y), F'_2(Y), \dots, F'_j(Y), \dots, F'_M(Y)]^T \quad (28)$$

where M is the number of fuzzy subsets (classes) and $F'_j(Y) = \text{Min}(f_{i,j}(x_N)) \quad i=1,2,\dots,N$.

After the MIN reasoning rule was applied to \mathbf{S} , a rescaling operation was performed in order to normalize the class proportion per pixel deduced from different fuzzy sets. The soft output vector \mathbf{F} can be expressed as follows (Melgani et al., 2000):

$$\mathbf{F} = [F_1(Y), F_2(Y), \dots, F_j(Y), \dots, F_M(Y)]^T \quad (29)$$

where

$$(30)$$

$$F_j(Y) = \frac{F'_j(Y)}{\sum_{k=1}^M F'_k(Y)}$$

The soft-classification step produces the membership maps for each class taking into consideration the degree of membership of each pixel per class.

3.1.1.3 Hardening or Defuzzyfication Process

A hardening process is performed using a MAX rule to convert the soft outputs into crisp outputs in order to generate a single classification map assigning each pixel to the class with a higher degree of membership (Melgani et al., 2000). For instance, pixel Y is assigned to class j if

$$\forall t \in 1,2,3 \dots, M \text{ and } t \neq j, \quad F_j(Y) \geq F_t(Y) \quad (31)$$

3.1.2 Fuzzy Maximum Likelihood (FML)

A supervised fuzzy-classification system based on statistical parameters known as Fuzzy Maximum Likelihood (FML) classifier was proposed by (Wang 1990). The method consists basically in the following steps: (1) estimate the fuzzy mean and fuzzy covariance matrix from training data which should be a representation of data softness, (2) estimate the membership values associated to each land cover type per pixel, and (c) finally a defuzzyfication process is performed in order to generate a single thematic map.

The soft representation of a geographical area is a form of representing the feature space into the fuzzy partition where partial membership of pixels in more than one class is allowed. A fuzzy partition of the feature space is represented by fuzzy sets (informational classes) on the universe X such that

$$\begin{aligned} \forall x \in X \\ 0 \leq f_j(x) \leq 1 \\ \sum_{x \in X} f_j(x) > 0 \end{aligned} \quad (32)$$

$$\sum_{j=1}^M f_j(x) = 1$$

where $f_j(x)$ is the membership function of fuzzy set j (class j), M is the number of informational classes, X is the whole pixels, and x are pixels (Wang 1990). The $M \times B$ fuzzy partition matrix, \mathbf{F} , can be written as follows (Wang 1990):

$$\mathbf{F} = \begin{bmatrix} f_1(x_1) & f_1(x_2) & \dots & f_1(x_B) \\ f_2(x_1) & f_2(x_2) & \dots & f_2(x_B) \\ \dots & \dots & \dots & \dots \\ f_M(x_1) & f_M(x_2) & \dots & f_M(x_B) \end{bmatrix} \quad (33)$$

where M and B are the number of classes and pixels, respectively.

Supervised hard-classification algorithms such as Maximum Likelihood use homogeneous training samples to train the classifier (Duda et al., 2001). Conversely, FML approach requires samples which take into consideration the mixture of land cover types in the scene (Wang 1990)(Schowengerdt 2007). The fuzzy mean, μ'_j , and fuzzy covariance matrix, Σ'_j , of land cover class j , which is represented as a fuzzy set, are needed as statistical parameters to train the FML classifier. The fuzzy mean of class j is defined as (Wang 1990)

$$\mu'_j = \frac{\sum_{i=1}^g f_j(x_i) x_i}{\sum_{i=1}^g f_j(x_i)} \quad (34)$$

where $f_j(x_i)$ is the membership function of class j , x_i is a sample pixel measurement vector, and g is the number of training samples.

The fuzzy covariance matrix of class j can be expressed as

$$\Sigma'_j = \frac{\sum_{i=1}^g f_j(x_i) (x_i - \mu'_j)(x_i - \mu'_j)^T}{\sum_{i=1}^g f_j(x_i)} \quad (35)$$

where $f_j(x_i)$ is the membership function of class j , x_i is a sample pixel measurement vector, g is the number of training samples, and μ'_j is the fuzzy mean of class j . The fuzzy mean and fuzzy covariance matrix are an extension of the conventional mean and covariance matrix. When the membership value of

class j , $f_j(x_i)$, is equal to 1 or 0, (34)-(35) become the conventional mean and covariance matrix statistics.

Each fuzzy set is described by its membership function which is based on the multidimensional gaussian membership function. Fuzzy mean and fuzzy covariance matrix replace the conventional mean and covariance matrix in the ML classification algorithm. A membership function of class j can be defined as follows (Wang 1990)

$$f_j(x) = \frac{P'_j(x)}{\sum_{k=1}^M P'_k(x)} \quad (36)$$

where

$$P'_k = \frac{1}{(2\pi)^{L/2} |\Sigma'_k|^{1/2}} e^{\left[-\frac{1}{2}(x-\mu'_k)^T \Sigma'_k{}^{-1} (x-\mu'_k)\right]} \quad (37)$$

and L is the dimension of data, M is the number of informational classes, and $1 \leq k \leq M$. The degree of membership associated to each land cover class depends on the position of the sample pixel, x_i , in the feature space. The membership function, $f_j(x)$, increases exponentially with the decrease of $(X - \mu'_k)^T \Sigma'_k{}^{-1} (X - \mu'_k)$. The term $\sum_{k=1}^M P'_k(x)$ is used as normalizing factor.

In order to obtain a soft training data, an iterative algorithm is used to generate the membership values of training data. At the initial stage, membership values are assumed to be either 0 or 1 associated to each class which becomes in a conventional mean and covariance matrix according to equation (34) and (35). New membership values (36) are calculated from conventional mean and covariance matrix which are used to recalculate fuzzy mean and fuzzy covariance matrix until the process reaches stable values for both fuzzy means and fuzzy covariance (Wang 1990)(Zhang and Foody 2001).

As we explained in this section, FML requires the use of soft-training data where apriori information of training samples coverage is needed. We proposed the use of the weight fractions obtained from a LMM method as the proportion coverage for training samples at initial stage in order to obtain the soft-training parameters.

3.1.3 Supervised Fuzzy C- Means (SFCM)

Fuzzy C – Means (FCM) is a well – known unsupervised sub-pixel classification algorithm (Bezdek et al., 1984) in which pixels are initially assigned randomly to clusters. The algorithm iteratively reassigns pixels to other clusters in order to minimize the generalized least square error function,

$$J_b = \sum_{i=1}^C \sum_{j=1}^M (v_{ji})^b (d_{ji})^2 \quad (38)$$

Let $X = \{x_1, x_2, \dots, x_g\}$ be a sample of C measured observations in a L – dimensional space. A fuzzy clustering is represented by a fuzzy set $\{V|v_{ji} \in [0, 1]\}$ where M and C are the number of clusters and pixels, respectively. b is a weight exponent, $1 \leq b \leq \infty$, which controls the data softness, increasing b tends to increase the degree of softness and vice versa (Zhang and Foody 2001)(Lucieer 2004). When b is set to 1, a hard classification is performed in which each pixel is allocated to one specific cluster. There are no criteria to select an optimum value of b . Authors (Bezdek et al., 1984)(Zhang and Foody 2001)(Lucieer 2004) suggest the use of a value for b in the range from $1.5 \leq b \leq 3.5$ depending on the degree of mixing in the scene. Perhaps, the computation of scene entropy (17) could be useful to set up the b parameter. $(d_{ji})^2$ is a measure of the distance between observed pixel, x_i , and the fuzzy cluster centers, μ_i . The most widely used $(d_{ji})^2$ are Euclidean (39) and Mahalanobis Distances (40).

$$(d_{ji \text{ ED}})^2 = (x_i - \mu'_j)^T (x_i - \mu'_j) \quad (39)$$

$$(d_{ji \text{ MahD}})^2 = (x_i - \mu'_j)^T \Sigma^{-1} (x_i - \mu'_j) \quad (40)$$

where μ'_j are the fuzzy cluster centers

v_{ji} is the membership value of an observed pixel vector x_i associated with cluster j and is computed from

$$v_{ji} = \frac{1}{\sum_{k=1}^M \left(\frac{d_{ji}}{d_{ki}}\right)^{2/(b-1)}} \quad (41)$$

v_{ji} has to satisfy the following constraints,

$$\begin{aligned} \sum_{i=1}^C v_{ji} &> 0, \quad j = 1, 2, \dots, M \\ \sum_{j=1}^M v_{ji} &= 1, \quad i = 1, 2, \dots, C \end{aligned} \quad (42)$$

Some applications require supervised methods to analyze remote sensed data. Zhang and Foody proposed supervised version of the FCM (Bezdek et al., 1984) algorithm (SFCM) using soft training data obtained from fuzzy means (43) and fuzzy covariance matrix (44) as training parameters of the classifier. Similarly FML has been derived.

$$\mu'_j = \frac{\sum_{i=1}^g v_{ji} x_i}{\sum_{i=1}^g v_{ji}} \quad (43)$$

$$\Sigma'_j = \frac{\sum_{i=1}^g v_{ji} (x_i - \mu'_j)(x_i - \mu'_j)^T}{\sum_{i=1}^g v_{ji}} \quad (44)$$

Deer (Deer et al., 1996)(Deer and Eklund 2001) proposed a Supervised Fuzzy Mahalanobis classifier which is also a modified version of the FCM algorithm using hard training data. In this case, μ_j and Σ_j are the conventional mean (45) and covariance matrix (46), respectively.

$$\mu_j = \frac{1}{g} \sum_{i=1}^g x_i \quad (45)$$

$$\Sigma_j = \frac{1}{g} \sum_{i=1}^g (x_i - \mu_j)(x_i - \mu_j)^T \quad (46)$$

where g is the number of pixel in the training data set for class j .

3.1.4 Linear Mixing Model (LMM)

LMM is also used as a soft classifier in this research work. LMM algorithm was described in details in Section 2.3.2. When LMM is used as a supervised soft classifier, it is assumed that the image analyst has prior knowledge of the scene and endmembers are determined from training data manually or as an average of training data (Foody and Cox 1994). Depending on the complexity of scene to be analyzed, a pre-processing step in order to determine a better representation of class endmembers is required. Unsupervised methods for unmixing of spectral data are an alternative to finding endmembers present in the scene before applying pre-processing techniques. Masalmah (Masalmah and Vélez-Reyes 2007) suggested the use of the Positive Matrix Factorization algorithms for the extraction of endmembers and abundance estimation in an unsupervised mode. Supervised methods such as Pixel Purity Index (PPI) (Boardman 1993)(Boardman et al., 1995), and others are used for this purpose as well (Plaza et al., 2004). PPI works over a reduced dimensional data calculating the pixel purity score for each point in the image cube by randomly generating L lines in the V -Dimensional Space. All the points are projected onto the lines, and the ones falling in the extremes of these lines are counted. The projections are repeated many times for random lines and those pixels at a certain cutoff threshold are declared “pure” pixels (Plaza et al., 2004).

3.1.5 Maximum Likelihood (ML) Algorithm

As part of the research, soft classification algorithms proposed to be included in the SSCT were compared with a conventional hard classification algorithm such as Maximum Likelihood (ML). ML is a per-pixel algorithm where each pixel is assigned to the class which it has the highest posterior probability (47) (Duda et al., 2001) (Richards 1995).

$$P(\omega_i|\mathbf{x}) = \frac{p(\mathbf{x}|\omega_i)P(\omega_i)}{\sum_{j=1}^M p(\mathbf{x}|\omega_j)P(\omega_j)} \quad (47)$$

where $P(\omega_i|\mathbf{x})$ is a posterior probability, $P(\omega_i)$ is a prior probability which in the case of ML is equal to $1/M$; M is the number of classes. $p(\mathbf{x}|\omega_i)$ is a class conditional probability density function (pdf).

ML simplifies to

choose i if $p(\mathbf{x}|\omega_i) > p(\mathbf{x}|\omega_j) \quad \forall j \neq i$, and $j=1, 2, 3, \dots, M$

If $p(\mathbf{x}|\omega_i)$ is a multidimensional Gaussian probability density function

$$p(\mathbf{x}|\omega_i) = \frac{1}{(2\pi)^{L/2} |\Sigma_i|^{1/2}} e^{\left[-\frac{1}{2}(\mathbf{x}-\mu_i)^T \Sigma_i^{-1} (\mathbf{x}-\mu_i)\right]} \quad (49)$$

where μ_i and Σ_i are the parameters for training the classifier, mean (45) of class i and covariance (46) of class i with dimension L , respectively. To avoid the computation of the exponential term, equation (49) can be reduced by applying a natural logarithm to $p(\mathbf{x}|\omega_i)$ which is a monotonically increasing function. The discriminant function of $p(\mathbf{x}|\omega_i)$ under ML conditions reduces to:

$$g_i(x) = \ln[p(\mathbf{x}|\omega_i)] = -(\mathbf{x} - \mathbf{v}_i)^T \Sigma_i^{-1} (\mathbf{x} - \mathbf{v}_i) - \ln|\Sigma_i| \quad (50)$$

The ML rule can be stated as follows:

$$x \in \omega_i \text{ if } g_i(x) > g_j(x) \quad \forall j \neq i, \text{ and } j=1, 2, 3, \dots, M$$

3.2 Summary

This chapter presented supervised soft classification algorithms based on Linear Mixing Model and fuzzy sets theory such as FML and SFCM with a Mahalanobis and Euclidean norms and fuzzy rule based algorithm such as FSCS which were included in the Spectral Soft Classification Tool. All those soft classification algorithms will be compared with a well known hard classifier, ML, as part of the research work.

CHAPTER 4

The Spectral Soft Classification Tool

This chapter presents the Spectral Soft Classification Tool (SSCT) which is an end to end classification system that provides supervised soft classification algorithms, visualization techniques, and accuracy assessment to evaluate the performance of soft classifiers using the fuzzy error matrix and conventional hard classification methods and other tools to measure the data softness as well. The SSCT will be added to the UPRM Hyperspectral Image Analysis Toolbox (HIAT). The routines developed and final integration will be performed by the LARSIP integration team.

4.1 Hyperspectral Image Analysis Toolbox (HIAT)

Researchers at the Laboratory for Applied Remote Sensing and Image Processing (LARSIP) have been working for the past 10 years on the analysis of multi/hyperspectral imagery being HIAT one of the products developed at LARSIP, UPRM. HIAT (Arzuaga-Cruz et al., 2004) (Rosario-Torres et al., 2005) is a MATLAB® Toolbox for the multi/hyperspectral image processing which provides hard classification and spectral unmixing functions similar to those available in commercial and non-commercial software such as ENVI® (ITT Visual Information Solutions 2007) and Multispec© (Biehl and Landgrebe 2002)(Landgrebe and Biehl 1994-2008). HIAT also includes original contributions in the area of feature extraction and bands selection (Vélez-Reyes and Jiménez-Rodríguez 1998). Figure 19 shows the data processing schema of the HIAT and proposed modification for soft classification. The green boxes in Figure 19 are functions already available at the toolbox. The blue boxes are the SSC modules that will be incorporate to HIAT. The LMM, FML, SFCM, and FSCS soft classification algorithms explained in Chapter 3 will be included into SSC Soft-Classification module. The approaches discussed in Section 2.3.3 to evaluate the performance of soft classifiers will be included into SSC Accuracy Assessment module. In addition, SSC will provide visualization tools as an aid to interpretation of soft classification output. The soft classification, visualization tools, and accuracy assessment modules shown in Figure 19 are described in Section 4.3 using an Enrique Reef, PR scene as an example to show the SSCT functionalities.

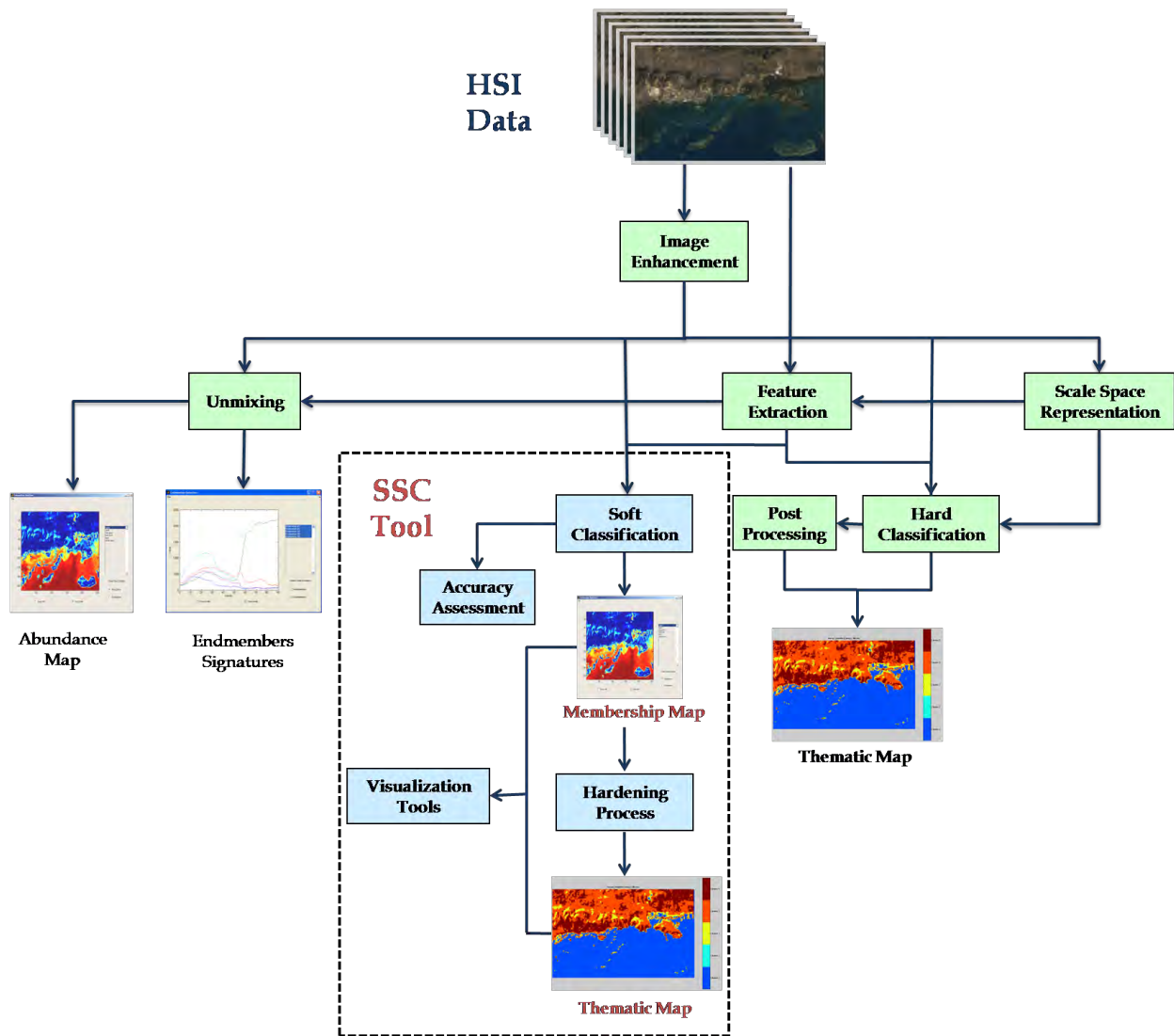


Figure 19: HIAT Processing Methodology including the proposed Spectral Soft Classification Tool

4.2 The Spectral Soft Classification Tool (SSCT)

As part of this work, we have developed an end to end soft classification tool, SSCT, which is shown in Figure 20, that will be incorporated into HIAT. SSCT will provide the image analysts a valuable tool for the analysis of spectral imagery. The soft-classification system is comprised of 5 steps: (1) pre-processing to remove atmospheric effects and denoised an image before apply classification algorithms, (2) feature extraction to reduce high dimensional data without a significant loss of information, (3) soft classification algorithms which take into consideration the mixing of pixels as part of the classification

process producing several fraction maps where each pixel represents the degree of membership of that pixel per informational class, (4) accuracy assessment using soft and non-soft ground truth data, and finally (5) visualization outputs which can be useful for interpreting the data softness using soft and hard outputs. An Enrique Reef at La Parguera, Puerto Rico scene is used next to show the SSCT functions.

A brief description of SSCT components is given in Table 3. A more detailed description is given in Appendix A.

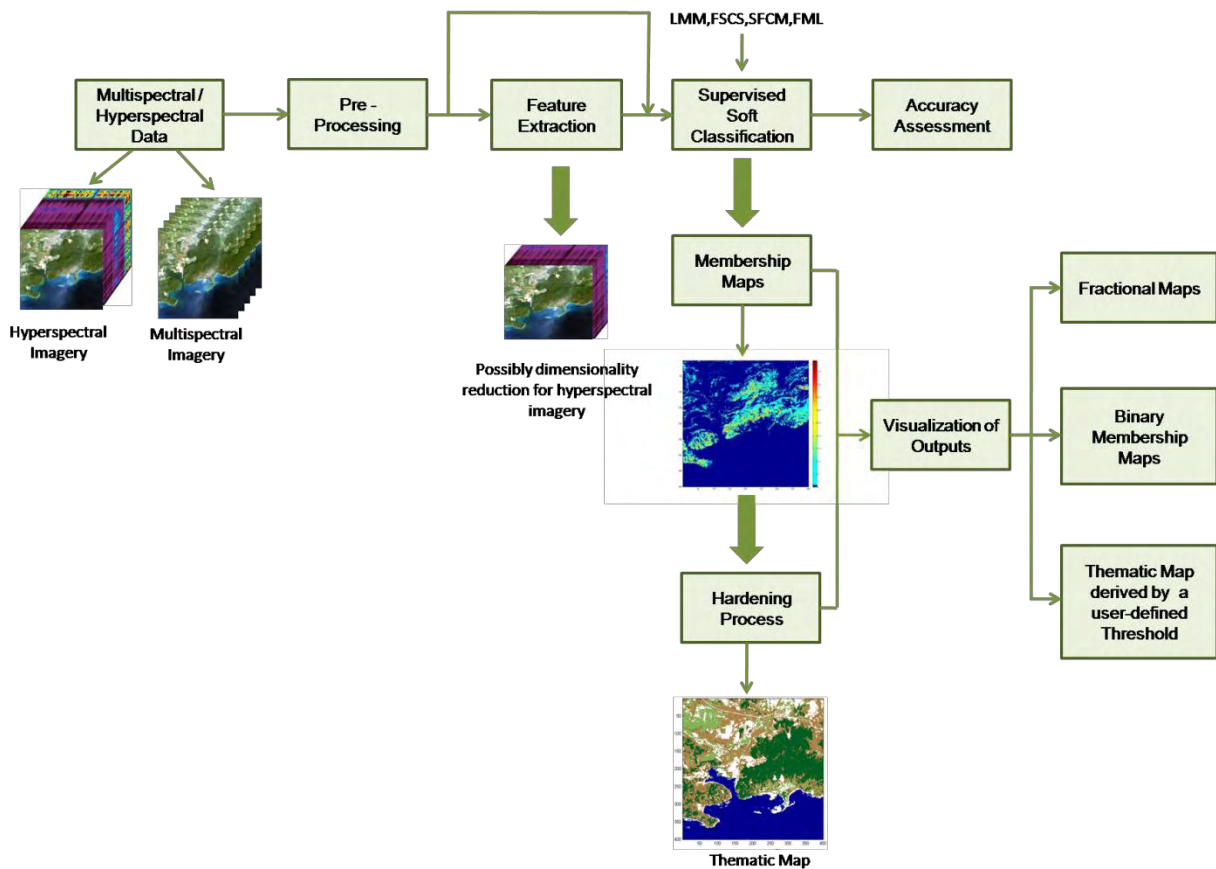


Figure 20: SSCT as an end-to-end soft classification system

Table 3: SSCT – Description of .m file functions

FUNCTION	DESCRIPTION
FracMaps	This function generates a RGB composite from three membership maps assigned to Red, Green, and Blue channels in order to explore the mixing among informational classes. (<i>Visualization Module</i>)
CorrCoefAnalysis	This function generates scatter plots between degree of membership derived by soft classification algorithms and soft-ground-truth data, and computes the correlation coefficient associated to each informational class. Soft ground truth data is required. (<i>Assessment Module</i>)
EucDist	This function estimates the separation of the degree of membership derived by soft classification algorithms and soft reference data based on the proportion coverage associated to each class in the pixel. Soft ground-truth data is required. (<i>Assessment Module</i>)
FEM	This function calculates the fuzzy error matrix to evaluate the performance of soft classification algorithms using fuzzy sets. Soft ground truth data is required. (<i>Assessment Module</i>)
Entropy_Img	This function generates an entropy image based on the membership maps derived by soft classification algorithms. (<i>Assessment & Visualization Module</i>)
Rescal	This function normalizes the degree of memberships to sum up to one. (<i>Complementary function</i>)
Defuzzy	This function generates a single classification map derived from membership maps produced by soft classification algorithms assigning the pixel to the class with the higher degree of membership. (<i>Complementary function & Soft Classification Module</i>)
LMMsc	This function generates a single classification map derived by LMM membership maps based on highest degree of membership. (<i>Soft Classification Module</i>)
FSCSsc	This function generates the FSCS membership maps and a single classification map based on highest membership value. (<i>Soft Classification Module</i>)
FMLsc	FMLsc function generates the FML membership maps and a single classification map based on highest degree of membership. At initial stage the degree of membership associated to each class is set to 1 or 0 ("pure pixels") in order to obtain the soft training parameters associated to each class iteratively. Training samples should be comprised from at least two classes. (<i>Soft Classification Module</i>)

FML_LMMsc	This function generates the FML membership maps and a single classification map based on highest degree of membership. LMM abundances are used to as the proportion coverage associated to each class in order to generate the soft training parameters. Training samples should be comprised from at least two classes. (<i>Soft Classification Module</i>)
FML_LMMscInit	This function generates the FML membership maps and a single classification map based on highest degree of membership. LMM abundances are used as the proportion coverage associated to each class in order to determine iteratively the soft training parameters. Training samples should be comprised from at least two classes. (<i>Soft Classification Module</i>)
ThMapThr	This function generates a single classification map with an unclassified class using a user defined threshold (between 0.01-0.99). (<i>Visualization Module</i>)
MemMapBinThr	This function generates binary maps using thresholds at 0.85, 0.7, 0.5, and 0.20 to visualize the spatial extent of a particular membership map. (<i>Visualization Module</i>)

4.3 Using the SSCT: Enrique Reef, La Parguera, Puerto Rico scene

4.3.1 Experimental Set-up

Figure 22 shows a subset, 25 x 48 pixels, of Enrique Reef, La Parguera located in the Southwestern of Puerto Rico Island used as hyperspectral data input for SSCT experiments. The scene was acquired in August 15, 2002 by HYPERION (Folkman et al., 2001), a hyperspectral sensor onboard Earth Observing (EO) – 1 satellite. HYPERION (Folkman et al., 2001) collects 220 unique spectral channels ranging from 0.4 to 2.5 μm with a 10nm bandwidth and 30m of spatial resolution for all bands as described in Table 4. Sea Grass, Mangrove, Sand, Reef Flat, and Deep Water were selected as informational classes. IKONOS imagery acquired in 2006 was used to show cover types location across Enrique Reef as shown in Figure 21.

Table 4: Specifications of HYPERION (EO-1) (Folkman et al., 2001) Hyperspectral sensor

Spectral Range	0.4-2.5 μm
Swath Width	7.5 km
Spatial Resolution	30 m
Spectral Resolution	220 channels
VNIR	Bands 8 – 57
SWIR	Bands 77 – 224
Temporal Resolution	200 days
Radiometric Resolution	12 bits

4.3.2 Land Cover References

We have used hard and soft land cover references available to validate the membership maps and classification maps derived by soft classification algorithms included in SSCT. Figure 24 shows a classification map of La Parguera, Puerto Rico region generated by the Biogeography Program of the National Oceanic and Atmospheric Administration (NOAA) National Centers for Coastal Ocean Science, which is part of the Center for Coastal Monitoring and Assessment (CCMA)⁷ (Kendall et al., 2001). They used aerial photographs of nearshore waters of Puerto Rico acquired in 1999 to study the benthic habitat types of the region and ground-truth points distributed across the region to validate the classification maps. The overall accuracy of La Parguera region was 93.6% which was estimated with 200 ground truth points as shown in Figure 25. A small percentage of submerged vegetation was misclassified as coral reef accordingly with (Kendall et al., 2001).

(Rivera-Borrero and Hunt 2007) has developed a classification map from 1 meter IKONOS PAN sharpened imagery shown in Figure 23(a) which was validated in the field with several ground control

⁷ <http://ccma.nos.noaa.gov/products/biogeography/benthic/welcome.html> Accessed in June 2008.

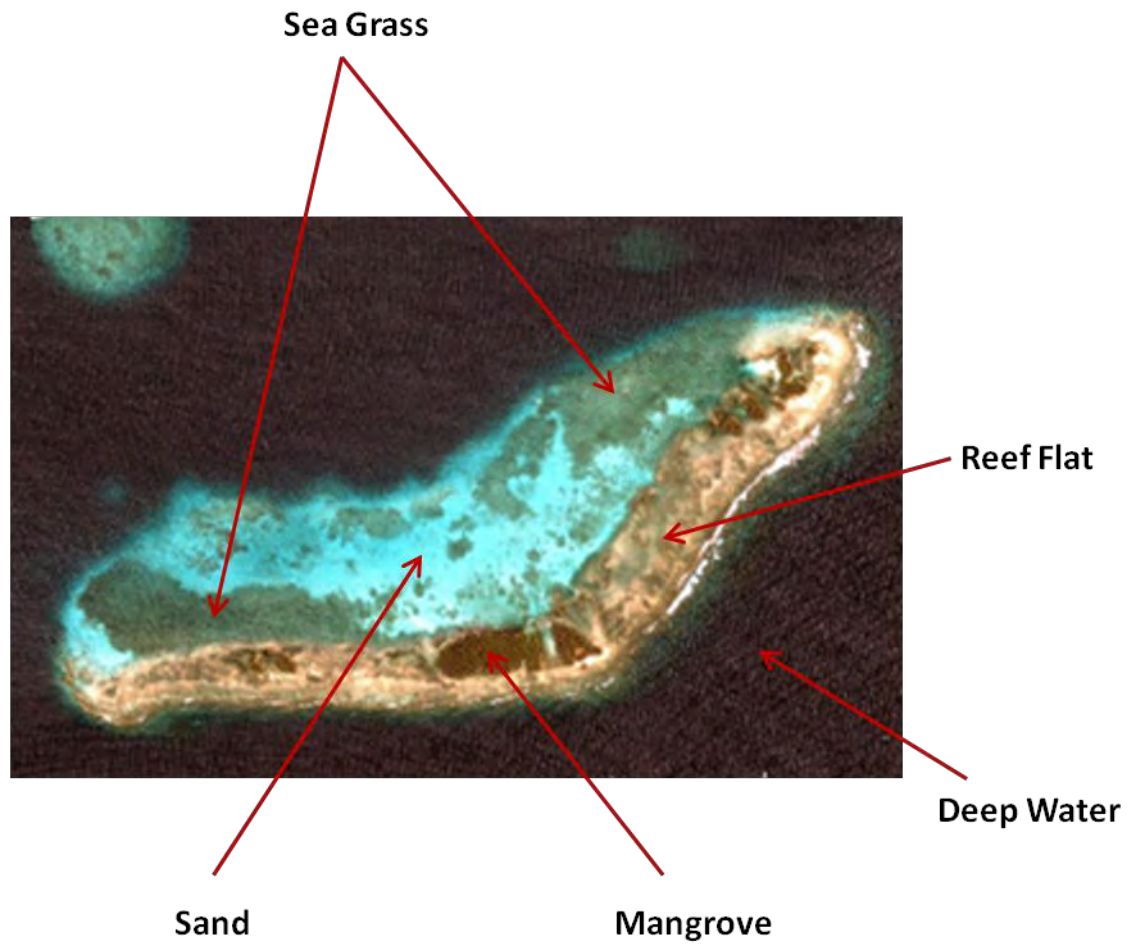


Figure 21: IKONOS true color image of Enrique Reef, La Parguera that shows informational classes selected for SSCT experiments



Figure 22: HYPERON true color image (bands 31-21-11) of Enrique Reef used as Hyperspectral data for SSCT experiments

points. The classes are labeled as follow: white for deep water, red for mangrove, green for sea grass, blue for sand, and coral color for reef flat region. He also produced a co-registration of both high spatial classification map and low spatial imagery from HYPERION as seen in Figure 23 (b). The image co-registration was performed using a polynomial method of degree two included in ENVI®⁸ (ITT Visual Information Solutions 2007). We have used the co-registration product of (Rivera-Borrero and Hunt 2007) to select the training samples/endmembers of supervised soft classification algorithms.

We have used soft references for each information class to evaluate the membership outputs obtained with SSCT soft classification algorithms. Those soft references come from abundance estimates derived from a co-registration of HYPERION imagery and IKONOS classification map (Rivera-Borrero and Hunt 2007) as shown in Figure 26 (a) – (e) for sea grass, sand, reef flat, mangrove, and deep water, respectively.

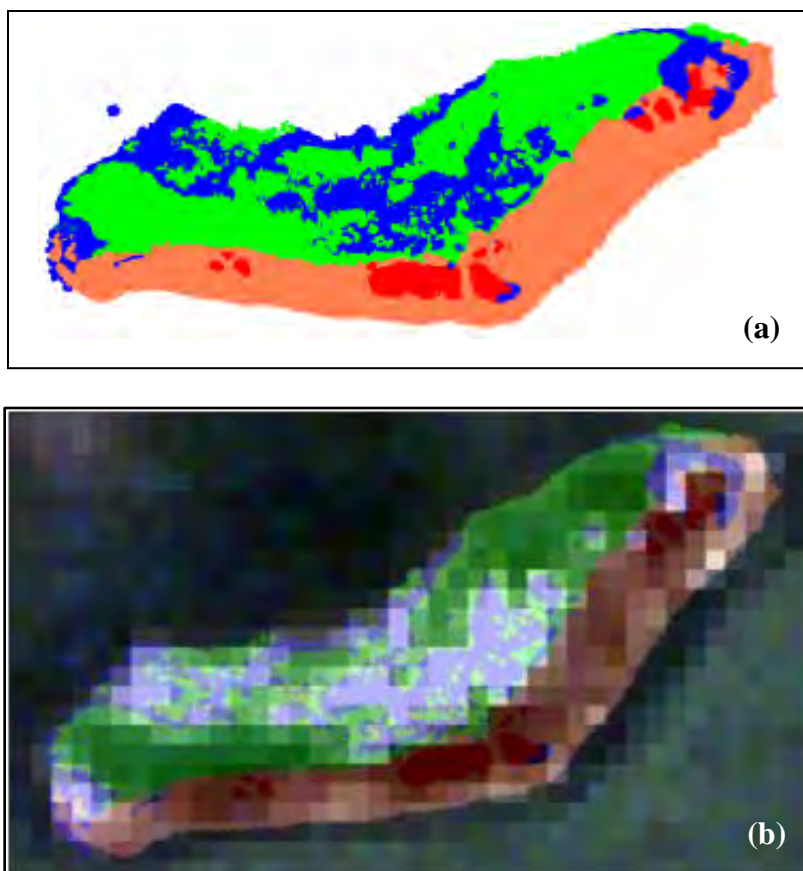


Figure 23: (a) IKONOS classification map, (b) Co-registration of IKONOS and HYPERION imagery used as Land Cover Reference for Enrique Reef scene (Rivera-Borrero and Hunt 2007).

⁸ <http://rsinc.com/envi/>. Accessed in June 2008.

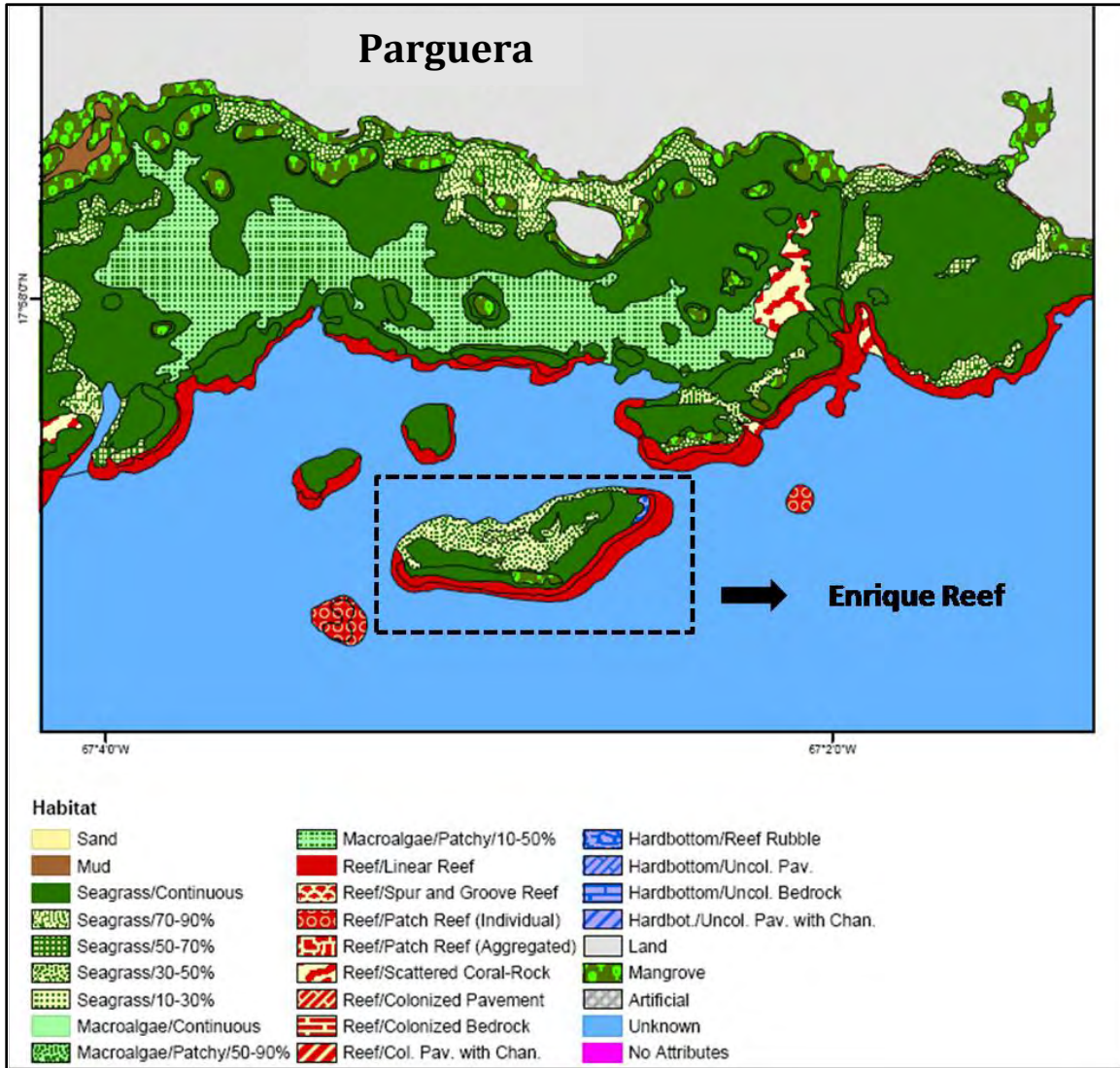


Figure 24: Benthic Habitat Map of La Parguera, PR generated in 1999 by CCMA, NOAA (Kendall et al., 2001)



Figure 25: Distribution of 200 ground truth points across the study area of La Parguera, PR (Kendall et al., 2001)

4.3.3 Pre-Processing

The soft-classification algorithms were applied to an atmospherically corrected hyperspectral imagery using a dark subtract band minimum algorithm available in ENVI® (ITT Visual Information Solutions 2007) in order to eliminate atmospheric effects. “Dark subtract” pixel is a simple method that finds out the minimum water pixel value in the infrared bands because in that region of the EM spectrum, water absorbs a lot of the incident energy that arrive to surface resulting in approximately all contribution from atmosphere (Chavez 1996).

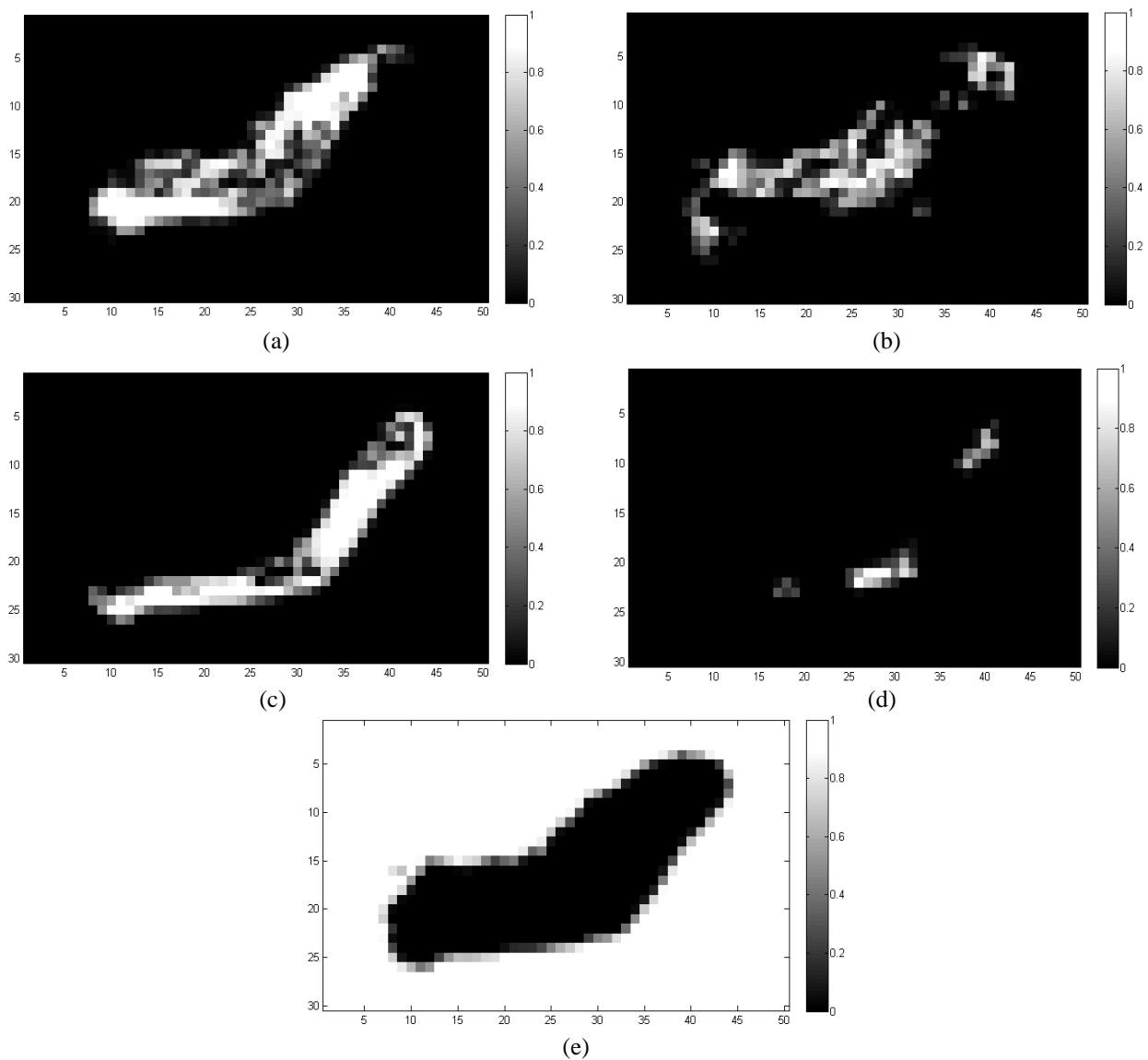


Figure 26: Abundances estimates derived from co-registration of IKONOS and HYPERION Imagery (Rivera-Borrero and Hunt 2007)

Once a simple atmospheric correction was done, principal components analysis (PCA) was used to denoise the hyperspectral imagery (Schowengerdt 2007).

Let be \mathbf{z} the principal component transform,

$$\mathbf{z} = \mathbf{V}^T \mathbf{x} + \mathbf{b} \quad (51)$$

where $\mathbf{V} = [\mathbf{v}_1, \mathbf{v}_2, \dots, \mathbf{v}_k]$ is the matrix of right covariance eigenvectors and bias \mathbf{b} is set to zero. Original data, \mathbf{x} , can be expressed as follows

$$\mathbf{x} = \mathbf{V}\mathbf{z} = \sum_{i=1}^k \mathbf{v}_i z_i = \sum_{i=1}^p \mathbf{v}_i z_i + \sum_{i=p+1}^k \mathbf{v}_i z_i \quad (52)$$

where k is the number of principal components which contains the total image variance and p is the number of principal components used to generated a restored image using signal components. PCs are ordered by decreasing variance such that PC_1 , is along the axis of maximum variance, PC_2 is along the second axis of maximum variance, and each succeeding axis has less variance. PCs are also uncorrelated

$$\text{cov}(z_i, z_j) = [C_z]_{ij} = 0 \quad \text{for } i \neq j$$

$$C_z = \begin{bmatrix} \lambda_1 & 0 & 0 & 0 \\ 0 & \lambda_2 & 0 & 0 \\ 0 & 0 & \ddots & 0 \\ 0 & 0 & 0 & \lambda_k \end{bmatrix} \quad (53)$$

where λ_i are the eigenvalues ordered in descending order.

Generally, any uncorrelated noise appears in the higher order components so that image can be restored eliminating those components. p is determined from equation (54) where T (percentage of variability) is usually selected above 95%. PCA filter 96% was chosen for the experiments shown in this chapter. The percentage of total variability is given by,

$$\%var(p) = \frac{\sum_{i=1}^p \lambda_i}{\sum_{i=1}^k \lambda_i} \times 100 \geq T \quad (54)$$

A re-constructed image, \mathbf{X}_p can be generated using the linear filter,

$$X_p = \sum_{i=1}^p v_i z_i = \mathbf{V}_p \mathbf{Z}_p = \mathbf{V}_p \mathbf{V}_p^T \mathbf{x} \quad (55)$$

where $\mathbf{V}_p = [\mathbf{v}_1, \mathbf{v}_2, \dots, \mathbf{v}_p]$ is a matrix formed by the first p eigenvectors of the covariance matrix, and $\mathbf{Z}_p = [\mathbf{z}_1, \mathbf{z}_2, \dots, \mathbf{z}_p]^T$ are the first p principal components.

A display of HYPERION raw band 9 image is shown in Figure 27 (a). On the other hand, Figure 27 (b) shows an image with 96% PCA filter which improved classification results. A graph of transect line 25 of both raw and denoised data is shown in Figure 27(c). As can be seen in Figure 27, PCA filter produced an image enhancement which could result in an improvement of classification accuracy.

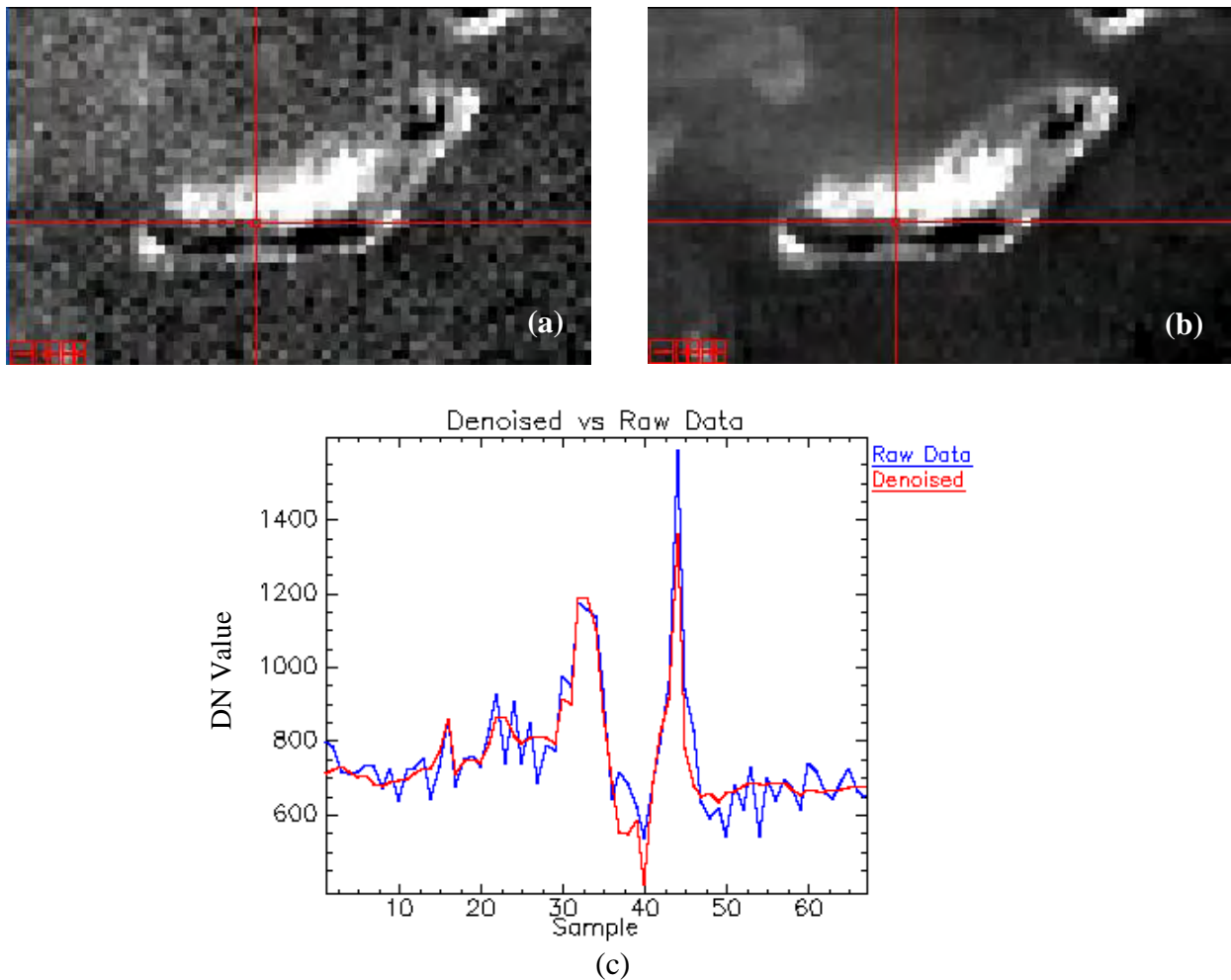


Figure 27: HYPERION (a) Band 9 raw image, (b) Band 9 - 96% PCA filter image, and (c) Line 25 of a first Enrique Reef, PR subset of 41 x 67 scene

4.3.4 Feature Extraction / Band Selection

There is a strong relation between number of training samples needed for accurate supervised classification and the number of bands which hyperspectral data is comprised (Landgrebe 2003). This is a problem in remote sensed data because in majority of cases training samples are limited. Hyperspectral data is comprised of correlated bands which in several cases results in redundant information. In addition, as the number of spectral channels increase computational cost and complexity increase. For this reason, feature extraction techniques are employ to reduce high dimensional data without a significant loss of information. Spectral band transformation and band selection such as Principal Components Analysis (PCA)(Schowengerdt 2007) and Singular Value Decomposition Subset Selection (SVDSS) (Vélez-Reyes and Jiménez-Rodríguez 1998) respectively are used for this purpose.

4.3.4.1 Singular Value Decomposition – Subset Selection (SVDSS)

SVDSS is a dimension reduction method which selects p -bands in an N -bands dimensional space in order to minimized loss of information. This method a difference of spectral band transformation techniques and it preserves the physical and spectral meaning of data which is an aid for human understanding.

Let be \mathbf{X} a matrix representation of a hyperspectral data where columns are arranged by stacking the columns of each single-band image. The SVDSS (Vélez-Reyes and Jiménez-Rodríguez 1998) selects the p most independent bands of the hyperspectral image.

$$\bar{\mathbf{X}} = \mathbf{X}\mathbf{P} = [\bar{\mathbf{X}}_1|\bar{\mathbf{X}}_2] = \mathbf{Q}\mathbf{R} \quad (56)$$

where \mathbf{X}_1 is an $N \times p$ matrix, \mathbf{X}_2 is an N by $N - p$ matrix, and \mathbf{P} is the pivoting matrix of the QR factorization (Vélez-Reyes and Jiménez-Rodríguez 1998)(Jiménez-Rodríguez et al., 2007) and p can be estimated using the percentage of variability in PCA. \mathbf{X}_1 contains the selected bands.

4.3.4.2 Feature Extraction/Band Selection for Enrique Reef scene

Soft-classification algorithms were applied to the Enrique Reef, PR scene. SVDSS was used as feature extraction method to reduce high-dimensional data from 220 bands to 14 bands which keep the 99% PCA of total data variability. HYPERION data file is comprised of 242 bands but actually there are

196 unique channels which have information that can be used to extract spectral information for classification purposes. Most of the remaining bands are located into the absorption bands regions.

First, a visual inspection was done to remove HYPERION noisy and damaged bands since Enrique Reef is significantly small scene. The mean of spectral response of training samples of deep water, mangrove, sea grass, reef flat, and sand for the 14 bands selected by SVDSS algorithm is shown in Figure 28. Table 5 describes the selected wavelengths and original HYPERION data set band number.

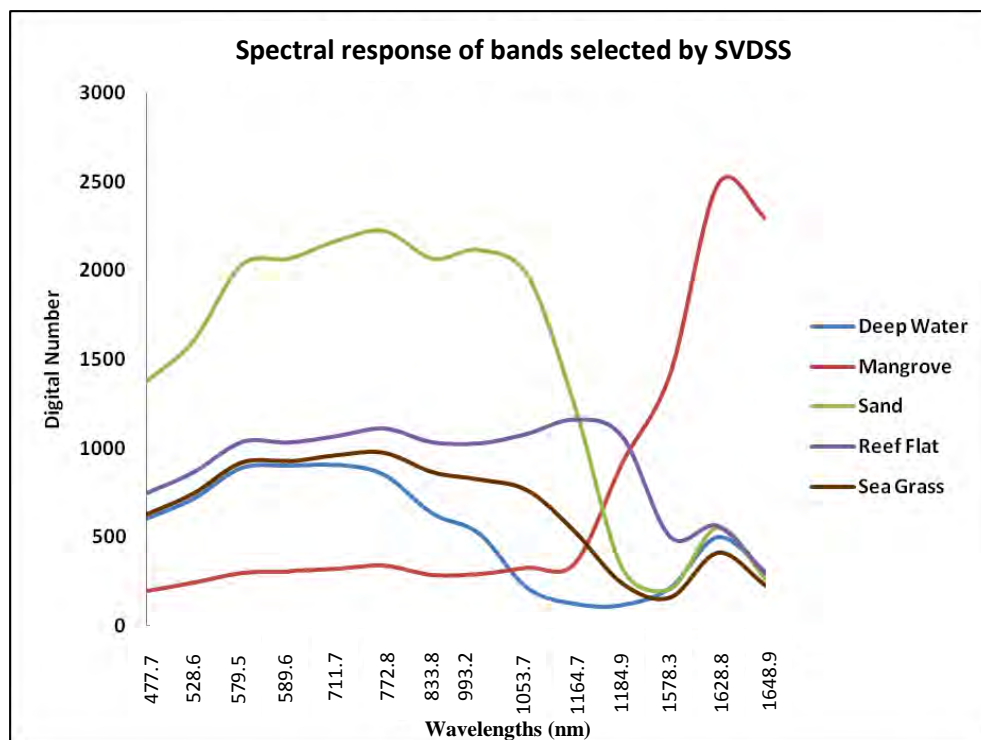


Figure 28: Mean training samples spectral response of bands selected by SVDSS

4.3.5 Soft Classification

This section shows membership maps related to pre-defined informational classes of Enrique Reef scene obtained with the four soft classification algorithms that were described in Chapter 3. These soft classification algorithms are (1) Supervised Fuzzy C- Means (SFCM), (2) Linear Mixing Model (LMM), (3) Fuzzy Maximum Likelihood (FML), and (4) Fuzzy Supervised Classification System (FSCS).

Table 5: Description of bands selected by SVDSS in terms of wavelengths and original band number in a HYPERION dataset

SVDSS Band Number	Original Band Number (HYPERION data file)	Wavelength (nm)
1	13	477.69
2	18	528.57
3	23	579.45
4	24	589.62
5	36	711.72
6	42	772.78
7	48	833.83
8	85	993.17
9	91	1053.69
10	102	1164.68
11	104	1184.87
12	143	1578.32
13	148	1628.81
14	150	1648.90

Figures 30-34 (a) – (d) show the membership maps outputs corresponding to Sea Grass, Sand, Reef Flat, Mangrove, and Deep Water, respectively obtained with soft classification algorithms included into SSCT. Figures 30-34 (e) also illustrate the abundance estimates derived from co-registration of IKONOS and HYPERION imagery from (Rivera-Borrero and Hunt 2007). Figure 29 (a) shows the training samples used for SFCM-Euclidean Norm and FSCS approaches. In the case of FML, and ML algorithms, it was necessary to add more samples to estimate the covariance matrix. The training samples for FML, and ML are shown in Figure 29 (b). The samples are distributed as follows: white for deep water pixels, green for sea grass pixels, blue for sand pixels, red for mangrove pixels, and yellow for reef flat pixels. On the other hand, the endmembers selected for LMM approach are shown in Figure 28 which was an average of the training samples used for SFCM and FSCS (see Figure 29 (a)).

Figure 30 (a) – (d) shows the sea-grass membership maps obtained with LMM, SFCM, FML, and FSCS approaches. Comparing the membership maps with the sea-grass soft reference (Figure 30 (e)), we can see that LMM, SFCM, and FML performed well on identifying the spatial distribution of sea grass.

Sea grass is mainly composed of *Thalasia testudinum* that has a faster change over time. FSCS identified the sea grass region quite well but it had problems to detect the mixture of pixels. In this scene, FSCS is working like a hard classifier except for few pixels. This is due to several factors such as the training samples since, Enrique Reef being a small scene, it is difficult to use entire pure pixels as training samples.

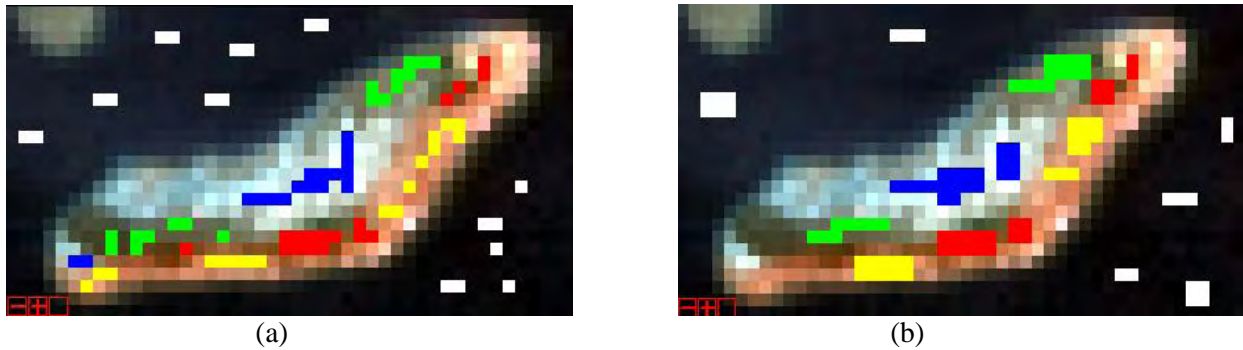


Figure 29: Training samples used for (a) SFCM, and FSCS, (b) FML, and ML

Figure 31 (a) – (d) shows the sand membership maps obtained with LMM, SFCM, FML, and FSCS approaches. Comparing the membership maps with the sand soft reference (see Figure 31 (e)), we can see that all methods performed well on identifying the spatial distribution of sand. As can be seen in FML outputs (see Figure 31 (c)), sands has some contribution in water pixels. This is due to the fact that FML required the use of soft parameters to obtain the degree of membership which were determined iteratively because we do not have an accurate proportions associated to each material for training pixels. FSCS identified the sand region quite well but it had problems to detect the mixture of pixels.

Figure 32 (a) – (d) shows the reef-flat membership maps obtained with LMM, SFCM, FML, and FSCS approaches. Comparing the membership maps with the reef-flat soft reference (see Figure 32 (e)), we can see that all methods performed quite well on identifying the spatial distribution of reef-flat. As can be seen in the SFCM outputs (see Figure 32 (b)), reef-flat had some contributions in the sea-grass region. This is due to the fact that several reef-flat training pixels could be comprised of certain percentage of sea grass. The reef-flat region contains a mixture of components such as sand, living and dead coral, and sea grass. On the other hand, FSCS identified the reef-flat region quite well but it had problems to detect the mixture of pixels.

Figure 33 (a) – (d) shows the mangrove membership maps obtained with LMM, SFCM, FML, and FSCS approaches. Comparing the membership maps with the mangrove soft reference (see Figure 33

(e)), we can see that SFCM and LMM methods produced the better membership output estimation. FSCS had problems to estimate the mixture of pixels. Due to training samples used, which does not come from just pure pixels, it overestimated the mangrove class and reef-flat class was misclassified.

Figure 34 (a) – (d) shows the deep-water membership maps obtained with LMM, SFCM, FML, and FSCS approaches. Comparing the membership maps with the deep-water soft reference (see Figure 34 (e)), we can see that all methods performed well on identifying the deep water regions. Although FML identified deep-water pixels, the proportion associated to this class was lower in comparison with remaining methods. This can be due to soft training parameters required for FML computation.

As can be seen in Figures 30-34 (a) – (d), LMM and SFCM membership maps had a good correlation between all informational classes and soft land references (see Figure 23 and Figures 30-34 (e)). Based on Enrique Reef results, SFCM seems to take into consideration the mixing of pixels as part of the classification process. It could be useful because LMM is a well known method to decompose a measured spectrum of a mixed pixel into its constituent spectra but depends on the scene, and methods employed to determine the endmembers, it can work well or not. The end-users can take advantage of soft-classification algorithms included in SSCT depending on the scene, and application of interest.

4.3.5.1 Hardening of Membership Map Outputs

A single thematic map was generated by a hardening process where pixels are assigned to the class which obtained the higher degree of membership. The thematic maps associated with LMM, SFCM, FSCS, FML, and FML initialized with LMM abundances are shown in Figure 35 (a) – (e). These classification maps were compared with Maximum Likelihood hard classification algorithm shown in Figure 35 (f). Figure 35 (g) shows a hardening output of soft references maps (see Figure 26 (a) – (e)). A second thematic map with 0.55 of threshold where pixels with less than 0.55 of pixel coverage appears as black and were assigned to unclassified class is shown in Figure 34 (h).

Comparing the IKONOS classification map (see Figure 23 (a) – (b)), IKONOS imagery (see Figure 21), and a hardened map obtained from soft references (see Figure 35 (g) – (h)), we can see that all thematic maps (Figure 35 (a) – (e)) obtained from soft classification provide a better representation of Enrique Reef remote sensed data than ML thematic map which produced an overestimation of mangrove

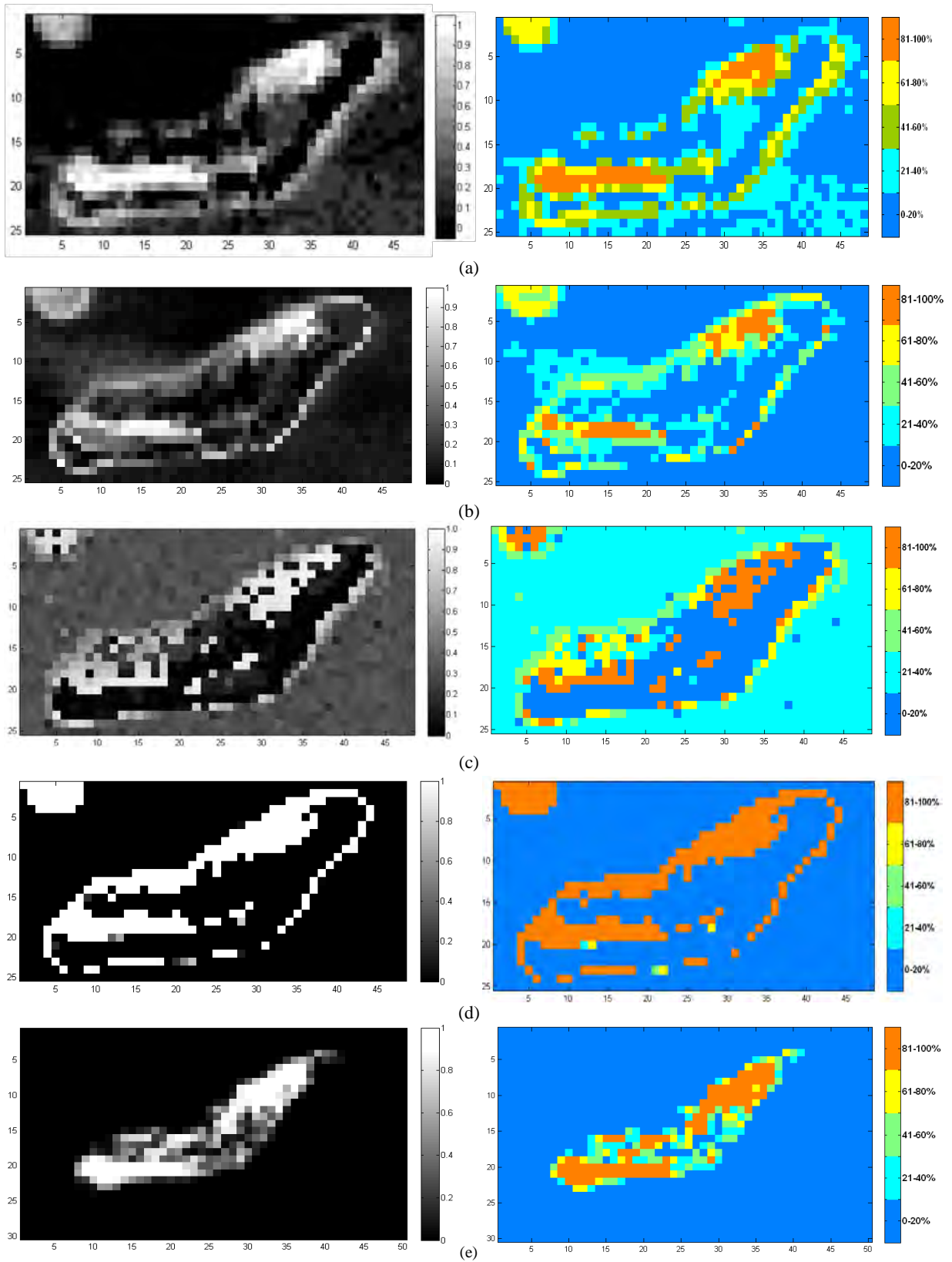


Figure 30: Sea Grass membership map using a 0-1 scale (left side) and ranges scale on the right side (0-20%, 21-40%, 41- 60%, 61-80%, 81-100%) obtained with (a) LMM, (b) SFCM, (c) FML, (d) FSCS, and (e) soft reference derived by co-registration of IKONOS and HYPERION imagery (Rivera-Borrero and Hunt 2007)

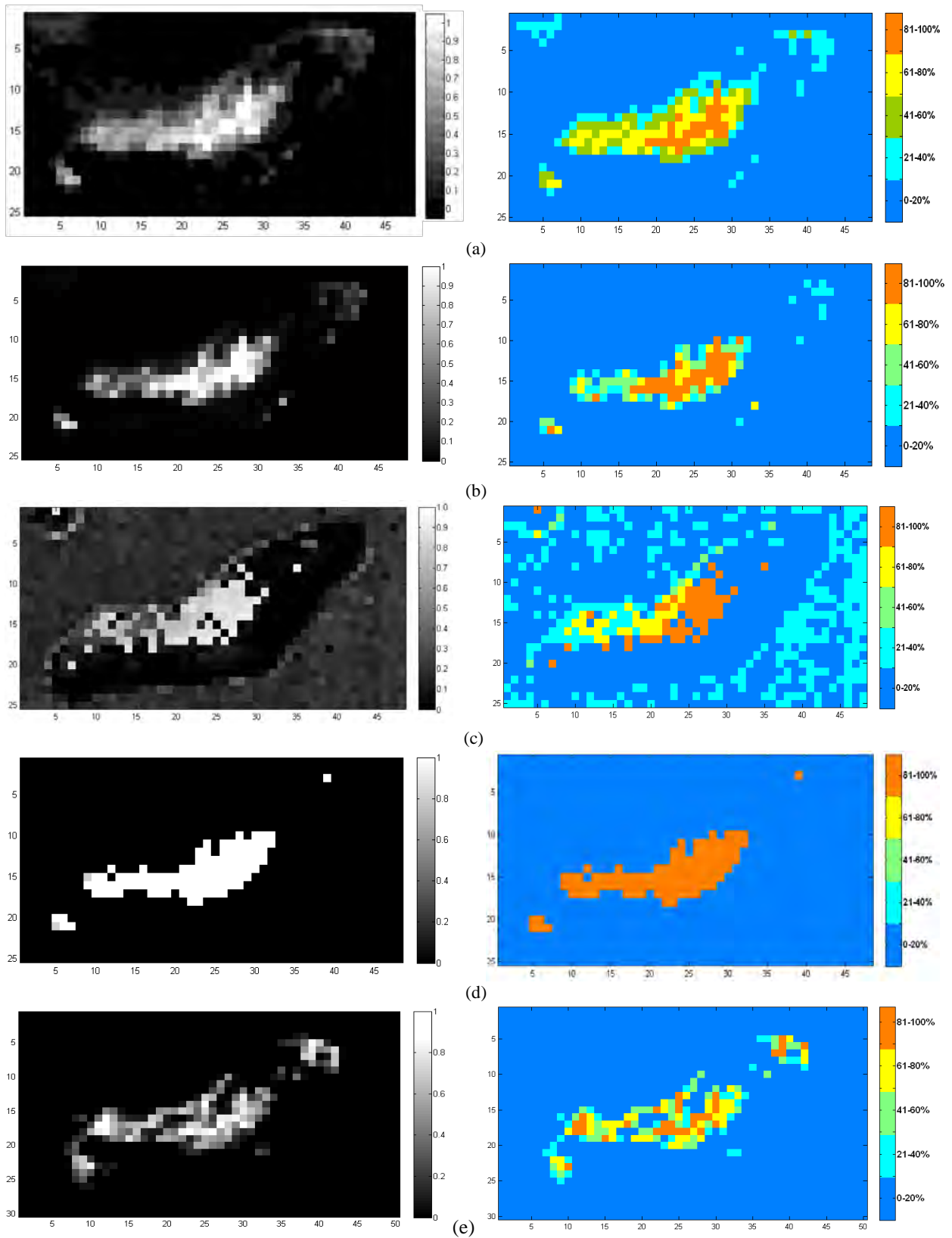


Figure 31: Sand membership map using a 0-1 scale (left side) and ranges scale on the right side (0-20%, 21-40%, 41- 60%, 61-80%, 81-100%) obtained with (a) LMM, (b) SFCM, (c) FML, (d) FSCS, and (e) soft reference derived by co-registration of IKONOS and HYPERION imagery (Rivera-Borrero and Hunt 2007)

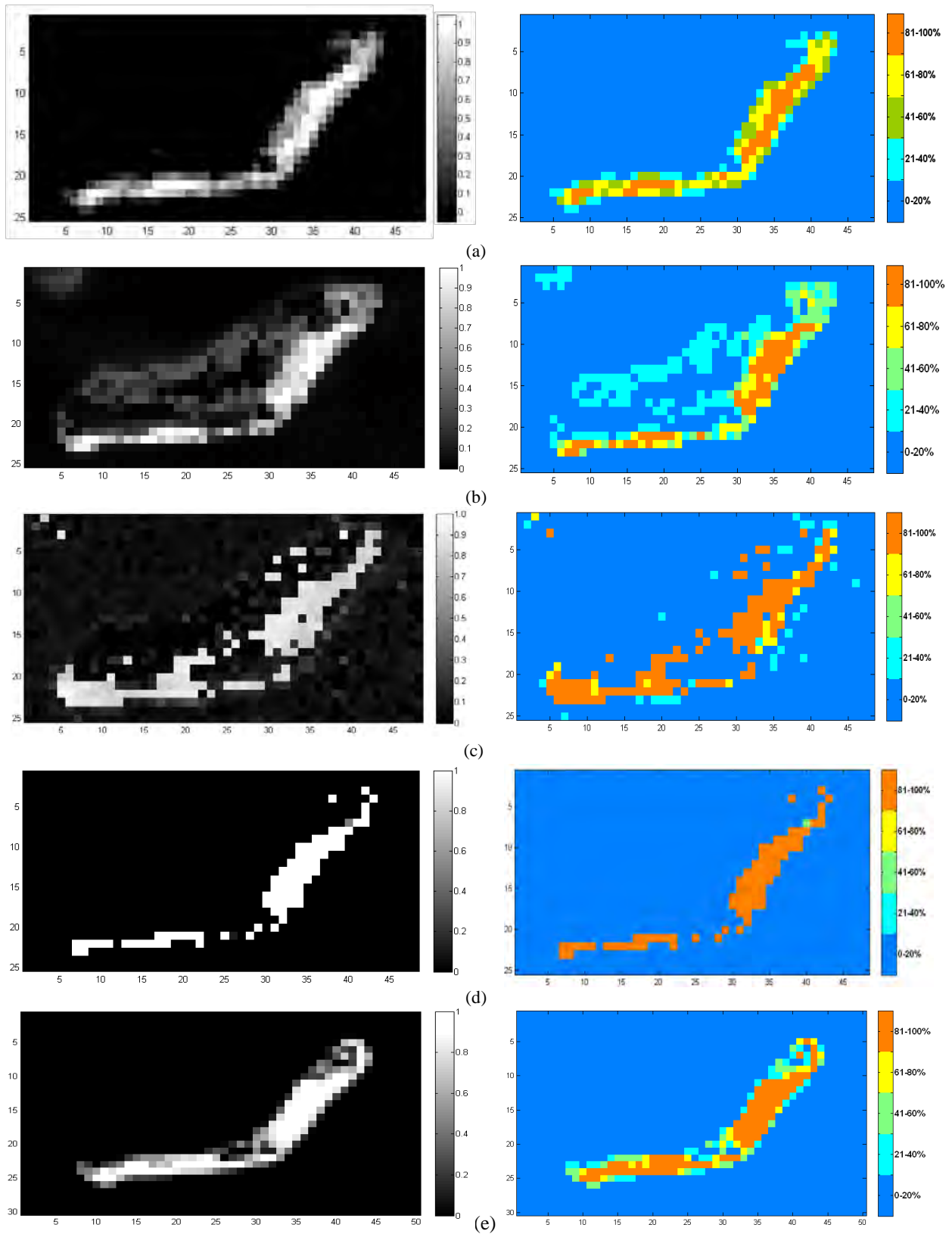


Figure 32: Reef Flat membership map using a 0-1 scale (left side) and ranges scale on the right side (0-20%, 21-40%, 41- 60%, 61-80%, 81-100%) obtained with (a) LMM, (b) SFCM, (c) FML, (d) FSCS, and (e) soft reference derived by co-registration of IKONOS and HYPERION imagery (Rivera-Borrero and Hunt 2007)

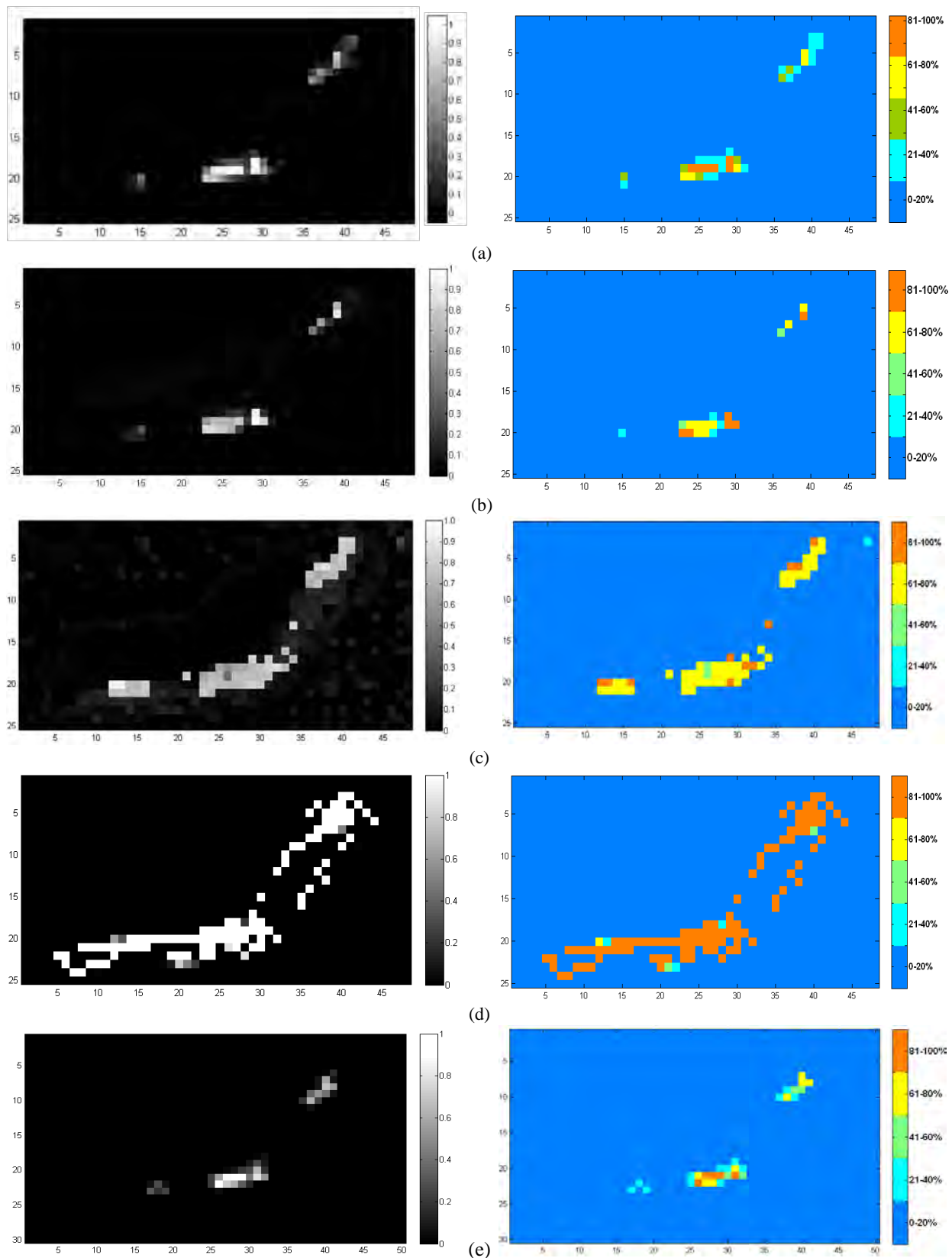


Figure 33: Mangrove membership map using a 0-1 scale (left side) and ranges scale on the right side (0-20%, 21-40%, 41-60%, 61-80%, 81-100%) obtained with (a) LMM, (b) SFCM, (c) FML, (d) FSCS, and (e) soft reference derived by co-registration of IKONOS and HYPERION imagery (Rivera-Borrero and Hunt 2007)

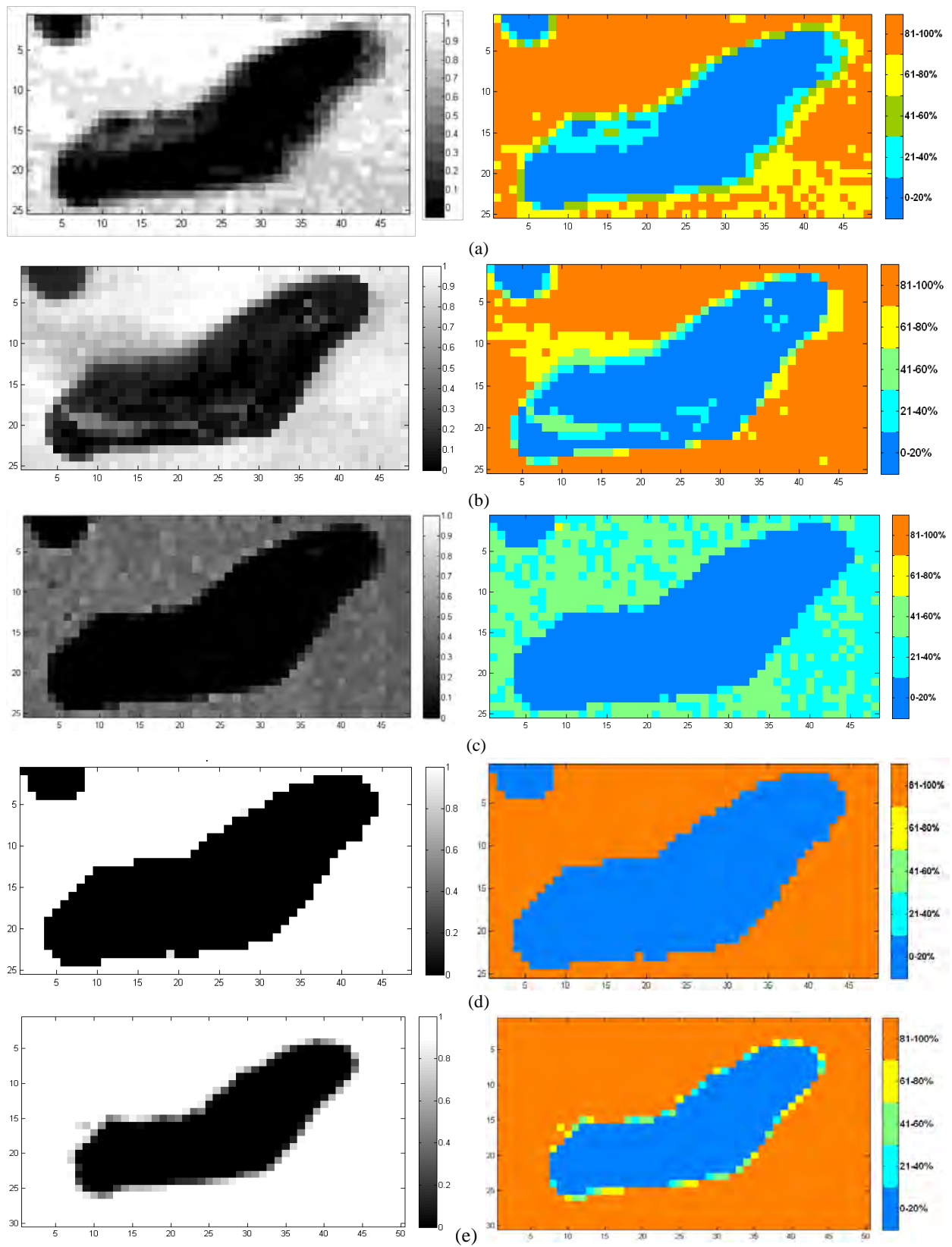


Figure 34: Deep Water membership map using a 0-1 scale (left side) and ranges scale on the right side (0-20%, 21-40%, 41-60%, 61-80%, 81-100%) obtained with (a) LMM, (b) SFCM, (c) FML, (d) FSCS, and (e) soft reference derived by co-registration of IKONOS and HYPERION imagery (Rivera-Borrero and Hunt 2007)

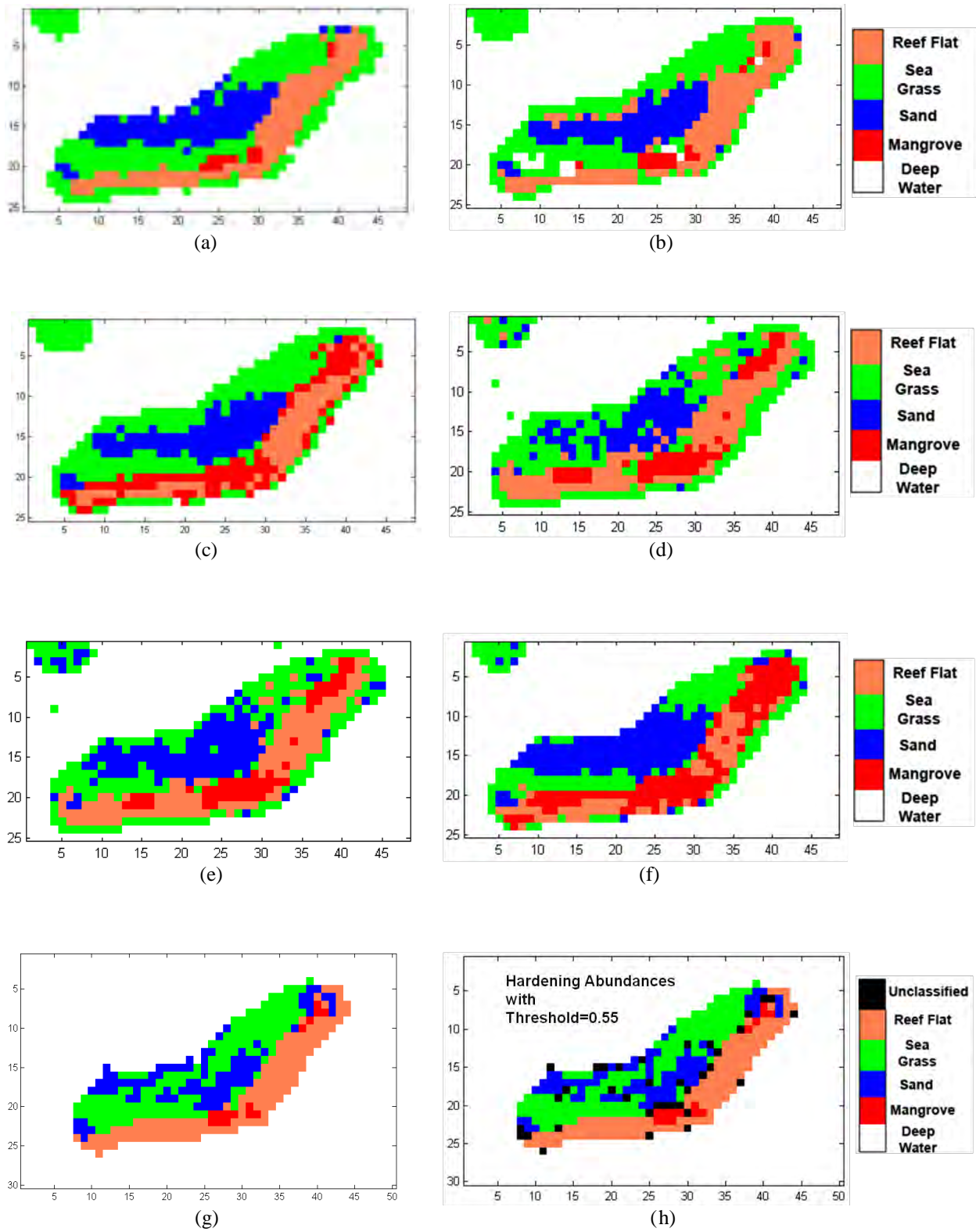


Figure 35: Classification maps obtained with (a) LMM, (b) SFCM, (c) FSCS, (d) FML, (e) FML-LMM to initialized, (f) ML, (g) hardening of soft references, and (h) threshold of 0.55 was applied to the classification map obtained in (g).

class. FSCS also produced an overestimation of mangrove class but obtained good identification of remaining informational classes. FML thematic map especially using LMM abundances to initialize the algorithm illustrates that FML improves the classification map obtained with the conventional ML algorithm for mangrove and sand classes.

SSCT visualization techniques to explore data softness of membership maps and hard outputs are described in next section.

4.3.6 Visualization Techniques

4.3.6.1 Fractional Maps

RGB composites are a useful tool to generated fractional color maps produced by a combination of three land cover membership maps assigned to red, green, and blue channels as shown in Figure 36 where Reef Flat, Sea Grass, and Sand were assigned to RGB channels (Schowengerdt 2007)(Bastin et al., 2002). As can be seen in Figure 36, the RGB composite allow us to explore the mixture between endmembers that it is not possible with a single thematic map derived by a hard classification.

4.3.6.2 Binary Maps

SSCT also provides binary maps to visualize the spatial extent of a particular land cover membership output as shown in Figures 37-39 for the case of Sand, Reef Flat, and Sea Grass, respectively. The user sets a threshold, for instance 0.85 and a binary image is generated which it shows the spatial extent of pixels with a degree of membership above the threshold. In that case, those pixels show a low data softness but depend on the thresholds and the study that users want to investigate it is possible to analyze the softness of membership output per land cover types. As can be seen in Figures 37 – 39, the user can set several thresholds to explore the softness of pixels associated to that informational class. For instance, if a user set thresholds at 0.85, 0.7, 0.5 and 0.2, the SSCT display an output in which pixels with degree of membership output from 0.85 to 1, 0.7 to 0.85, 0.5 to 0.7, and 0.2 to 0.5 exhibit different colors as can be seen in the right side of Figures 37 – 39. On the other hand, the left side of Figures 37 – 39 show the spatial extent of pixels for varying threshold from 0-1. The visualization of transition zones could be a key in the study of climate change of vegetation types or regions where field

work expeditions are expensive and could be intrusive on an ecosystem (Lucieer 2006)(Bastin et al., 2002).

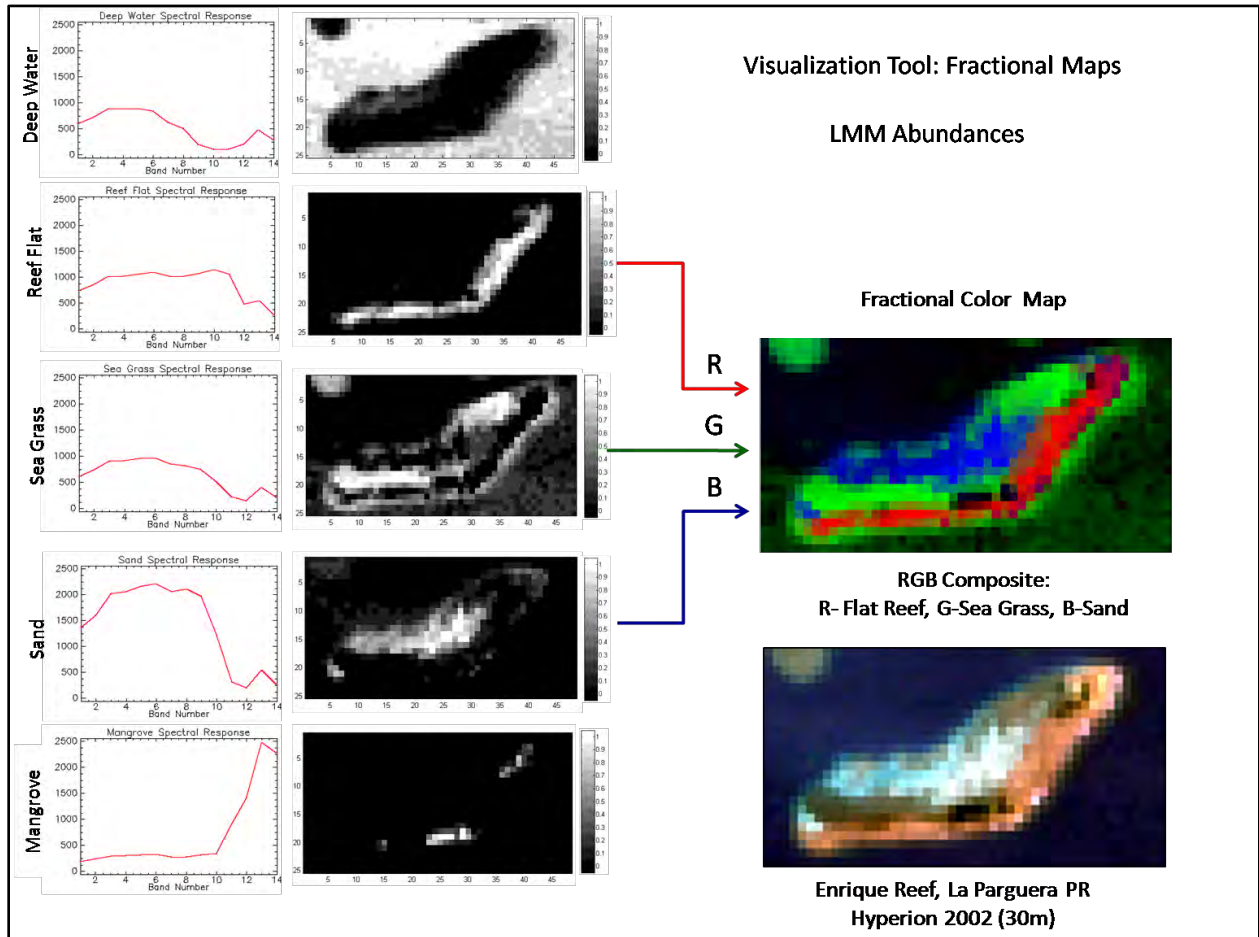


Figure 36: Fraction color maps derived by a combination of Reef Flat, Sea Grass, and Sand membership maps in the RGB channels

4.3.6.3 Thematic Map Derived by a User-Defined Threshold

A defuzzification or hardening process produce a single thematic map derived from membership maps which contain information about the proportions associated to each informational class. For that reason, visualization techniques that take advantage of this could be useful to image analysts who sometimes prefer to analyze a single classification map instead of several fraction or membership maps. We proposed the use of a user-defined threshold because if a pixel has the higher degree of membership

of a particular class less than 50% pixel coverage for instance should not be assigned to this land cover type in a hardening process. All those pixels which have winning classes with less than 50% of pixel coverage were assigned to unclassified label which appear as black in Figure 40 (b). On the other hand, Figure 40 (c) illustrates a thematic map where pixels with area coverage less than 0.5 were given similar colors of the class which obtained the higher degree of membership. In that case, the image analyst can explore data softness by thresholds and labels colors. As can be seen in Figure 40 (b)-(c), unclassified pixels are located in the boundaries between classes and regions which have mixtures between classes accordingly with co-registration of HYPERION and IKONOS imagery (see Figure 23 (b)). Further SSCT outputs for classification maps visualization are shown in Figure 41.

4.3.7 Accuracy Assessment

Accuracy assessment is a key element of any classification system to evaluate the accuracy of classification maps and membership outputs. In literature several methods to evaluate the performance of soft classifiers in terms of measure the degree of mixing, and fuzzy error matrix which is an extension of the conventional hard assessment taking into consideration the weights obtained per informational class. Correlation coefficient analysis was also performed to study linear relation between soft reference data and weights obtained from soft classification algorithms. All the methods included in the SSCT are explained in details in Section 2.3.3.

4.3.7.1 Measures of the Degree of Mixing

In Section 2.3.3.1, we discussed different methods that can be used to analyze the soft classification outputs in term of how fuzzy data is and to measure the strength of fuzzy partitioning. There is no standard to evaluate soft classifiers but the use of several approaches could give us a better idea of how accurate is the results obtained from membership outputs and hardened process.

Figures 42 – 45 show the entropy values of estimated membership outputs obtained with LMM, SFCM, FML, and FSCS approaches. We expect that pixels with high degree of mixing should have high entropy values. On the other hand, if a pixel is almost pure it should get a low entropy value. Following this concept, we can appreciate that LMM and SFCM entropy images in Figures 42 - 43 obtained higher

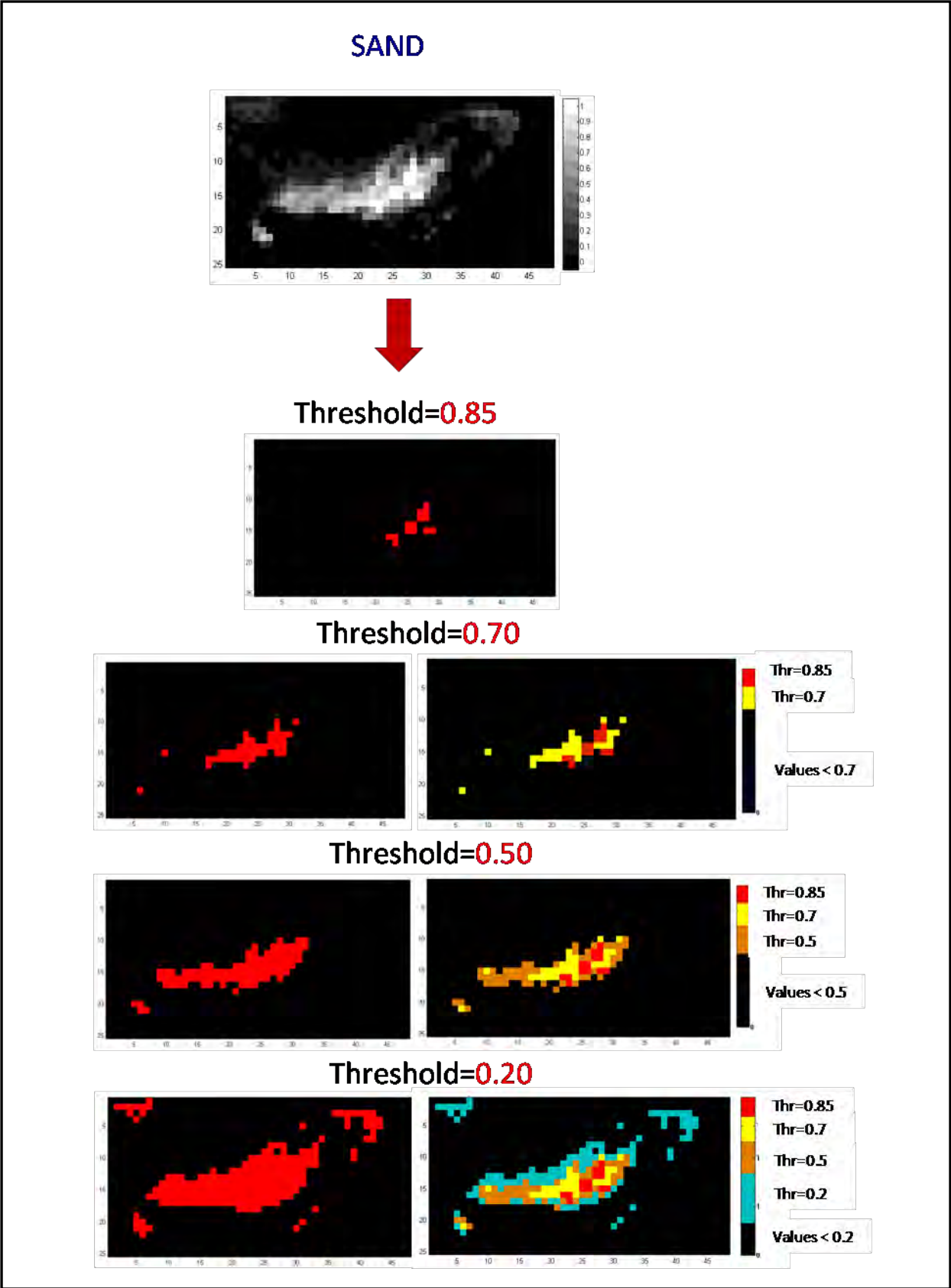


Figure 37: Binary maps of sand LMM abundances derived by user-defined thresholds of 0.85, 0.7, 0.5, and 0.2

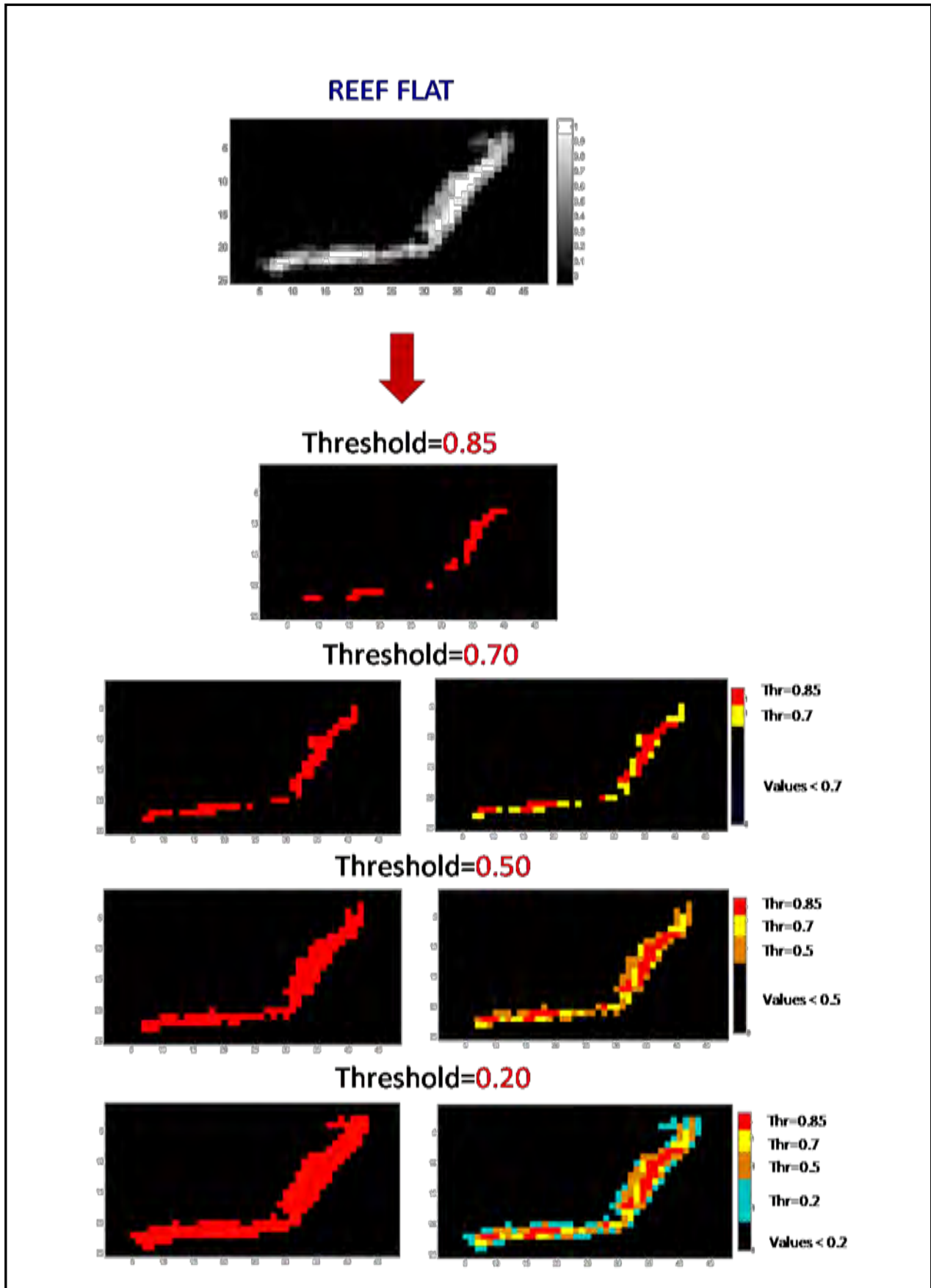
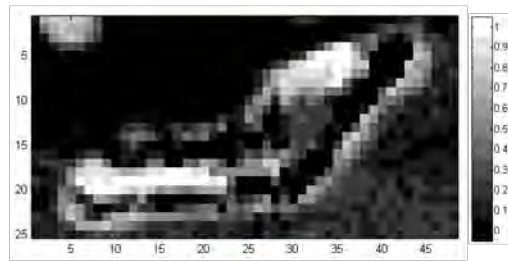
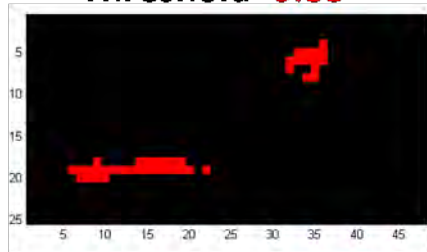


Figure 38: Binary maps of reef-flat LMM abundances derived by user-defined thresholds of 0.85, 0.7, 0.5, and 0.2

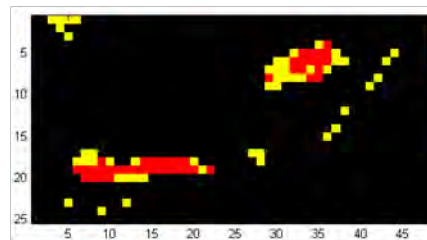
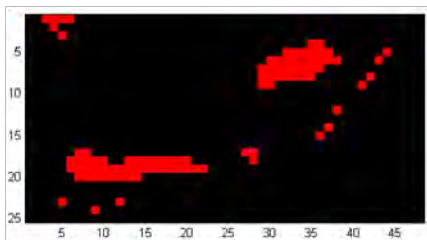
SEA GRASS



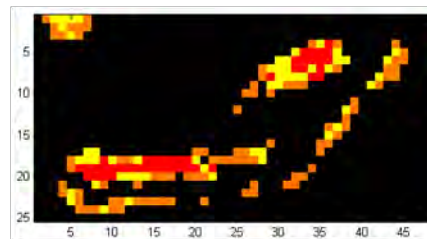
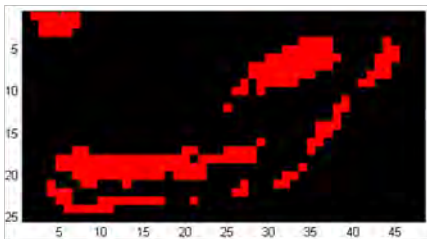
Threshold=0.85



Threshold=0.70



Threshold=0.50



Threshold=0.20

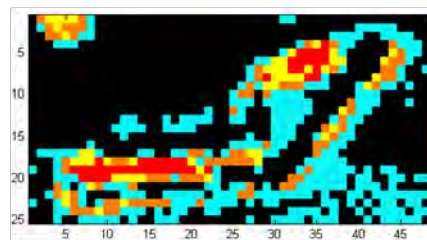
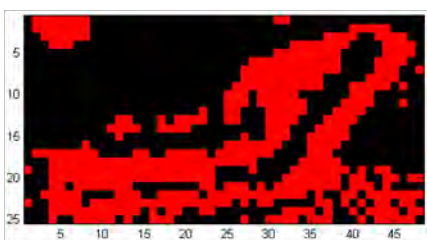


Figure 39: Binary maps of sea-grass LMM abundances derived by user-defined thresholds of 0.85, 0.7, 0.5, and 0.2

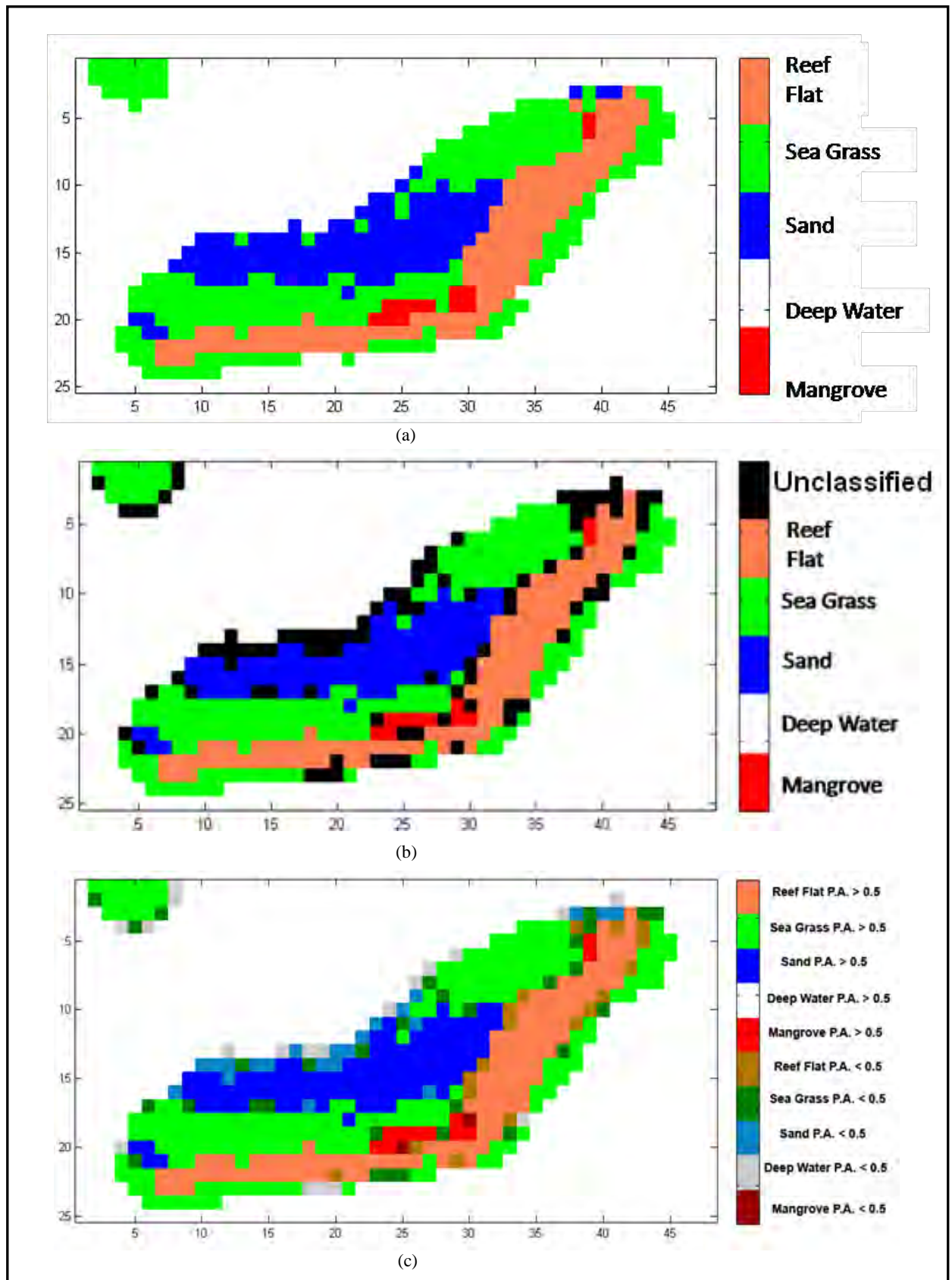


Figure 40: (a) Hardening LMM abundances, (b) with threshold of 0.5 (unclassified class), and (c) with threshold of 0.5 and specified by class label which obtained higher degree of membership.

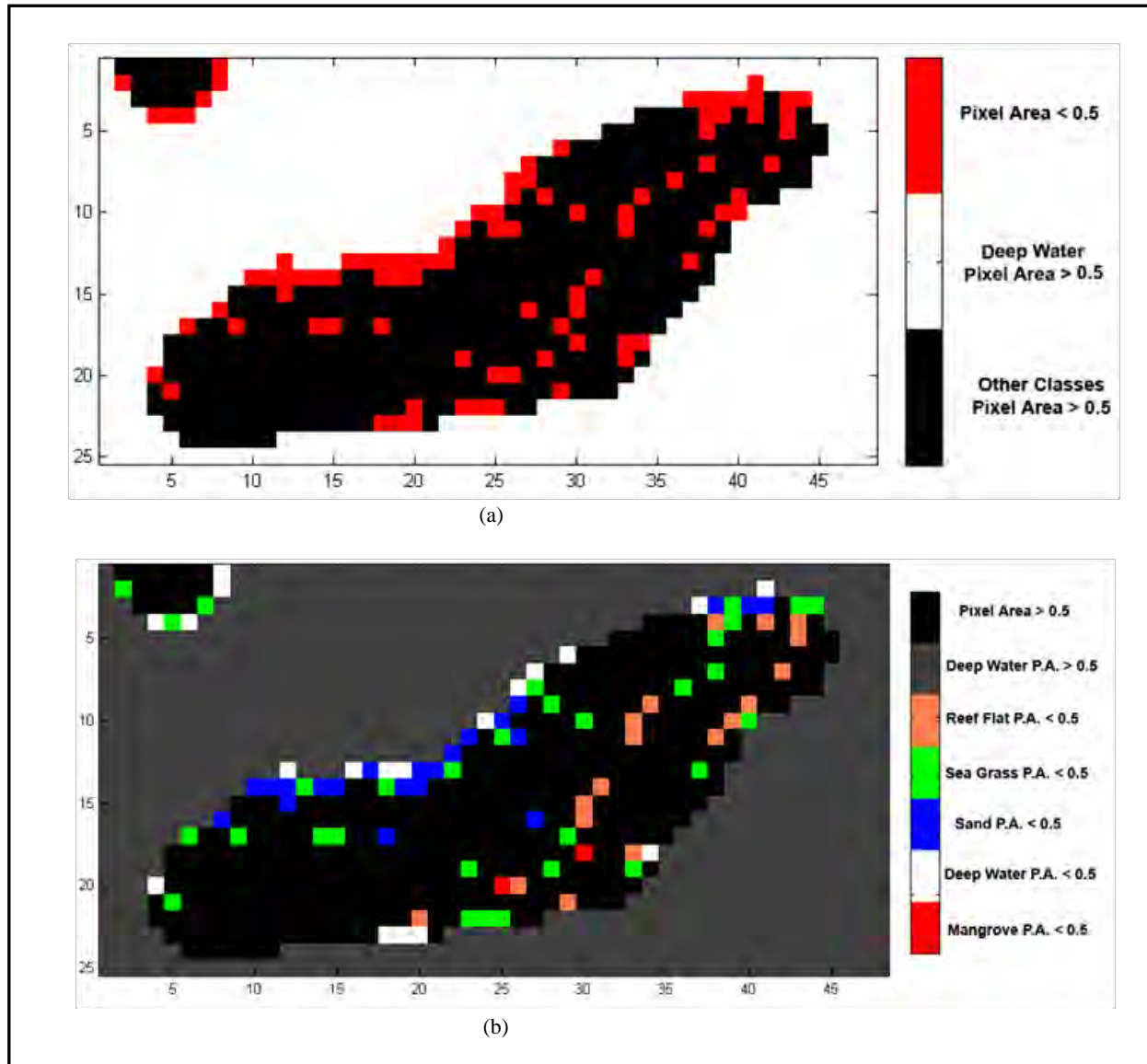


Figure 41: Thematic map with threshold ($T=0.5$). (a) Pixels with $T < 0.5$ are in red, (b) pixels with $T < 0.5$ are labeled by the class which obtained higher weight.

entropy values for regions such as sea-grass, reef-flat, and some portion of sand habitats in the benthic habitat classification map generated by Biogeography Program of NOAA-CCMA shown in Figure 24 (Kendall et al., 2001). Conversely, lower entropy values in Figure 42-43 (LMM and SFCM) were assigned to continuous sea grass region in the benthic habitat reference map in Figure 24.

In contrast, Figure 44 shows entropy values for a FSCS approach. It presents a few higher entropy values. It has sense in our entropy interpretation because FSCS had problems in detecting mixture of

pixels as can be seen in the membership maps generated by this method in Section 4.3.5 (see Figures 30 – 34 (d)). Accordingly to results, it is evident that for Enrique Reef scene, FSCS does not provide weight fractions associated with each informational class per pixel although it produced a better classification map (defuzzification step) than ML thematic map. For that reason, entropy images could be a useful tool for image analyst in order to analyze membership outputs obtained from soft classification algorithms.

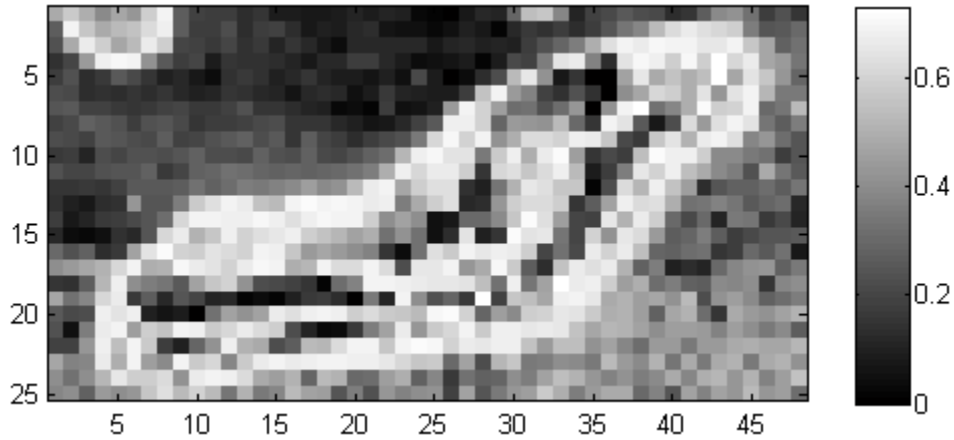


Figure 42: Entropy values derived from estimated LMM abundances

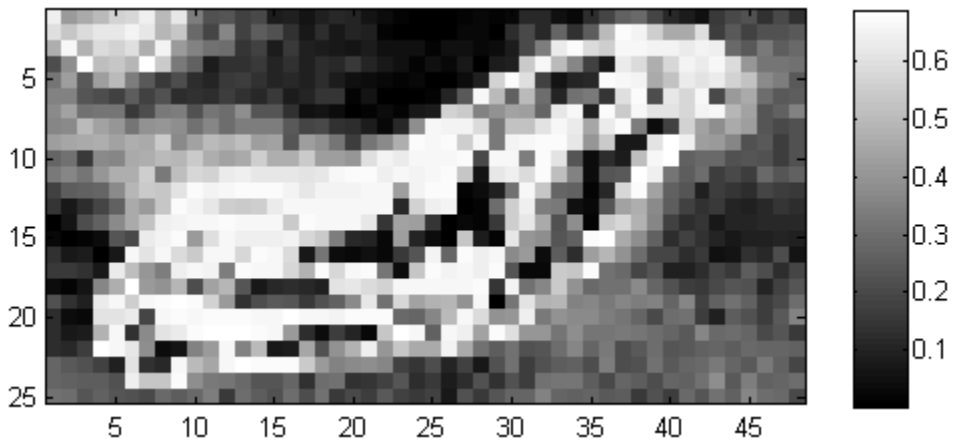


Figure 43: Entropy values derived from estimated SFCM membership outputs

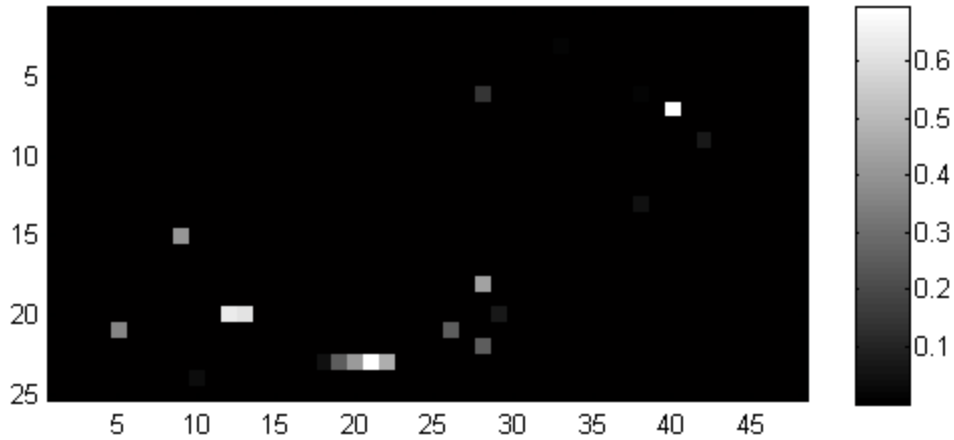


Figure 44: Entropy values derived from estimated FSCS membership outputs

Figure 45 illustrates an entropy image obtained from FML membership outputs. As can be seen in Figure 34 (c), FML had difficulties to estimate weight fractions associated with the deep-water class. As a result, degrees of membership obtained were lower. In spite of FML difficulties, Deep Water is still distinguishable in comparison with remaining land cover types in the scene. Hence, it is expected that water region gets high entropy values as shown in Figure 45. Sea grass, reef flat, and mangrove pixels also obtain high entropy values which are comparable with mixture regions showed in the NOAA Benthic classification map in Figure 24.

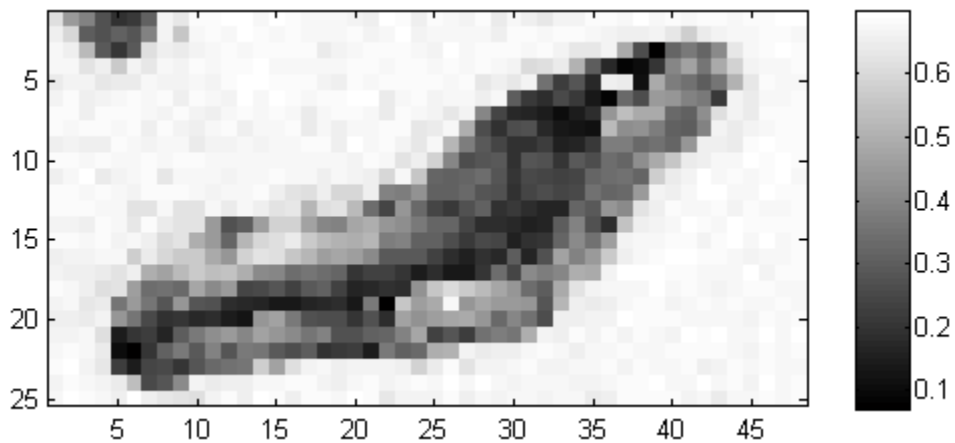


Figure 45: Entropy values derived from estimated FML membership outputs

SSCT provides other methods to measure the degree of mixing from fraction map results such as Euclidean Distance (2.3.3.1.3). Table 6 shows Euclidean Distance and entropy computations. As the mean entropy value is closer to maximum entropy, it is an indication of high mixing of pixels. On the contrary, if the mean entropy value is closer to the minimum entropy, it means that the classifier was acted as hard classifier, how was the case of FSCS. A lower mean entropy value can also be produced by the analysis of a scene with little mixing. As shown in Table 6, both LMM and SFCM show similar degree of mixing as can be seen in entropy images of both methods. Accordingly with entropy results in Table 6, FML show a higher mixing of membership outputs due to deep-water estimation difficulty. When the soft data reference is available, Euclidean Distance approach can be used. Euclidean Distance results for Enrique Reef scene shown in Table 6 were computed using LMM abundances as soft reference data. SFCM obtained the lower Euclidean Distance value which means minor difference between SFCM estimated membership outputs and LMM membership values.

Table 6: Measures Degree of Mixing for SFCM, FSCS, FML, and LMM

Classes	LMM	SFCM	FSCS	FML
Min Entropy	0	0.0016	0	0.0707
Max Entropy	0.7305	0.6900	0.6931	0.6980
Mean Entropy	0.3830	0.3462	0.0050	0.5476
Euclidean Distance	Used as Soft Reference Data	0.0158	0.0492	0.0646

4.3.7.2 Fuzzy Error Matrix (FEM)

A Fuzzy Error Matrix analysis (see Section 2.3.3.2) (Binaghi et al., 1999) could be a better approach instead of conventional hard assessment to evaluate the performance of soft classifiers when soft ground truth data is available. FEM is an extension of the confusion error matrix but takes into consideration estimated weight fraction to get the producer's, user's, and overall accuracies. The quality of fractional weights used as soft ground truth data is crucial to compute accuracy percentages that really measure the performance of a soft classifier. Therefore, lower overall accuracy does not denote bad performance of a soft classifier. Hence, the expertise of an image analyst will be a plus in the analysis and

interpretation of results. This could be a reason of why FEM is not used as standard accuracy assessment for soft classification.

Tables 8 – 11 shows the FEM of SFCM, FML, FML-LMM (LMM abundances used to initialize FML algorithm) and FSCS approaches using LMM abundances as soft references data. Testing samples used to generate FEM are shown in Figure 48 which were the same as those used for a conventional hard assessment. A bar graph of FEM overall accuracies relative to LMM abundances is shown in Figure 49. Tables 7 shows a perfect matching among estimated and soft reference which represent an ideal case in order to facilitate the interpretation of new measures obtained from SFCM, FML, and FSCS degree of memberships. Accordingly with FEM results, SFCM attained the finest performance obtaining 87% of overall accuracy relative to LMM abundances. Examining FML error matrix which obtained overall accuracy of 65% relative to LMM abundances, we note that producer’s accuracy for deep-water class is 43.2%. This indicates an underestimation of degree of memberships for deep-water class as can be seen in their membership map in Figure 34 (c) and the entropy image in Figure 45. FML using LMM abundances to initialize the FML algorithm obtain a 71% of overall accuracy relative to LMM abundances used as soft reference data. It shows an improvement in comparison with FML outputs. On the other hand, FSCS user’s accuracy relative to LMM abundances for mangrove class is 58.9% which indicates an overestimation of this class as can be appreciated in FSCS membership and thematic maps in Figures 33 (d) and 35 (c).

Table 7: Fuzzy Error Matrix reference derived by a Perfect Matching of testing samples (ideal case)

	R_{DeepWater}	R_{mangrove}	R_{sand}	R_{SeaGrass}	R_{ReefFlat}	Total grades	User's Accuracy
C_{DeepWater}	47.9234	1.2657	3.9842	4.9989	1.7112	47.9234	100.0%
C_{mangrove}	1.2657	9.0763	1.0955	1.796	1.7883	9.0763	100.0%
C_{sand}	3.9842	1.0955	26.9968	3.4309	2.2404	26.9968	100.0%
C_{SeaGrass}	4.9989	1.796	3.4309	34.4129	3.211	34.4129	100.0%
C_{ReefFlat}	1.7112	1.7883	2.2404	3.211	28.5908	28.5908	100.0%
Total grades	47.9234	9.0763	26.9968	34.4129	28.5908		
Producer's Accuracy	100.0%	100.0%	100.0%	100.0%	100.0%		
Overall Accuracy	100.0%						

Table 8: Fuzzy Error Matrix derived from SFCM membership values (C) and LMM abundances used as Soft Reference (R)

	$R_{DeepWater}$	$R_{mangrove}$	R_{sand}	$R_{SeaGrass}$	$R_{ReefFlat}$	Total grades	User's Accuracy
$C_{DeepWater}$	44.3909	1.7085	3.6043	8.4081	1.9723	50.117	88.6%
$C_{mangrove}$	1.298	7.8416	0.8452	1.8201	1.7041		
C_{sand}	2.4217	0.771	23.1321	2.1354	1.0271		
$C_{SeaGrass}$	6.0157	1.6416	4.3233	25.6303	2.8175		
$C_{ReefFlat}$	2.7136	1.5856	3.4278	4.8943	26.677		
Total grades	47.9234	9.0763	26.9968	34.4129	28.5908		
Producer's Accuracy	92.6%	86.4%	85.7%	74.5%	93.3%		
Overall Accuracy	86.9%						

Table 9: Fuzzy Error Matrix derived from FML membership values (C) and LMM abundances used as Soft Reference (R)

	$R_{DeepWater}$	$R_{mangrove}$	R_{sand}	$R_{SeaGrass}$	$R_{ReefFlat}$	Total grades	User's Accuracy
$C_{DeepWater}$	20.6949	0.3547	1.7796	4.205	0.6915	20.8512	99.3%
$C_{mangrove}$	2.8054	7.8116	2.0047	3.617	7.4001		
C_{sand}	12.4903	1.4106	20.7128	8.4714	1.6107		
$C_{SeaGrass}$	19.2057	2.5465	6.5788	23.4983	2.3443		
$C_{ReefFlat}$	4.9374	1.9358	7.8078	10.141	23.6336		
Total grades	47.9234	9.0763	26.9968	34.4129	28.5908		
Producer's Accuracy	43.2%	86.1%	76.7%	68.3%	82.7%		
Overall Accuracy	65.5%						

Table 10: Fuzzy Error Matrix derived from FML-LMM (LMM abundances used to initialize the FML algorithm) membership values (C) and LMM abundances used as Soft Reference (R)

	R _{DeepWater}	R _{mangrove}	R _{sand}	R _{SeaGrass}	R _{ReefFlat}	Total grades	User's Accuracy
C _{DeepWater}	24.2345	0.3447	1.7751	4.1855	0.6816	24.3795	99.4%
C _{mangrove}	2.2937	7.5928	1.992	3.3371	7.566	14.6622	51.8%
C _{sand}	11.5625	1.831	23.3752	8.0598	1.7188	34.1253	68.5%
C _{SeaGrass}	16.3717	2.9081	6.2443	25.7575	2.65	39.3612	65.4%
C _{ReefFlat}	5.9635	1.8708	5.9794	8.9857	23.4693	34.4721	68.1%
Total grades	47.9234	9.0763	26.9968	34.4129	28.5908		
Producer's Accuracy	50.6%	83.7%	86.6%	74.8%	82.1%		
Overall Accuracy	71.0%						

Table 11: Fuzzy Error Matrix derived from FSCS membership values (C) and LMM abundances used as Soft Reference (R)

	R _{DeepWater}	R _{mangrove}	R _{sand}	R _{SeaGrass}	R _{ReefFlat}	Total grades	User's Accuracy
C _{DeepWater}	43.918	0.1512	1.5541	3.8863	0.4901	50	87.8%
C _{mangrove}	0.7958	8.2398	0.4551	1.6579	2.8516	14	58.9%
C _{sand}	1.8895	0.1776	22.8093	1.6112	0.512	27	84.5%
C _{SeaGrass}	0.7524	0.2639	1.2107	25.3405	0.4329	28	90.5%
C _{ReefFlat}	0.5677	0.2438	0.9676	1.917	24.3042	28	86.8%
Total grades	47.9234	9.0763	26.9968	34.4129	28.5908		
Producer's Accuracy	91.6%	90.8%	84.5%	73.6%	85.0%		
Overall Accuracy	84.8%						

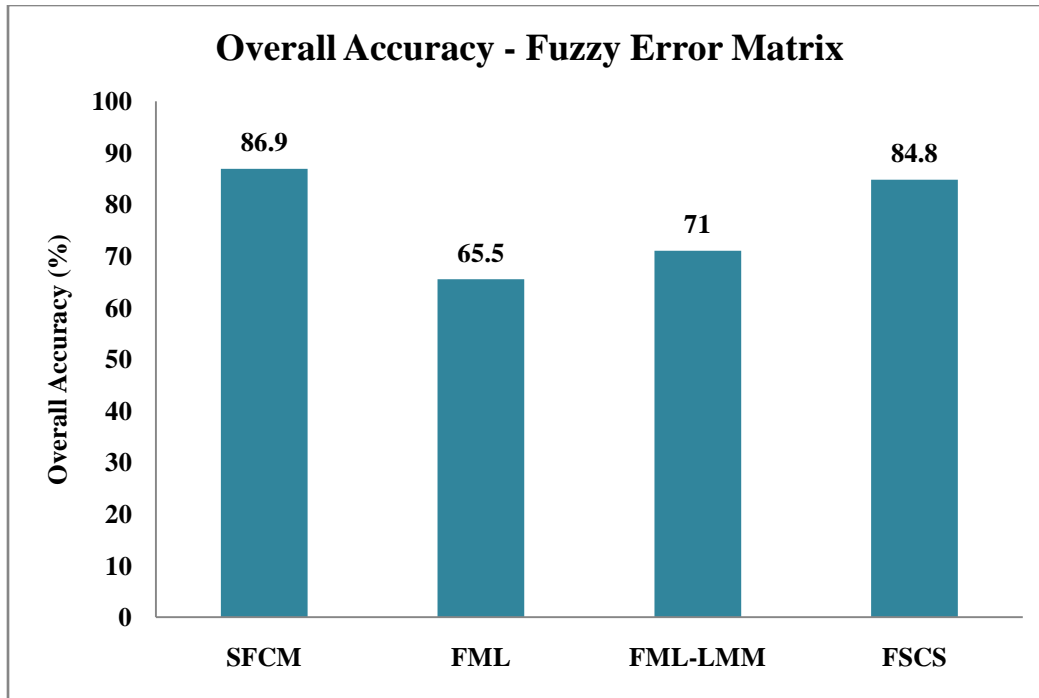


Figure 46: Fuzzy Error Matrix overall accuracy of SFCM, FML, FML-LMM, and FSCS approaches

4.3.7.3 Linear Relationship among Membership Outputs and Soft Reference Data

SSCT also provides the option to generate a scatter plot comparing estimated degree of membership and soft ground truth data in order to measure linear correlation between estimated and actual data. Table 12 illustrates the correlation coefficients and Root Mean Square (RMS) error obtained for SFCM, FSCS, and FML approaches. LMM abundances were used as soft reference data. The LMM abundances and SFCM were found to be strongly and significant correlated by correlation coefficient average of 87.4%. Scatter plots for each SFCM land cover composition is shown in Figure 47. Mangrove, sand, reef flat, and deep water are strongly correlated obtaining correlation coefficients of 0.93, 0.92, 0.89, and 0.92 respectively. Examining the RMS error, we can see that SFCM obtained the lower RMS error relative to LMM abundances as shown in Table 12. Accordingly with results shown in this chapter where LMM abundances were used as soft reference data in order to show SSCT Accuracy Assessment module functionalities and to compare fuzzy classification methods with a LMM approach, SFCM seems that takes into consideration the mixing of pixels as part of the classification process. Therefore, it could

produce a decomposition of a pixel into its constituent spectra comparable as LMM can do from fuzzy point of view.

Table 12: Correlation coefficient (ρ_{XY}) and RMS error of SFCM, FML, and FSCS using LMM abundances as soft reference data

Classes	Correlation Coefficient			RMS Error		
	SFCM	FML	FSCS	SFCM	FML	FSCS
Deep Water	0.9173	0.9338	0.9112	0.1500	0.1349	0.1552
Mangrove	0.9324	0.6631	0.5256	0.0317	0.0656	0.0746
Sand	0.9230	0.5699	0.8586	0.0776	0.1658	0.1034
Sea Grass	0.7048	0.3619	0.6319	0.1799	0.2363	0.1965
Reef Flat	0.8905	0.6846	0.8085	0.1001	0.1604	0.1292
Average	0.8736	0.6427	0.7473	0.1079	0.1526	0.1318

4.3.7.4 Conventional Hard Assessment

The most widely used method for hard classification assessment is known as Confusion Error Matrix (refer to Section 2.3.3). In the majority of cases, image analyst does not have available soft ground truth data to perform a fuzzy error matrix. In that case, a conventional hard assessment could be conducted to evaluate a thematic map derived from a hardening process although it is not the best way to evaluate the performance of soft classifiers. Commonly, testing samples are selected from “pure” or almost “pure” pixels because we have to know the label of those pixels in order to relate it to producer’s or user’s accuracy in confusion matrix analysis. As a result, we expect that soft and hard classifiers obtain a higher overall accuracy as shown in Figure 49 while soft and hard algorithms obtained an overall accuracy above 90%. Accordingly with these results, FML obtained the lower accuracy of 89.2% inclusive below ML algorithm but if we compare FML and ML classification maps (see Figure 35 (d) and (f)) with land cover references (refer to Section 4.3.2), we can see that FML improved classification result especially for mangrove and sand classes. FML using LMM abundances to initialize the algorithm obtained accuracy of 94% improving FML performance in terms of overall accuracy percentage and

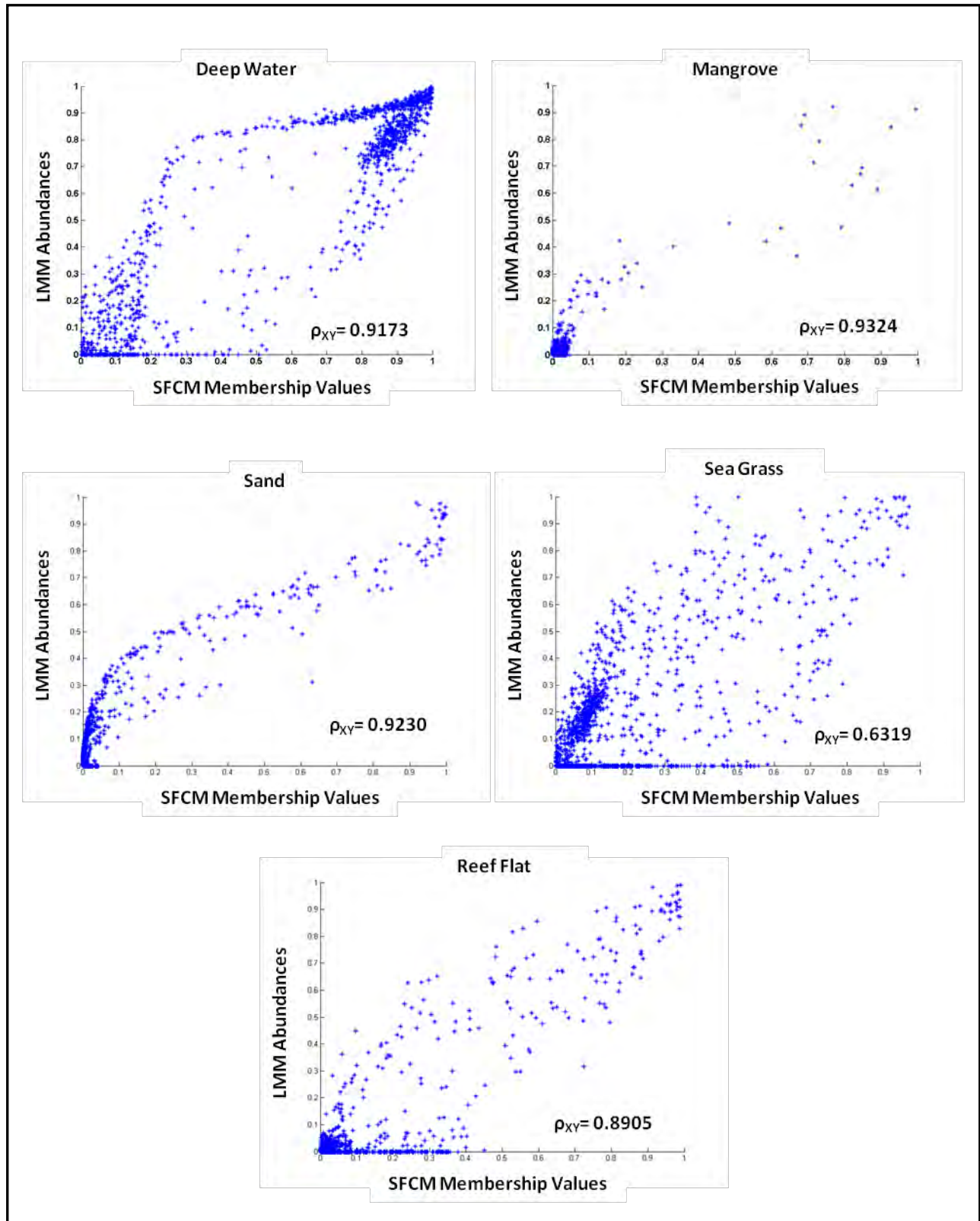
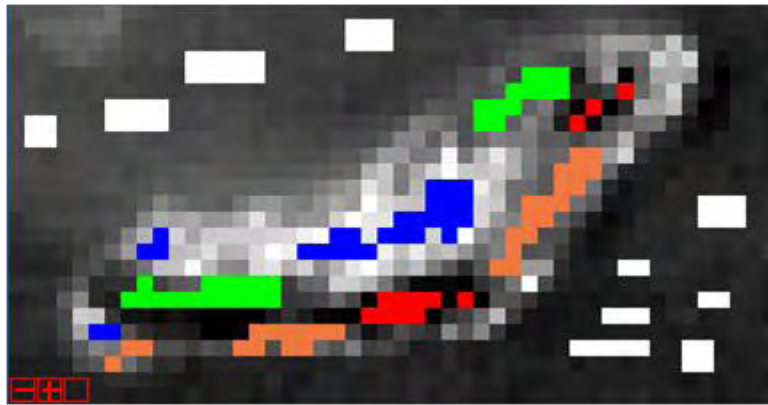


Figure 47: Relationships between SFCM and LMM for deep water, mangrove, sand, sea grass, and reef flat informational classes

classification maps (see Figure 35 (d)-(e)). Figure 48 (white for deep-water, green for sea-grass, red for mangrove, blue for sand, and coral for reef-flat) shows testing samples selected for a confusion error matrix analysis shown in Tables 13-18 for LMM, SFCM, FML,FML-LMM, FSCS, and ML approaches, respectively.



(a)

Cover Type	No. of Samples
Deep Water	50
Mangrove	12
Sand	27
Sea Grass	28
Reef Flat	30

(b)

Figure 48: (a) Enrique Reef Testing Samples selected for a hard assessment, (b) Number of samples per informational class

Table 13: Confusion Error Matrix of a LMM thematic map derived by a hardening LMM abundance maps

	Deep Water	Mangrove	Sand	Sea Grass	Reef Flat	User's Accuracy
Deep Water	50	0	0	0	0	100%
Mangrove	0	9	0	0	0	100%
Sand	0	0	27	0	0	100%
Sea Grass	0	2	0	28	0	93.3%
Reef Flat	0	1	0	0	30	96.8%
Number of Testing Samples	50	12	27	28	30	
Producer's Accuracy	100%	75%	100%	100%	100%	
Overall Accuracy		98.0%				

Table 14: Confusion Error Matrix of a SFCM thematic map derived by a hardening SFCM membership maps

	Deep Water	Mangrove	Sand	Sea Grass	Reef Flat	User's Accuracy
Deep Water	50	0	0	2	0	96.2%
Mangrove	0	12	0	0	0	100%
Sand	0	0	27	0	0	100%
Sea Grass	0	0	0	28	0	100%
Reef Flat	0	0	0	0	30	100%
Number of Testing Samples	50	12	27	28	30	
Producer's Accuracy	100%	100%	100%	93.3%	100%	
Overall Accuracy		98.7%				

Table 15: Confusion Error Matrix of a FML thematic map derived by a hardening FML membership maps

	Deep Water	Mangrove	Sand	Sea Grass	Reef Flat	User's Accuracy
Deep Water	50	0	0	0	0	100%
Mangrove	0	12	0	0	3	80%
Sand	0	0	22	3	0	88%
Sea Grass	0	0	1	20	0	95.2%
Reef Flat	0	0	4	5	27	75%
Number of Testing Samples	50	12	27	28	30	
Producer's Accuracy	100%	100%	81.5%	71.4%	90%	
Overall Accuracy		89.2%				

Table 16: Confusion Error Matrix of a FML-LMM (LMM abundances used to initialize the FML algorithm) thematic map derived by a hardening FML-LMM membership maps

	Deep Water	Mangrove	Sand	Sea Grass	Reef Flat	User's Accuracy
Deep Water	50	0	0	0	0	100%
Mangrove	0	12	0	0	3	80%
Sand	0	0	26	2	0	92.9%
Sea Grass	0	0	1	23	0	95.8%
Reef Flat	0	0	0	3	27	90%
Number of Testing Samples	50	12	27	28	30	
Producer's Accuracy	100%	100%	96.3%	82.1%	90%	
Overall Accuracy		93.9 %				

Table 17: Confusion Error Matrix of a FSCS thematic map derived by a hardening FSCS membership maps

	Deep Water	Mangrove	Sand	Sea Grass	Reef Flat	User's Accuracy
Deep Water	50	0	0	0	0	100%
Mangrove	0	12	0	0	2	85.7%
Sand	0	0	27	0	0	100%
Sea Grass	0	0	0	28	0	100%
Reef Flat	0	0	0	0	28	100%
Number of Testing Samples	50	12	27	28	30	
Producer's Accuracy	100%	100%	100%	100%	93.3%	
Overall Accuracy		98.6 %				

Table 18: Confusion Error Matrix of a ML thematic map

	Deep Water	Mangrove	Sand	Sea Grass	Reef Flat	User's Accuracy
Deep Water	50	0	0	0	0	100%
Mangrove	0	12	0	0	7	63.2%
Sand	0	0	27	0	0	100%
Sea Grass	0	0	0	27	0	100%
Reef Flat	0	0	0	1	23	95.8%
Number of Testing Samples	50	12	27	28	30	
Producer's Accuracy	100%	100%	100%	96.4%	76.7%	
Overall Accuracy		94.6 %				

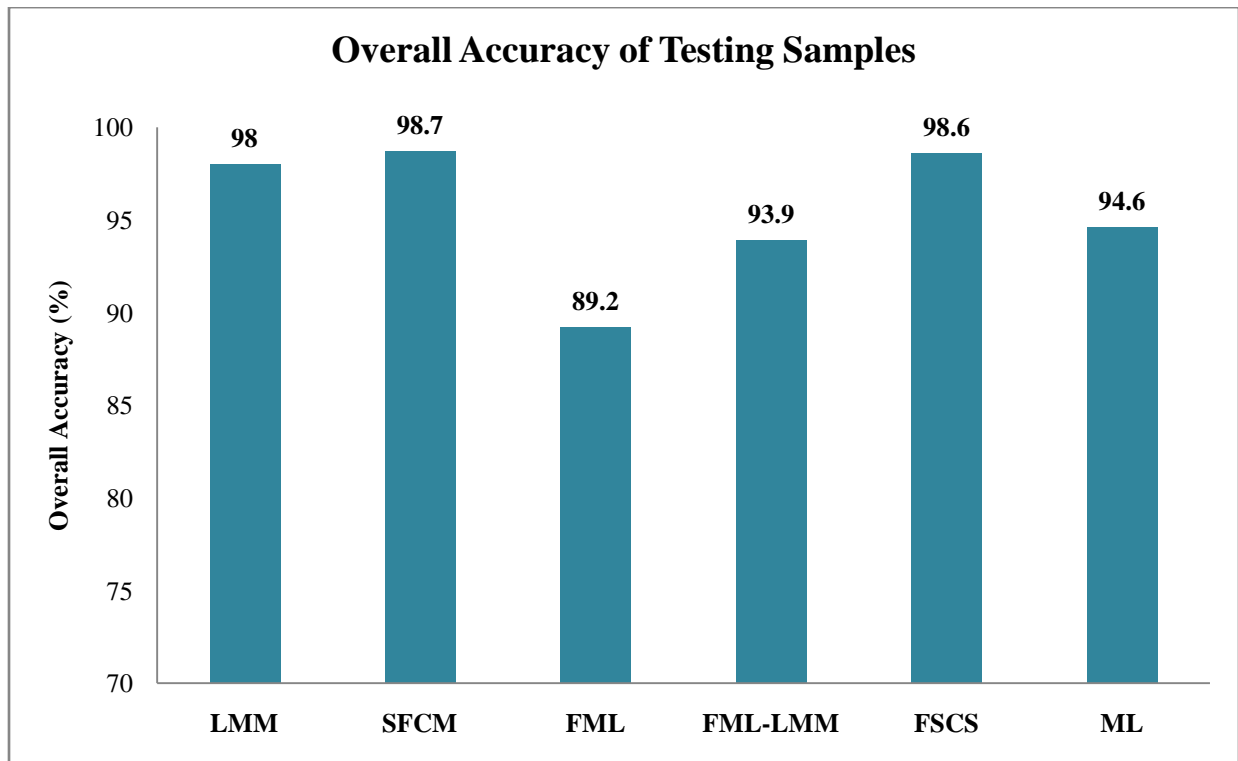


Figure 49: Confusion error matrix overall accuracy percentage of testing samples of LMM, SFCM, FML, FML-LMM, ML, and FSCS approaches

4.4 Summary

This chapter explained the Spectral Soft Classification Tool (SSCT) functions in term of soft classification algorithms (LMM, SFCM-Euclidean norm, FSCS, and FML), visualization techniques for membership outputs and thematic maps derived from membership maps, and accuracy assessment to evaluate the performance of soft classifiers which can give a better idea of how softness data is when a combination of techniques are applied. An Enrique Reef, La Parguera, Puerto Rico scene was used to explain the SSCT capabilities.

CHAPTER 5

Experimental Results using Real Data

This chapter presents results of applying the SSCT to an ETM+ image from Lajas, Puerto Rico. Membership maps and classification maps derived from a soft classification using LMM, FML, SFCM, and FSCS algorithms are studied in this chapter.

5.1 Multispectral Case Study

A description of the Enhanced Thematic Mapper (ETM)+⁹ and characteristics of the imagery used for experimental results are summarized next. The multispectral imagery was acquired on February 20, 2002 using an ETM+ on-board Landsat 7. ETM+ has a spectral resolution of 7 bands from visible to the long infrared region of the electromagnetic spectrum and 1 panchromatic band. It has a temporal resolution of 16 days and radiometric resolution of 8 bits with a swath width of 185 km. Table 19 summarizes specifications of the ETM+ sensor. The imagery data was downloaded at no cost from the Global Land Cover Facility (GLCF)¹⁰ at the University of Maryland. A subset of 752 x 212 pixels shown in Figure 50 was performed in order to generate a land remote sensed scene around Lajas, PR. A spectral subset also was performed to use bands 1 – 5, 7 with a 30m of spatial resolution for classification processes.

Table 19: Specifications of ETM+ sensor on – board Landsat 7

Band / Channel	Region of Electromagnetic Spectrum	Wavelength (λ) - μm	Spatial Resolution (meters)
Band 1	Visible - Blue	0.45 – 0.52	30m
Band 2	Visible - Green	0.52 – 0.60	30m
Band 3	Visible - Red	0.63 – 0.69	30m
Band 4	Near Infrared (NIR)	0.76 – 0.90	30m
Band 5	Middle Wave Infrared (MWIR)	1.55 – 1.75	30m
Band 6	Far Infrared (thermal)	10.40 – 12.50	60m
Band 7	MWIR	2.08 – 2.3	30m
Band 8	Panchromatic (PAN)	0.52 - 0.90	15m

⁹ Landsat 7 Science Data Users Handbook: <http://landsathandbook.gsfc.nasa.gov/handbook.html>

¹⁰ GLCF is a center for land cover change research using remotely sensed satellite data. Through the Earth Science Data interface (ESDI) at GLCF, it is possible to download scenes from different sensors at no cost. <http://www.landcover.org/index.shtml>

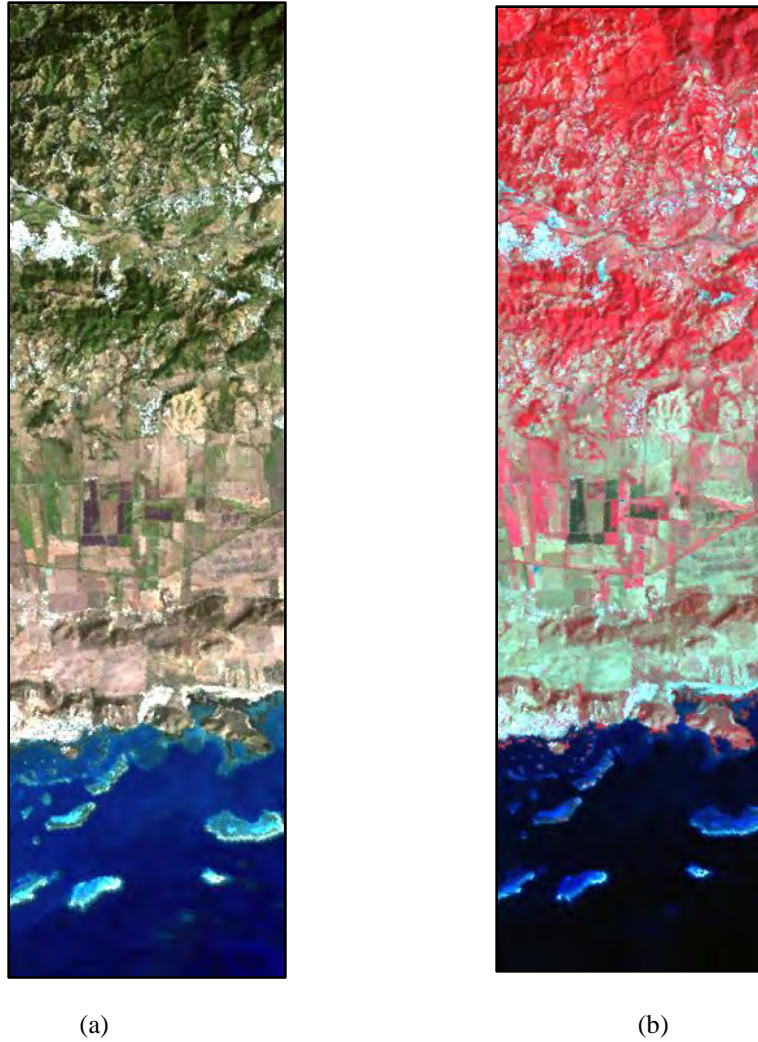
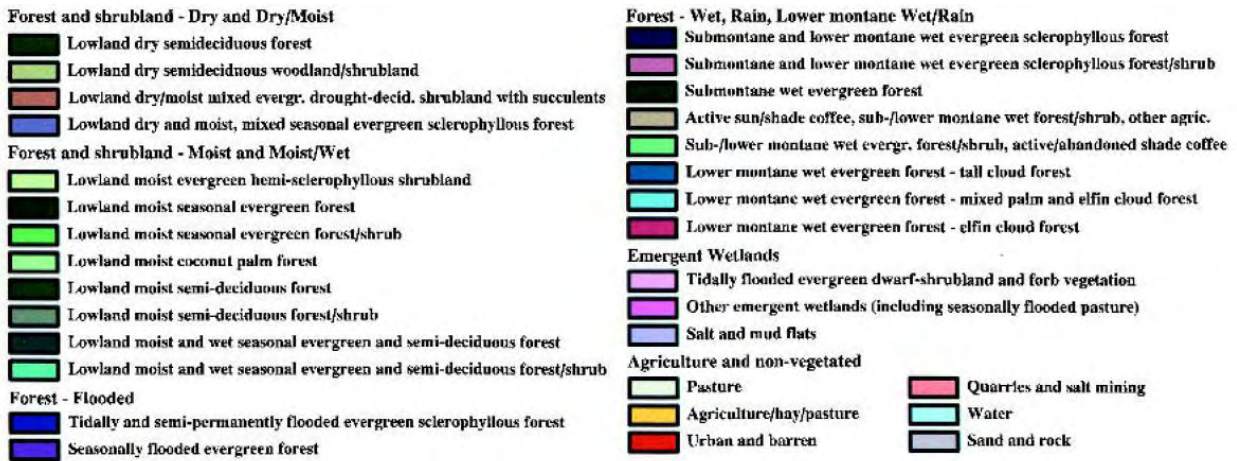
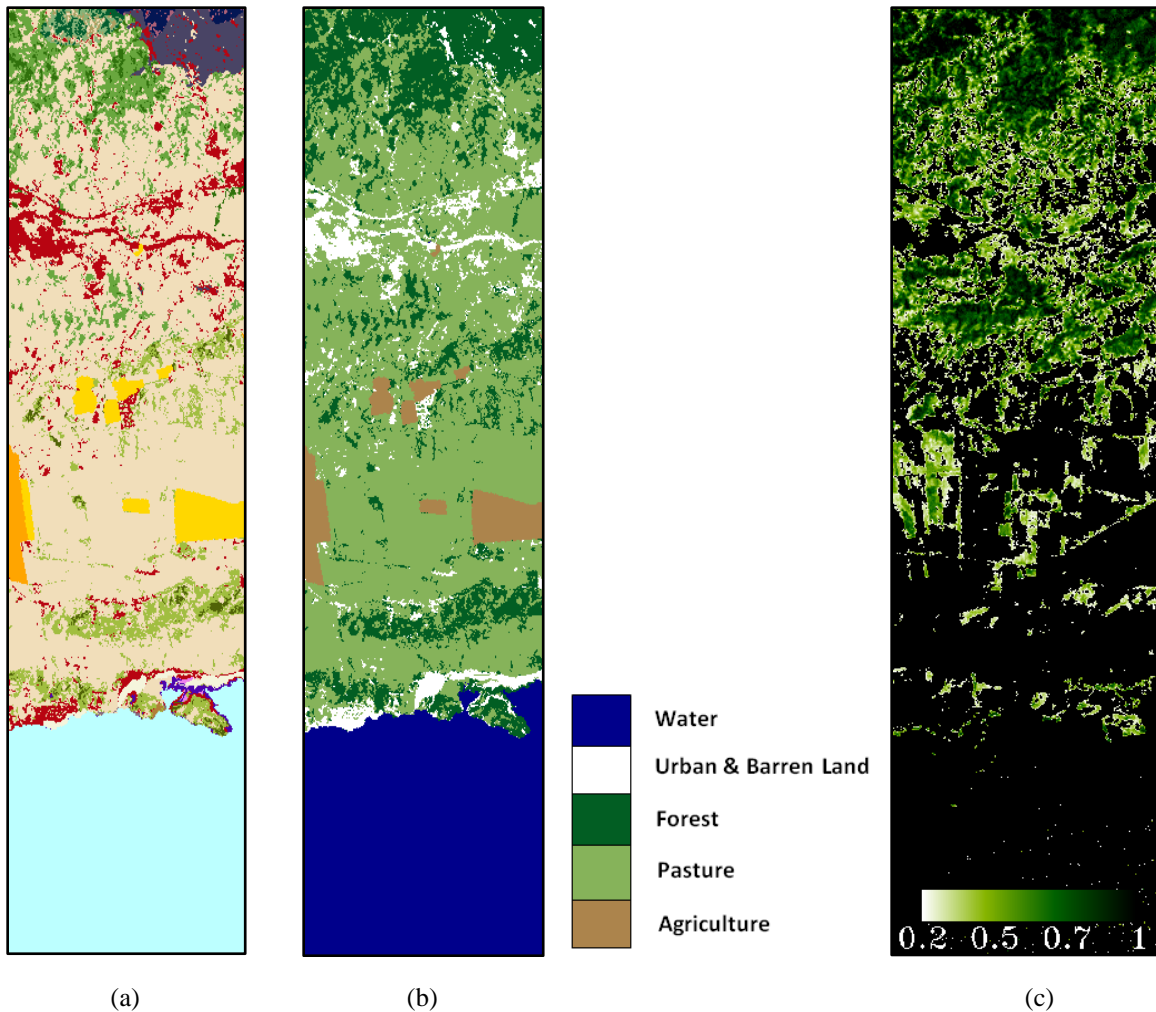


Figure 50: A true color (bands 3-2-1) and color infrared images (bands 4-3-2) of Lajas, PR scene acquired with an ETM+ sensor.

5.1.1 Ground Truth Reference: USDA Puerto Rico Land Cover 1991

We have used the USDA PR Land Cover 1991 (Helmer et al., 2002) shown in Figure 51 (a)-(b) to select representative training samples of informational classes. Due to spatial resolution limitation, it is not appropriate to use the original land cover types shown in Figure 51 (a) and (d). Figure 51 (b) shows a modification of land cover types using only five informational classes: water, urban and barren land, forest, pasture, and agriculture. Normalized Difference Vegetation Index (NDVI) (Schowengerdt 2007) was computed to compare the membership maps and thematic maps obtained with soft classification algorithms for a forest class. NDVI could be useful to evaluate this area taking into consideration the difference in years between Land Cover Reference (1991) and multispectral imagery (2002).



(d)

Figure 51: USDA Puerto Rico Land Cover Reference 1991 (Helmer et al., 2002) (a) Original Thematic Map, and (b) Modified thematic map after perform a merge of classes, (c) NDVI of a scene, (d) legend of USDA Land Cover showed in (a)

A distribution in terms of number of pixels and approximate area coverage of original land cover types present in the Lajas scene and how those classes were merge into new informational classes is described in Table 20.

Table 20: Distribution of original and modified land cover types of the USDA PR Land Cover 1991 (Helmer et al., 2002) for classification purposes

Original land cover types in Lajas, PR scene (USDA PR Land Cover 1991)	Num. of pixels per class	Percentage area coverage (%)	Modified land cover types	Num. of pixels per class	Percentage area coverage (%)
Water	40,187	25.21	Water	40,187	25.21
Pasture	77,925	48.88	Agriculture	83,222	52.2
Agriculture	5,297	3.32			
Lowland dry semi deciduous forest	1,014	0.64			
Lowland dry semi deciduous woodland/shrub land	8,336	5.23			
Lowland dry mixed evergreen drought-deciduous shrub land with succulents	58	0.04			
Lowland dry and moist, mixed seasonal evergreen sclerophyllous forest	3,566	2.24			
Lowland moist seasonal evergreen forest/shrub	10,255	6.43			
Submontane and lower montane wet evergreen sclerophyllous forest	711	0.45	Forest	25,850	16.21
Submontane wet evergreen forest	552	0.35			
Active sun/shade coffee, submontane and lower montane wet forest/shrub	271	0.17			
Submontane and lower montane wet evergreen forest/shrub and active/abandoned shade coffee	654	0.41			
Tidally and semi-permanently flooded evergreen sclerophyllous forest	433	0.27			
Urban & Barren	9,251	5.80	Urban & Barren Land	10,165	6.38
Sand & Rock	914	0.57			
TOTAL	159,424	100		159,424	100

5.1.2 Soft Classification Results

SFCM, FML, LMM, and FSCS algorithms were applied to an atmospherically corrected multispectral image using the dark subtract band minimum algorithm available in ENVI® (ITT Visual Information Solutions 2007). Figure 52 shows the spectral response of water, urban & barren, forest, pasture, agriculture classes selected manually from the image. These endmembers were used to obtain LMM-1 membership maps shown in Figure 53. As a comment, LMM-1 refers to LMM using endmembers selected manually from the image. A classification map derived from a hardening process of LMM-1 membership maps is shown in Figure 54 (a). Figure 54 (b) shows a thematic map with the unclassified class which was produced by a threshold of 0.50. The USDA PR Land Cover 1991 is shown in Figure 54 (c) in order to compare classification results.

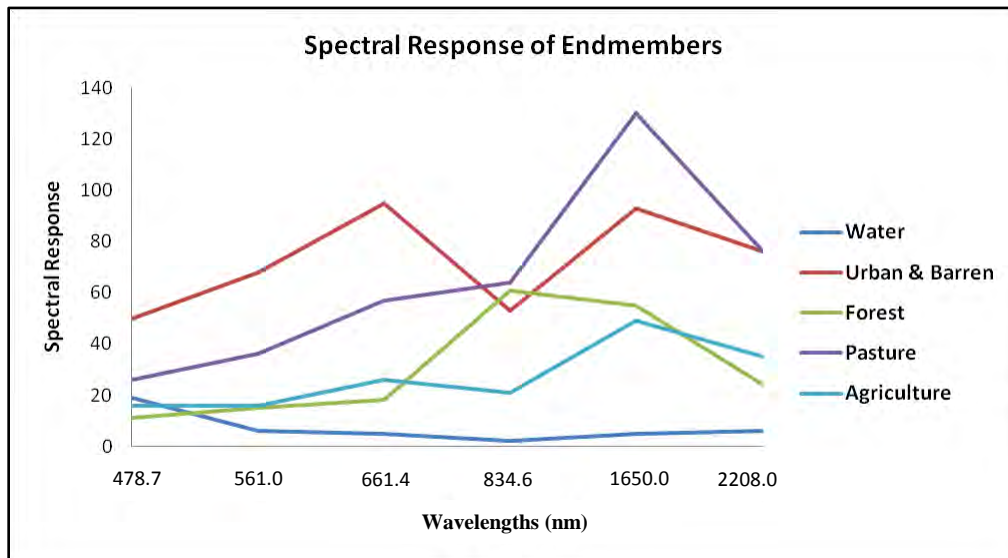


Figure 52: Spectral response of informational classes used to compute LMM-1

Due to the complexity of scene in terms of the number of endmembers that could be representative of materials present in the scene based on the USDA Land Cover Reference (Helmer et al., 2002) shown in Figure 51 (a), and the low spectral resolution of the sensor to discriminate between two classes with similar spectral response such as agriculture and pasture cover types, LMM-1 computed using PPI (Boardman 1993)(Boardman et al., 1995) or endmembers selected manually from the image is not working completely well for water, and pasture classes. An agriculture class is detected in forest

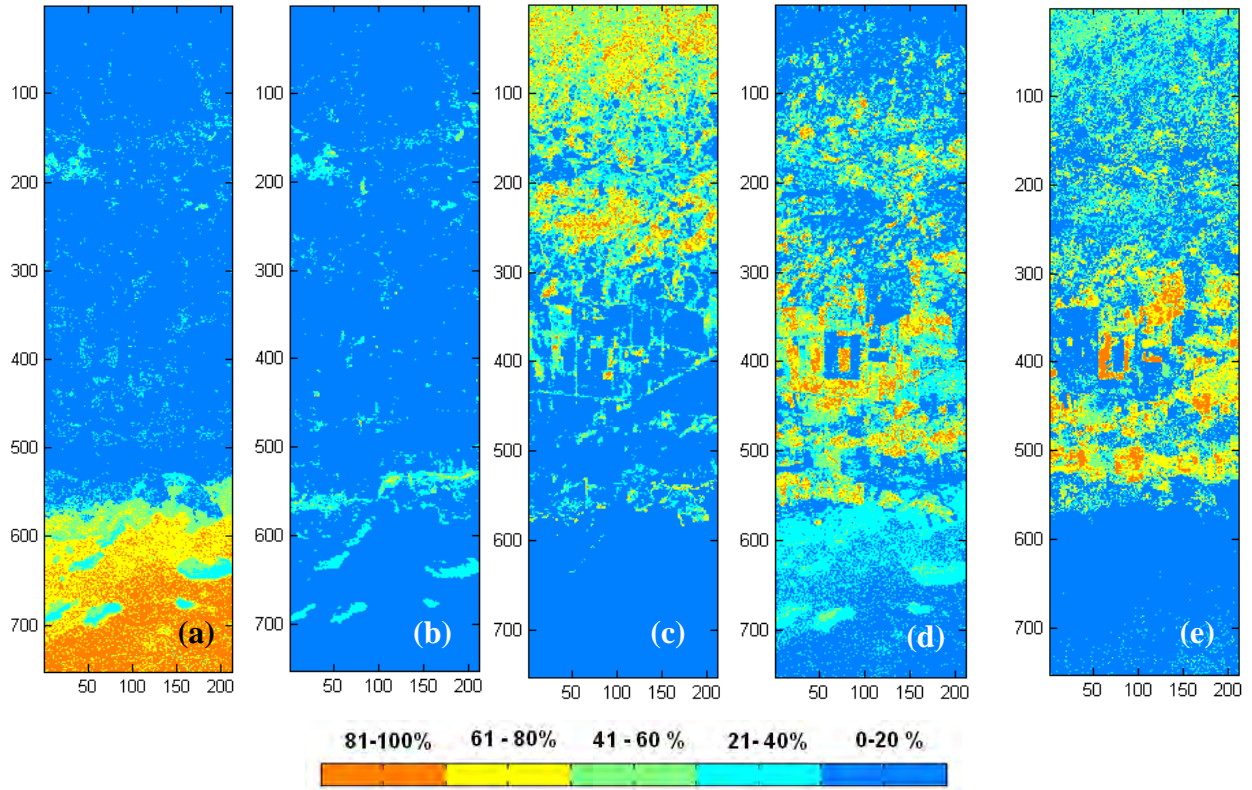


Figure 53: Membership maps obtained using a LMM-1 (endmembers selected manually from the image) of (a) Water, (b) Urban and Barren Land, (c) Forest, (d) Pasture, and (e) Agriculture. A scale based on ranges were used (0-20%, 21-40%, 41-60%, 61-80%, and 81-100%)

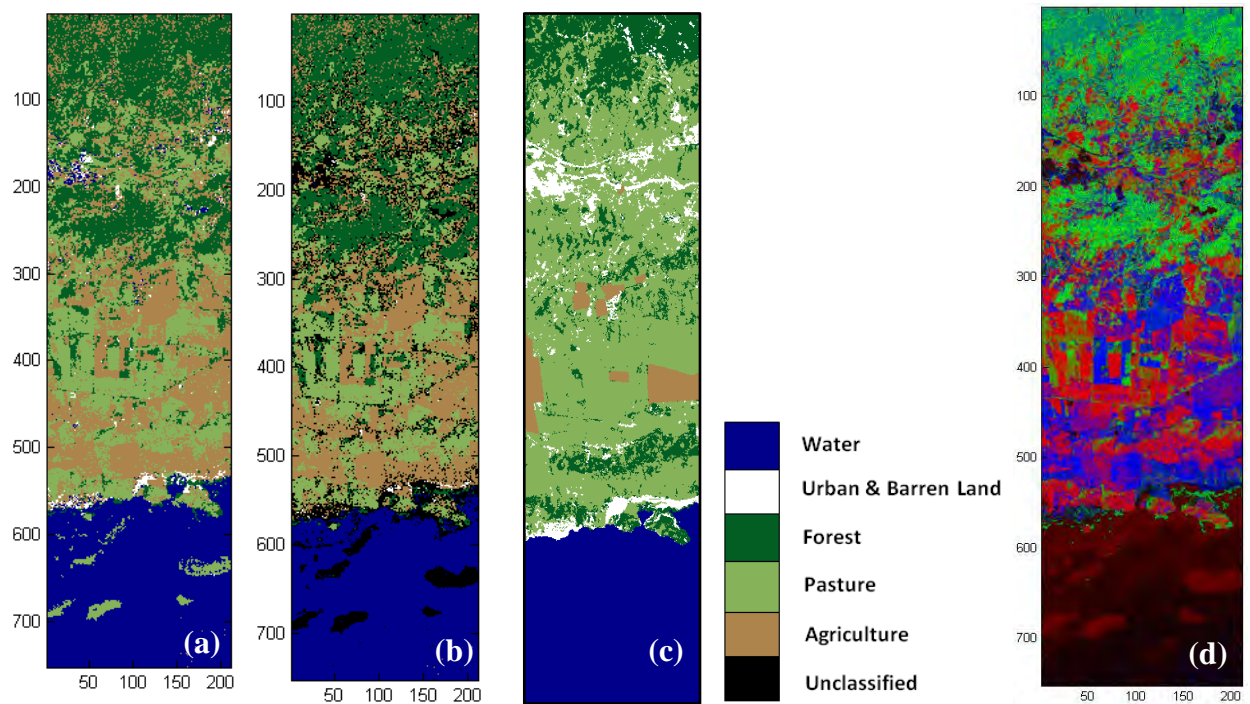


Figure 54: (a) Classification map derived from LMM-1 hardening process, (b) threshold of 0.5 was applied, (c) USDA PR Land Cover Reference 1991 (Helmer et al., 2002), and (d) LMM-1 Fractional Map, R-Pasture, G-Forest, B-Agriculture

areas according to NDVI output (see Figure 51 (c)). However, comparing NDVI output (see Figure 51 (c)) and Land Cover Reference (see Figure 54 (c)) the classification map derived from a hardening process and shown in Figure 54 (a) seemed to capture this class accurately. The fractional map shown in Figure 54 (d) where the degree of memberships from pasture, forest, and agriculture classes were assigned to RGB channels respectively gives us an idea of the mixing among these classes especially between pasture and agriculture classes.

The second approach based on Positive Matrix Factorization (PMF) (Masalmah and Vélez-Reyes 2007) was used in order to determine a better representation of endmembers especially for water, pasture, and agriculture classes. A PMF algorithm developed by Masalmah and Vélez-Reyes was applied to land remote sensed scene using endmembers selected manually for LMM-1 to initialize the algorithm (refers in this work as LMM-2 for differentiation of LMM-1). We found that 5 or 10 iterations performed well to refine the spectral response of the endmembers selected manually from the image. If a higher number of iterations are used, the algorithm can find new spectral responses that could correspond to other materials in the scene which are not necessarily related to the informational classes chosen previously. Figure 55 shows spectral response of water, urban & barren, forest, pasture, agriculture classes derived from the PMF algorithm.

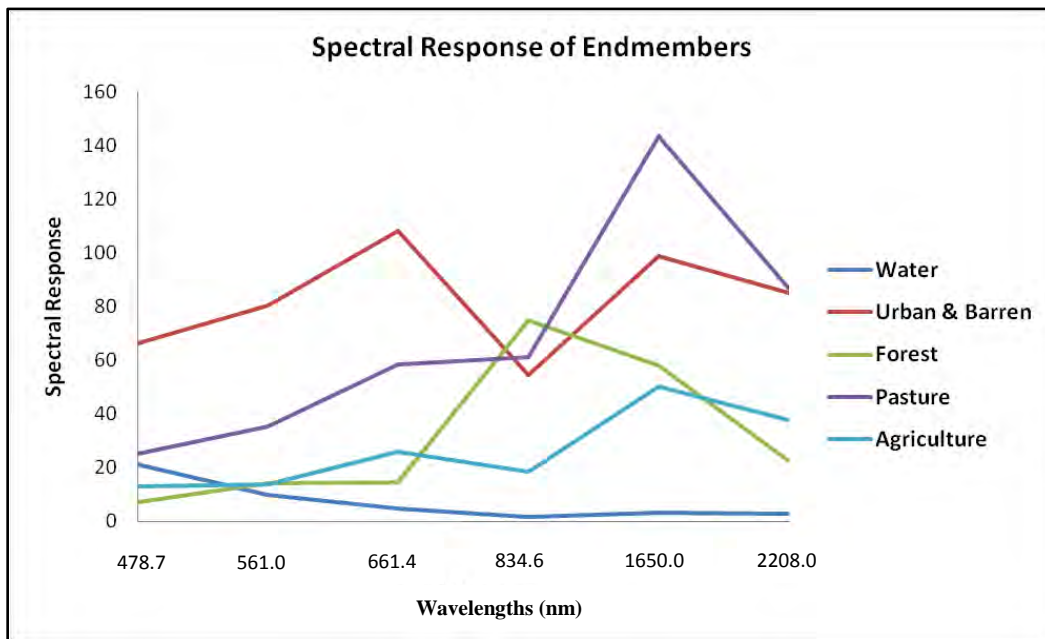


Figure 55: Spectral response of informational classes used to compute LMM-2 (derived from PMF algorithm (Masalmah and Vélez-Reyes 2007))

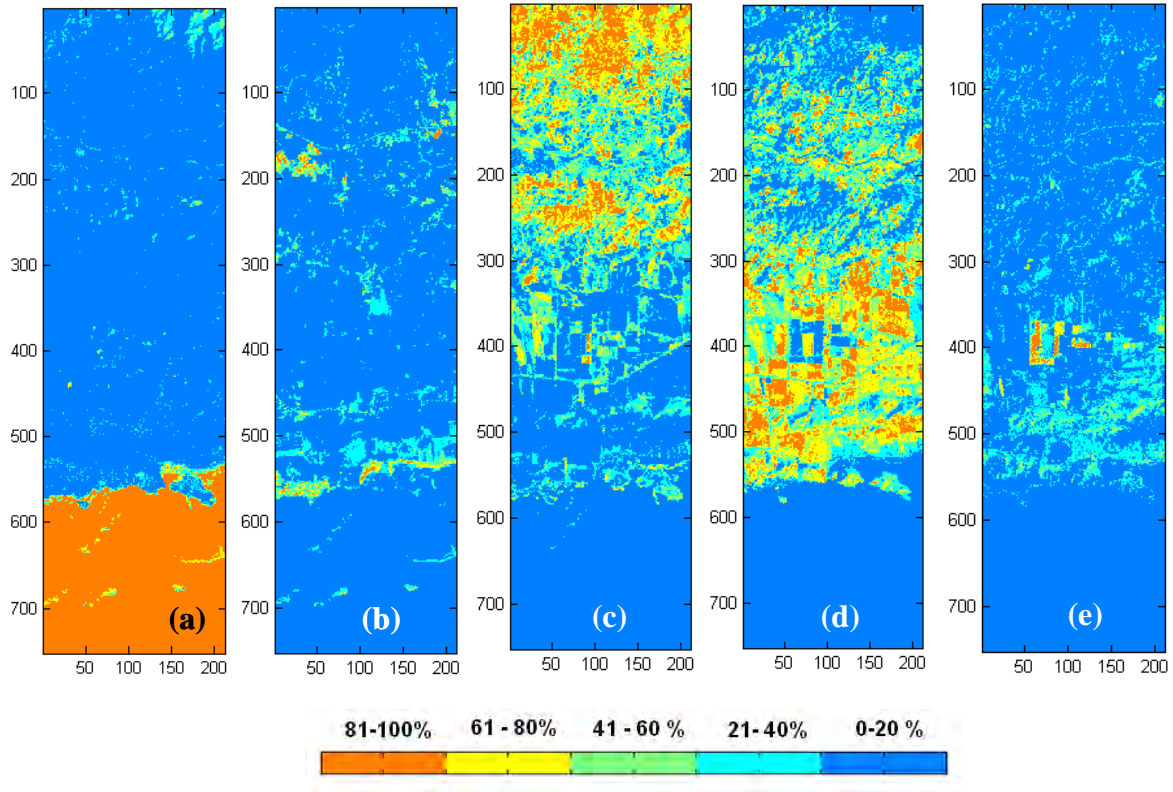


Figure 56: Membership maps obtained using a LMM-2 (PMF initialized with endmembers selected manually from the image) of (a) Water, (b) Urban and Barren Land, (c) Forest, (d) Pasture, and (e) Agriculture. A scale based on ranges were used (0-20%, 21-40%, 41-60%, 61-80%, and 81-100%)

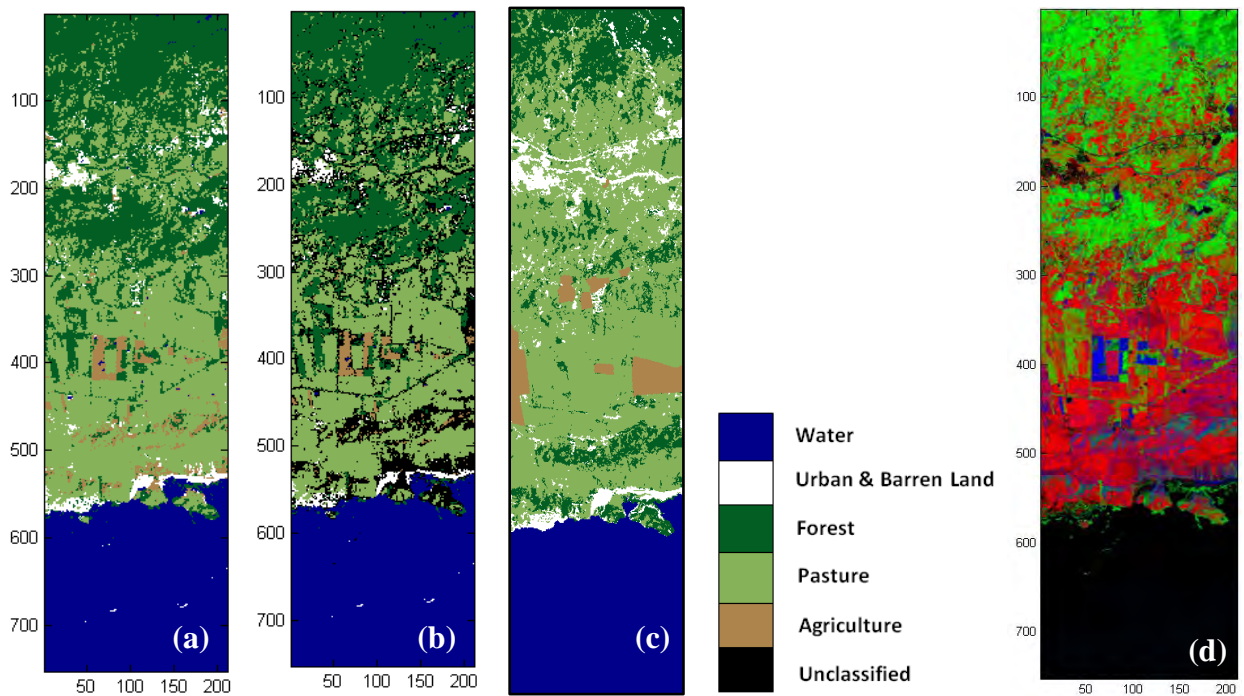


Figure 57: (a) Classification map derived from LMM-2 hardening process (b) threshold of 0.5 was applied, (c) USDA PR Land Cover Reference 1991 (Helmer et al., 2002), and (d) LMM-2 Fractional Map, R-Pasture, G-Forest, B-Agriculture

Figure 56 (a) – (e) shows membership maps obtained from a LMM-2. As can be seen in Figure 56 (a) – (e), membership maps obtained with LMM-2 approach improves the output in comparison with LMM-1. Water class is uniformly defined with higher degree of membership for their region. Comparing NDVI output (see Figure 51 (c)), we can see that pixels with higher degree of membership for a forest class correspond to the pixels which obtained high NDVI values. In addition, agriculture membership map shows a reduction in pixels assigned to agriculture which were saturated using LMM-1. However, the use of a high spectral resolution sensor in the case of LMM-1 could improve the performance of the classifier because it provides a higher discrimination between materials which has similar spectral signatures. Figure 57 (d) shows a fractional map where the degree of memberships from pasture, forest, and agriculture classes were assigned to RGB channels respectively. The fractional map shown in Figure 57 (d) shows the mixing among pasture and agriculture classes and between pasture and forest in the boundaries or transition zones among these informational classes.

The classification maps derived from hardening of LMM-2 membership maps including the unclassified class are shown in Figures 57 (a)-(b). It performed well in comparison with NDVI output (see Figure 51 (c)) and Land Cover Reference Figure 57 (c). The unclassified pixels in Figure 57 (b) are located mainly in urban and barren areas which has sense because this class in practical situations is comprised by various land cover types.

Figure 58 shows training samples used to train (a) SFCM and FSCS algorithms. FML algorithm uses mixed pixels as training data. For that reason, original samples were modified to assure that majority of training samples corresponds to a mixture of classes. FML training samples are shown in Figure 58 (b). Figure 58 (c) shows testing samples used to compute a confusion error matrix.

Membership maps obtained with SFCM are shown in Figure 59 (a) – (e). Comparing them with NDVI output (see Figure 51 (c)) and land cover reference (see Figure 60 (c)), we can see that SFCM performed well in terms to detect the degree of membership per informational class and classification map derived from a SFCM hardening process. The agriculture membership map shows slight saturation of agriculture area that could be due to the fact of training samples used and the low spectral resolution of a ETM+ sensor. The use of a hyperspectral sensor can improve the results for agriculture class because it provides high spectral resolution that could be useful for discriminating between materials which have similar spectral responses such as agriculture and pasture classes. The fractional map shown in Figure 60 (d) where the degree of memberships from pasture, forest, and agriculture classes were assigned to RGB

channels respectively gives us an idea of the mixing among these informational classes and the slight saturation of agriculture class is also appreciated.

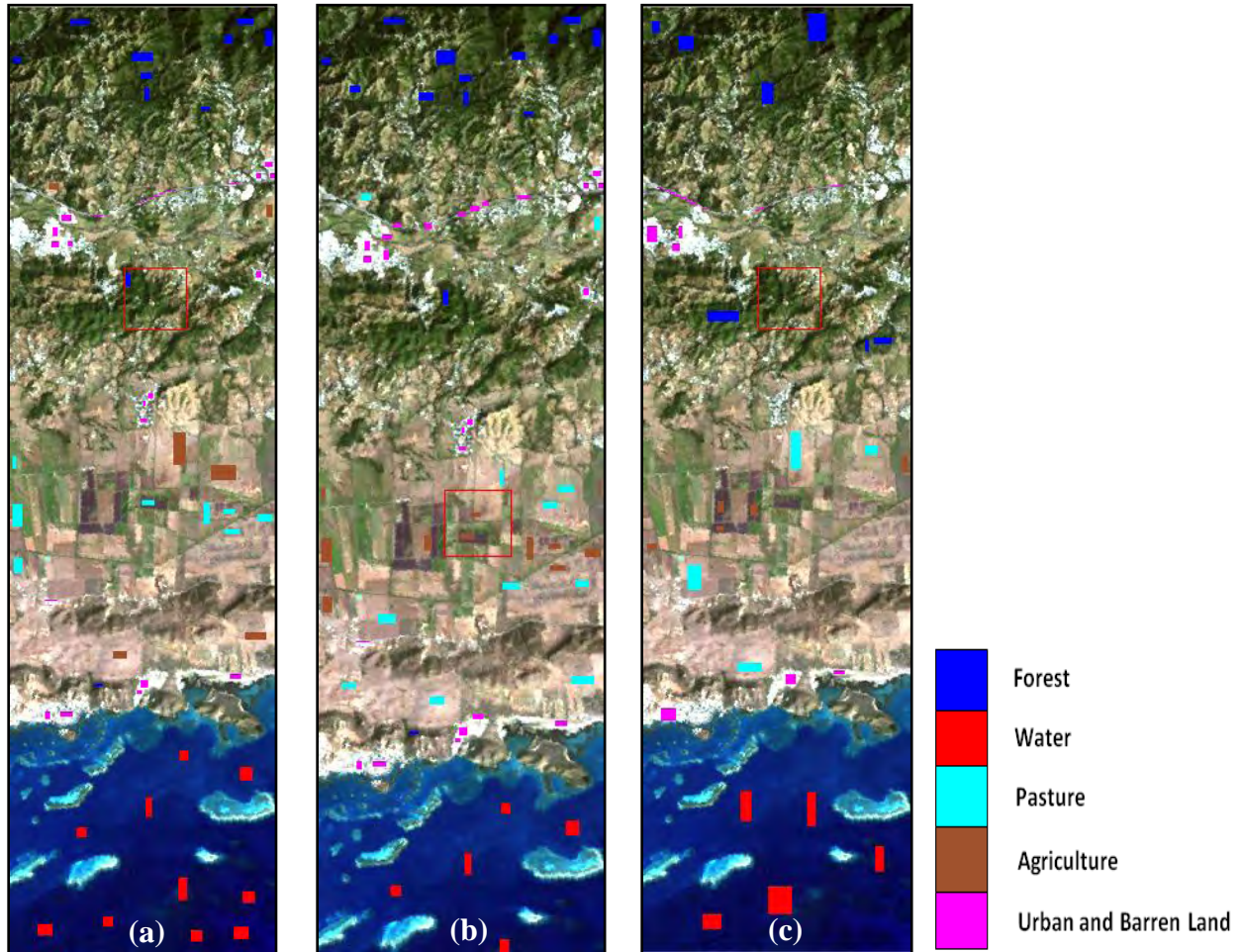


Figure 58: Training samples of (a) SFCM, and FSCS, (b) FML, and (c) testing samples

Figure 61 (a) – (e) shows membership maps obtained with FSCS. As can be seen, FSCS performed well in determining the spatial distribution of informational classes but the majority of degrees of membership per pixel were allocated in the 81-100% range. In addition, FSCS shows a slight saturation of the agriculture class that could be appreciate in the classification map (see Figure 62 (a)) derived from a hardening process and in the fractional map derived from degree of memberships from pasture, forest, and agriculture shown in Figure 62 (c). This can be improved using a hyperspectral imagery which can provide a better discrimination between pasture and agriculture class because of the higher spectral resolution.

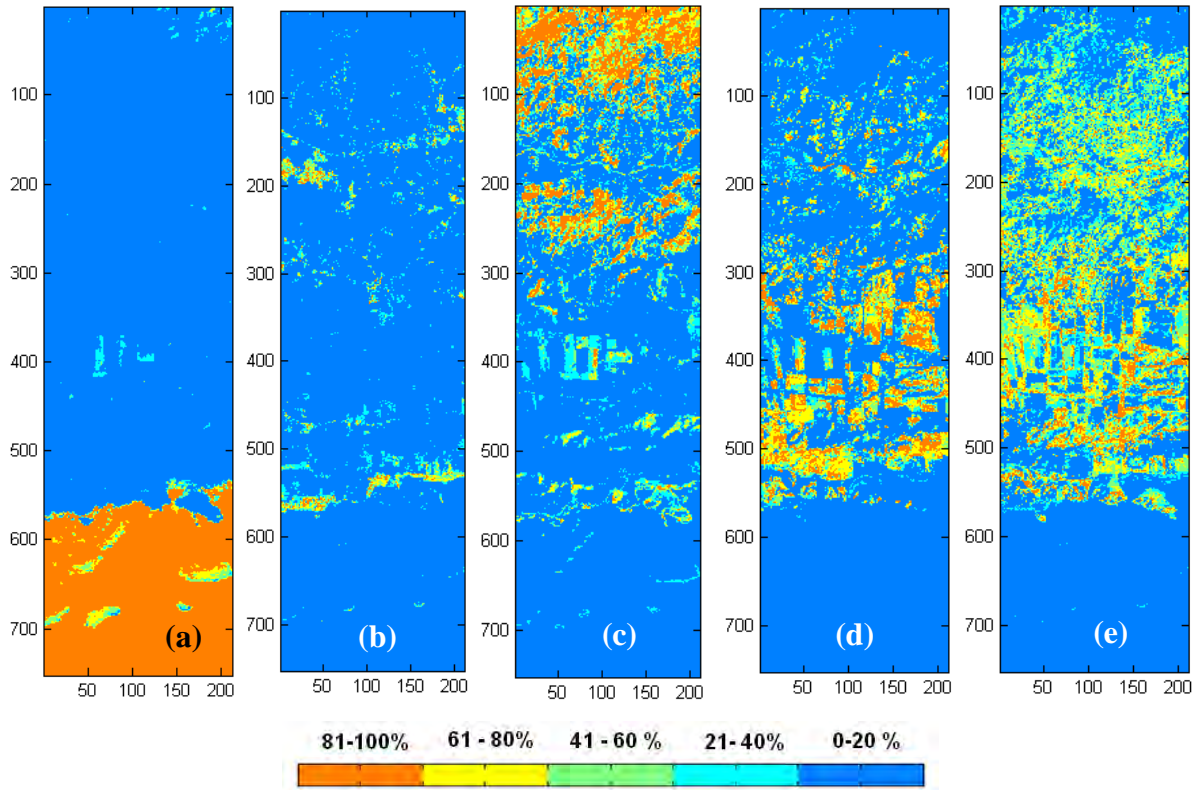


Figure 59: Membership maps obtained using a SFCM-Euclidean Norm of (a) Water, (b) Urban and Barren Land, (c) Forest, (d) Pasture, and (e) Agriculture. A scale based on ranges were used (0-20%, 21-40%, 41-60%, 61-80%, and 81-100%)

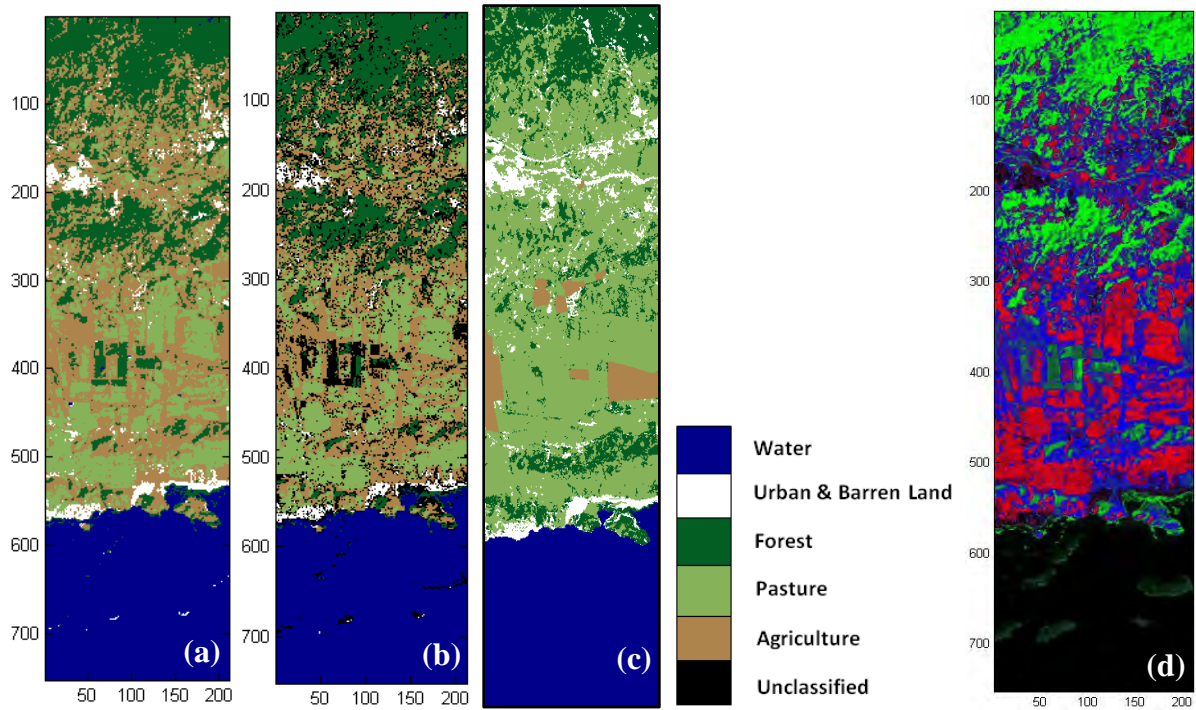


Figure 60: (a) Classification map derived from SFCM-Euclidean Norm hardening process (b) threshold of 0.5 was applied (c) USDA PR Land Cover Reference 1991 (Helmer et al., 2002), and (d) SFCM Fractional Map, R-Pasture, G-Forest, B-Agriculture

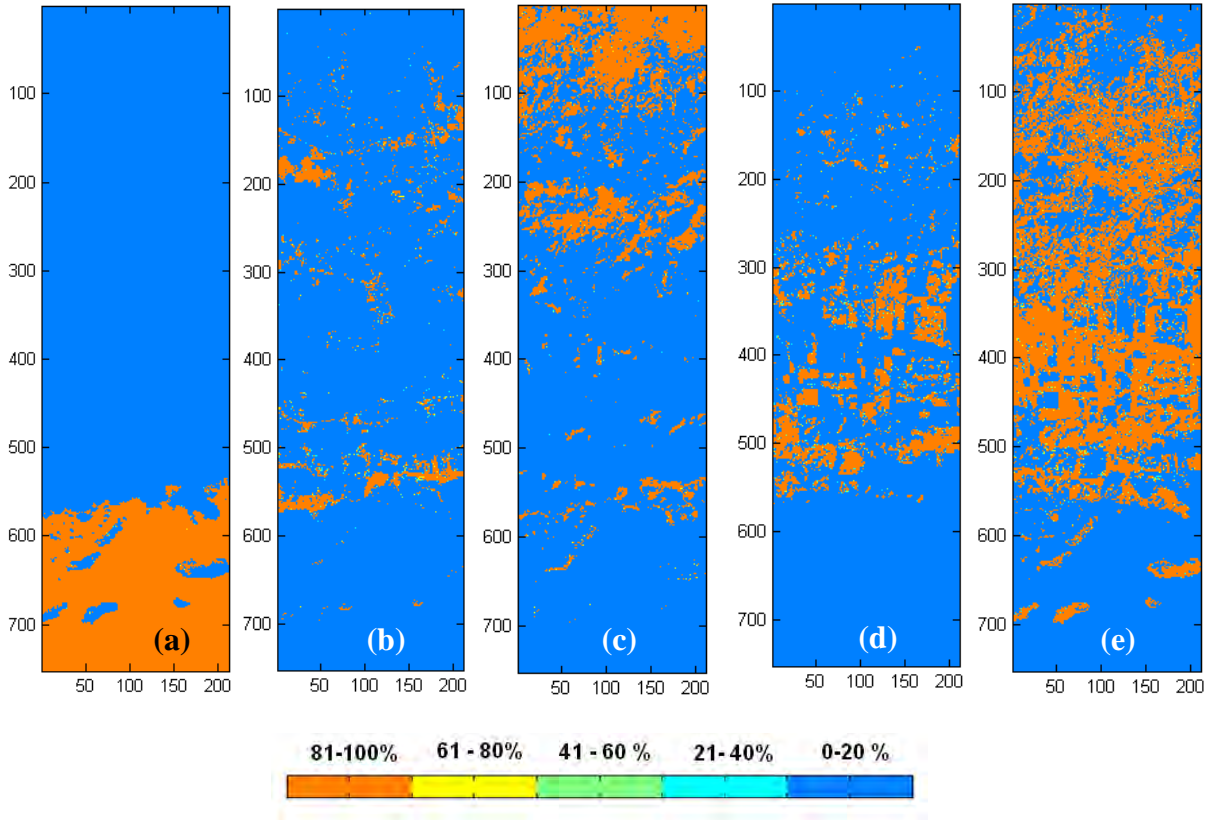


Figure 61: Membership maps obtained using a FSCS of (a) Water, (b) Urban and Barren Land, (c) Forest, (d) Pasture, and (e) Agriculture. A scale based on (0-20%, 21-40%, 41-60%, 61-80%, and 81-100%) ranges were used.

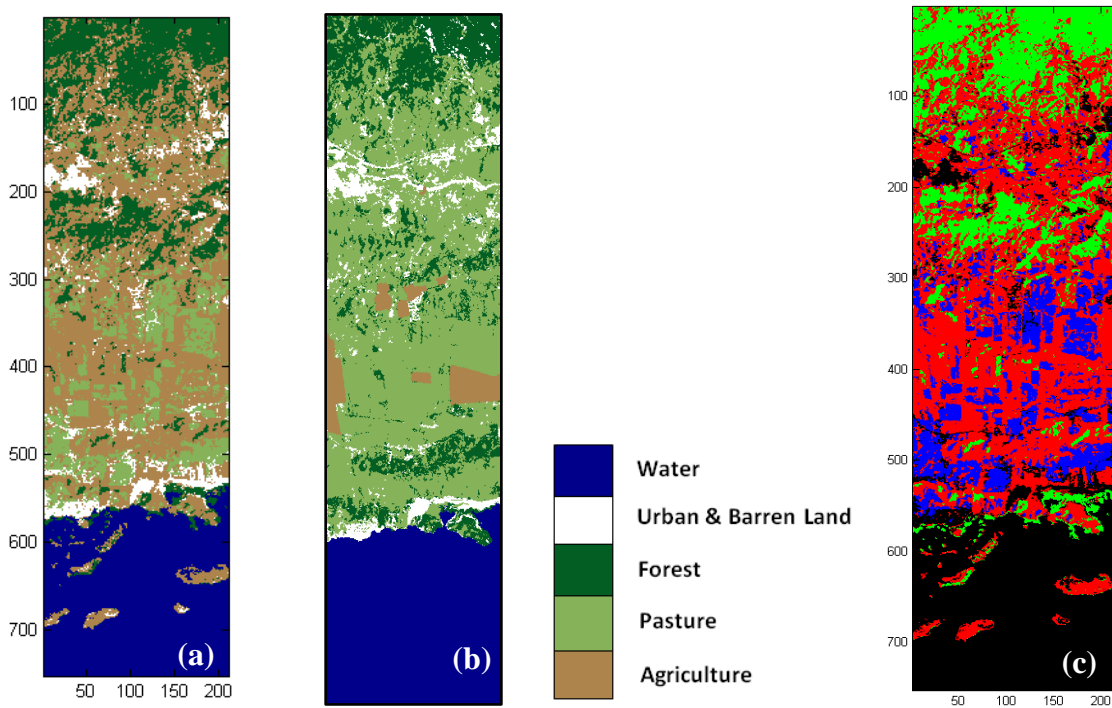


Figure 62: (a) Classification map derived from FSCS hardening process, and (b) USDA PR Land Cover Reference 1991 (Helmer et al., 2002), and (c) FSCS Fractional Map, R-Pasture, G-Forest, B-Agriculture

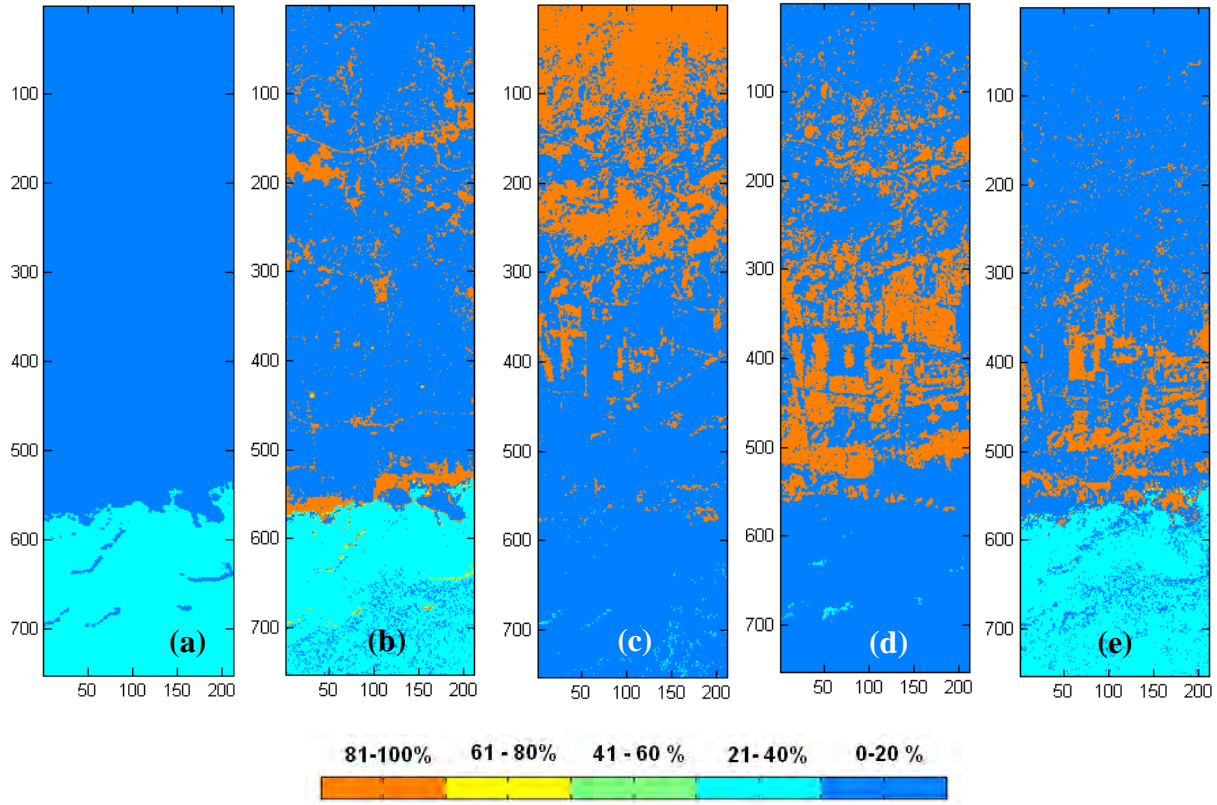


Figure 63: Membership maps obtained using a FML-initialized with LMM of (a) Water, (b) Urban and Barren Land, (c) Forest, (d) Pasture, and (e) Agriculture. A scale based on (0-20%, 21-40%, 41-60%, 61-80%, and 81-100%) ranges were used.

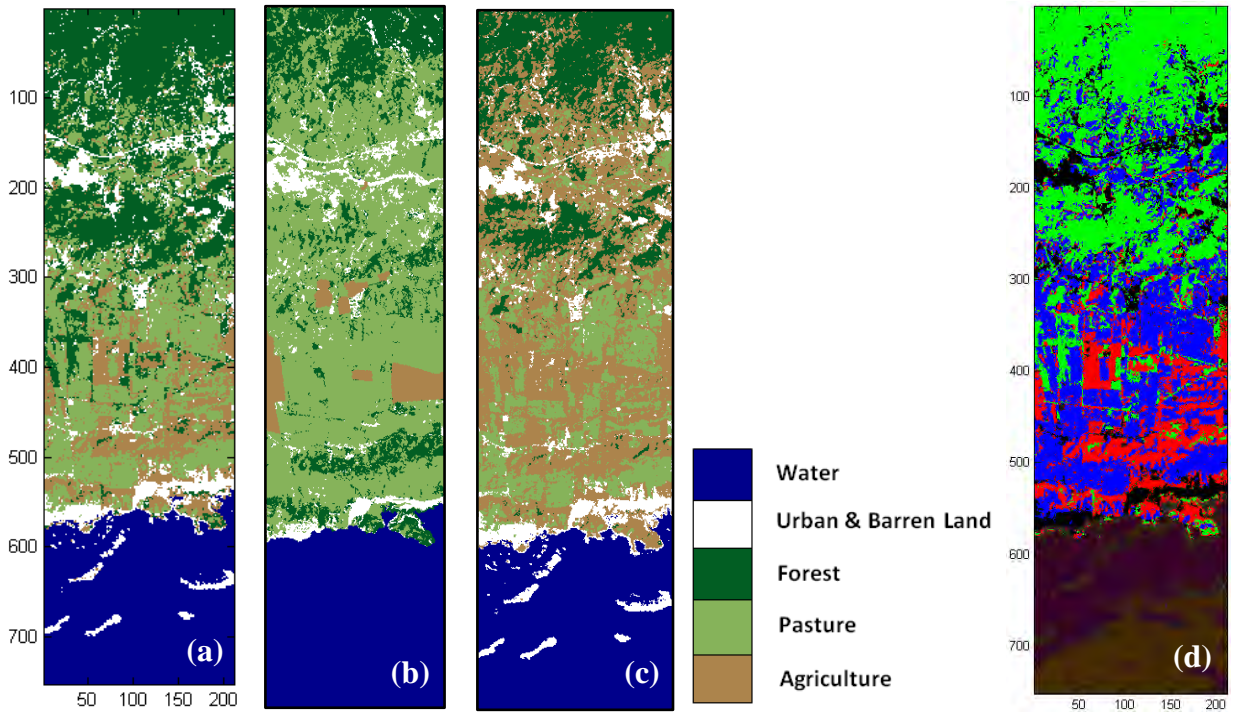


Figure 64: (a) Classification map derived from FML-initialized LMM hardening process (b) USDA PR Land Cover Reference 1991 (Helmer et al., 2002), (c) Maximum Likelihood, (d) FML Fractional Map, R-Pasture, G-Forest, B-Agriculture

Membership maps obtained with FML are shown in Figure 63 (a) – (e). Using LMM abundances at initial stage to obtain soft training data improves significantly the classification map derived by a hardening process in comparison with conventional ML thematic map as can be seen in Figures 64 (a) (FML) and 64 (c) (ML), respectively.

As can be seen in the membership maps and thematic maps derived with a LMM-1, LMM-2, SFCM, FSCS, and FML (see Figures 53-54, 56-57, 59-64), FML-initialized with LMM abundances, LMM-2 and SFCM provides better representation of the multispectral remote sensed scene in terms of membership maps and thematic maps accordingly with NDVI outputs (see Figure 51 (c)) and land cover reference (see Figure 51 (b)). LMM-1, and FSCS probably improves their results if a hyperspectral imagery is used as can be seen with the Enrique Reef scene studied in Chapter 4.

The confusion error matrices for LMM-1, LMM-2, SFCM, FSCS, and FML approaches are shown in Tables 21-26 respectively. All approaches with the exception of LMM-1 obtained above 90% of overall accuracy as we can see in Figure 65. LMM-1 obtained a lower overall accuracy by the low spectral resolution of Lajas imagery in comparison of Enrique scene where high spectral resolution imagery was used for the same approach. For that reason, classes with similar spectral signatures, such as agriculture and pasture, and urban and barren land pixels which typically are a mixture of materials failed in determine an accurate proportion associated to specially these classes and then the hardening step does not produced good results. This conventional hard assessment is not the best way to evaluate the performance of soft classifiers because, as can be seen in classification maps derived from a hardening process, soft classification outputs provide a better representation for this low spatial resolution imagery than ML accordingly to NDVI output (see Figure 51 (c)) and the land cover reference (see Figure 51 (b)).

5.2 Summary

In this chapter, we present experiments using a multispectral imagery of Lajas, PR acquired with an ETM+ sensor. Soft classification results in terms of membership maps and classification maps derived from a hardening of degree of membership were conducted for the LMM-1 (endmembers selected manually from the image), LMM-2 (PMF algorithm initialized with endmembers selected manually from the image) (Masalmah and Vélez-Reyes 2007), SFCM, FSCS, and FML (initialized with LMM)

Table 21: Confusion Error Matrix of a LMM-1 thematic map derived by a hardening LMM-1 abundance maps

	Water	Urban & Barren Land	Forest	Pasture	Agriculture	User's Accuracy
Water	1143	98	0	0	0	92.1%
Urban & Barren Land	0	123	0	0	3	97.6%
Forest	0	17	799	0	24	95.1%
Pasture	0	59	0	216	9	76.1%
Agriculture	0	152	145	447	197	20.9%
Number of Testing Samples	1143	449	944	663	233	
Producer's Accuracy	100%	27.4%	84.6%	32.6%	84.5%	
Overall Accuracy		72.2 %				

Table 22: Confusion Error Matrix of a LMM-2 thematic map derived by a hardening LMM-2 abundance maps

	Water	Urban & Barren Land	Forest	Pasture	Agriculture	User's Accuracy
Water	1143	1	0	0	6	99.4%
Urban & Barren Land	0	355	0	2	0	99.4%
Forest	0	31	944	0	32	93.7%
Pasture	0	54	0	661	46	86.9%
Agriculture	0	8	0	0	149	94.9%
Number of Testing Samples	1143	449	944	663	233	
Producer's Accuracy	100%	79.1%	100%	99.7%	64.0%	
Overall Accuracy		94.8 %				

Table 23: Confusion Error Matrix of a SFCM thematic map derived by a hardening SFCM membership maps

	Water	Urban & Barren Land	Forest	Pasture	Agriculture	User's Accuracy
Water	1143	0	0	0	3	99.7%
Urban & Barren Land	0	331	0	8	0	97.6%
Forest	0	4	937	0	120	88.3%
Pasture	0	42	0	646	2	93.6%
Agriculture	0	72	7	9	108	55.1%
Number of Testing Samples	1143	449	944	663	233	
Producer's Accuracy	100%	73.7%	99.3%	97.4%	46.4%	
Overall Accuracy		92.2 %				

Table 24: Confusion Error Matrix of a FSCS thematic map derived by a hardening FSCS membership maps

	Water	Urban & Barren Land	Forest	Pasture	Agriculture	User's Accuracy
Water	1143	0	0	0	0	100%
Urban & Barren Land	0	399	0	36	0	91.7%
Forest	0	0	924	0	25	97.4%
Pasture	0	17	0	519	0	96.8%
Agriculture	0	33	20	108	208	56.4%
Number of Testing Samples	1143	449	944	663	233	
Producer's Accuracy	100%	88.9%	97.9%	78.3%	89.3%	
Overall Accuracy		93.0 %				

Table 25: Confusion Error Matrix of a FML (initialized using LMM) thematic map derived by a hardening FML membership maps

	Water	Urban & Barren Land	Forest	Pasture	Agriculture	User's Accuracy
Water	1143	0	0	0	0	100%
Urban & Barren Land	0	425	0	6	4	97.7%
Forest	0	1	944	0	20	97.8%
Pasture	0	23	0	638	2	96.2%
Agriculture	0	0	0	19	207	91.6%
Number of Testing Samples	1143	449	944	663	233	
Producer's Accuracy	100%	94.7%	100%	96.2%	88.8%	
Overall Accuracy		97.8 %				

Table 26: Confusion Error Matrix of a ML thematic map

	Water	Mangrove	Sand	Sea Grass	Reef Flat	User's Accuracy
Water	1143	0	0	0	0	100%
Urban & Barren Land	0	929	0	0	2	99.79%
Forest	0	0	551	19	0	96.67%
Pasture	0	0	4	420	4	98.13%
Agriculture	0	15	108	10	227	63.06%
Number of Testing Samples	1143	449	944	663	233	
Producer's Accuracy	100%	98.4%	83.1%	93.5%	97.4%	
Overall Accuracy		95.3 %				

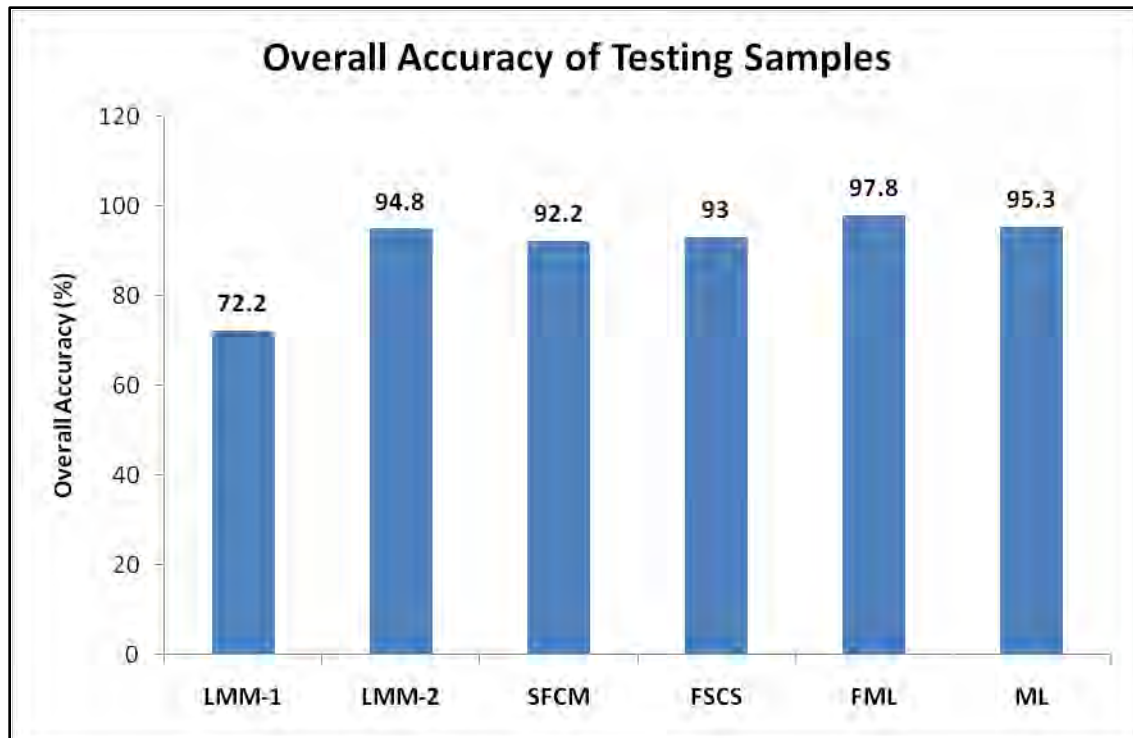


Figure 65: LMM-1, LMM-2, SFCM, FSCS, FML, and ML overall accuracy percentage of testing samples

approaches. A confusion error matrix analysis was used to assess the performance of soft classification algorithms due soft ground truth data was not available for this scene.

Based on the multispectral scene studied in this chapter, LMM-2 approach using the endmembers selected manually from the image to initialize the PMF algorithm (Masalmah and Vélez-Reyes 2007) improves significantly the membership maps and classification map derived from a hardening process in comparison with LMM-1. As we can observe experimentally, the PMF algorithm (Masalmah and Vélez-Reyes 2007) provides better results than LMM-1 because it refine the endmembers selected manually from the image resulting in a better representation of cover types chosen as informational classes. The FML approach using LMM abundances to initialize the algorithm also improves significantly the classification map derived by a hardening process in comparison with conventional ML thematic map. In summary, SFCM, LMM-2, and FML initialized with LMM abundances provides the better representation of the multispectral scene in terms of membership maps and classification maps accordingly with NDVI output and the USDA PR Land Cover Reference (Helmer et al., 2002). The FSCS and LMM-1 can improves their outputs using a hyperspectral sensor which provides a better discrimination between

materials that have similar spectral response such as agriculture and pasture classes taking advantage of its high spectral resolution.

CHAPTER 6

Conclusions and Future Work

6.1 Conclusions

In this chapter, we summarize the major results obtained from the investigation. In chapter 1, we have presented the motivations for the research, problem statement, and the objectives that we accomplished during the research work. Chapter 2 discussed a theoretical background and literature review needed to understand the proposed work. Supervised soft classification algorithms studied in the research were explained in Chapter 3. As part of the research, we developed an end to end classification system called Spectral Soft Classification Tool (SSCT) that will be incorporated to the Hyperspectral Image Analysis Toolbox (HIAT) developed over the past eight years by UPRM researchers at the Laboratory for Applied Remote Sensing and Image Processing (LARSIP). An Enrique Reef scene at Lajas, PR acquired with HYPERION sensor was used to show the SSCT functionalities. Further experiments using multispectral data are described in Chapter 5.

A comparative study of supervised fuzzy logic algorithms and linear mixing model used as soft classifiers was performed during this research. The research demonstrates that soft classifiers could be an alternative of hard classification of low spatial resolution imagery because they are more appropriate to describe and model the real variation of landscape remote sensed images which are imprecise naturally.

Based on the Lajas scene, Linear Mixing Model (LMM) and Supervised Fuzzy C-Means (SFCM) approaches have good correlation among all membership maps and classification maps. The use of LMM abundances to initialize the FML algorithm improves significantly the classification derived by a hardening process in comparison with the conventional ML thematic map. On the other hand, the use of PMF algorithm to refine the endmembers selected manually from the image improves the membership maps obtained from LMM-1 using the endmembers selected manually from the image or using the PPI method.

Accordingly with Enrique Reef results, we can conclude that LMM and SFCM membership maps have a good correlation among all informational classes and soft ground truth data. Fuzzy Supervised Classification System (FSCS) had problems to detect the mixtures of pixels although it produced good classification maps in comparison with ground truth data available with an exception of mangrove class which was overestimated. Fuzzy Maximum Likelihood (FML) using LMM abundances estimates to initialize the soft-training data improves the thematic map obtained with a conventional Maximum Likelihood algorithm especially for sand and mangrove classes. FML assuming pure training samples to initialize the soft training data also improves the hard Maximum Likelihood classification map but FML-using LMM to initialize soft training data obtained higher overall accuracy percentages in terms of the traditional confusion error matrix and fuzzy error matrix. All classification maps derived from soft classification algorithms provided a better representation of Enrique Reef scene in comparison with a ML thematic map which produced an overestimation of the mangrove and sand classes.

In addition, a soft classification tool was developed. SSCT intends to group many efforts of researchers in the area of soft classification in order to provide a valuable tool to image analysts and end users to analyze multi/hyperspectral imagery in terms of fractional maps and thematic maps derived from a soft classification algorithms, visualization techniques, and accuracy assessment.

Actually, we cannot eliminate data softness from end users at all but the use of visualization techniques are an aid in the visual interpretation and analysis of soft classification outputs. Fractions maps are useful to generate a RGB composite of three membership maps assigning them to red, green, and blue channels. It allows us to explore the mixing among classes which is not possible using a single classification map derived from a hard classification. Also, binary membership maps provide a tool to visualize how the spatial distribution of a particular class is changing through the different thresholding set by end users depends on the application of interest. The visualization of thematic maps derived from a soft classification is another valuable tool because we can take advantage of information about the proportion of pixel coverage obtained with membership maps and it can be used to select a threshold and establish an unclassified class to explore the area of mixing among classes assigning a similar color of the class which obtained the higher degree of membership. Those classification maps are also helpful because they take into consideration the mixed pixels and could be a complement in the analysis of a particular scene because sometimes the image analysts prefer to use a single classification map instead of several membership maps.

We presented the use of entropy images to visualize the areas of significant degree of mixing among classes. Entropy is a measure of information that we are trying to use to evaluate degree of mixing since the degree of membership obtained from soft classification, although they are not probabilities, they are fraction values that ranges from 0 – 1. An entropy computation of an almost pure pixel produces a lower value. On the contrary, an entropy computation of a pixel which has a higher degree of mixing between classes produces a higher value. Following this concept, entropy images was generated to provide an additional tool to evaluate the degree of mixing in a scene.

The use of a fuzzy error matrix, and Euclidean distance presented in this research to evaluate the performance of soft classifiers provides a complement of the conventional accuracy assessment based on the confusion error matrix. We have not found in literature any method that solves the accuracy assessment issue of soft classification outputs satisfactorily. However, the uses of several approaches could give us a better idea of how accurate is the results obtained from a membership outputs and hardening process.

In summary, soft methods are another way to model low spatial resolution remote sensed data by naturally taking into consideration the mixing of pixels as part of the classification process.

6.2 Future Work

Soft classification based on Linear Mixing Model and Fuzzy Logic algorithms was addressed during the research. As a future work, neural networks and neuro-fuzzy methods can be study in order to compare which method could provide better results to model the real variation of landscape remote sensed imagery. The use of Support Vector Machine (SVM) to calculate the degree of membership associated to informational classes and composite kernels, which incorporate spatial and spectral information was proposed by Gu, Liu, and Zhang . Their study revealed an improvement in classification accuracies by the use of composite kernels.

This research have studied supervised soft classification approach where prior knowledge of image analyst is required to determine a good representation of training samples in order to train soft classifiers. Unsupervised soft classification could be study in order to also provide an automated tool without significant interaction of end users. Unsupervised methods are also useful in supervised case study because provide an idea of class patterns that could be used to select training samples and

endmembers for a supervised mode. Some initial results based on the Positive Matrix Factorization (PMF) (Masalmah and Vélez-Reyes 2007) were discussed in Chapter 5.

Accuracy assessment of soft classifiers is still a big issue. This research studied methods proposed in literature to evaluate the performance of soft classifiers but they are sensitive to the use of a higher accurate proportion coverage of each informational class per pixel as a soft ground truth data which in practical situations is difficult to obtain. It is needed to conduct further investigation on how we can assess soft classifiers taking into consideration the multiclass assignment problem and using soft ground truth data.

Monitoring land cover changes is a key of different applications such as forestry, environment, geology, agriculture, and others. It could be useful to study how soft classification can be used to detect the transition zones of diverse classes (membership maps) by the use of temporal images and change detection algorithms.

The Spectral Soft Classification Tool functionalities shown in Chapter 4 need to be incorporated in HIAT. These functions will complement the existing functions available in HIAT for hard classification, supervised and unsupervised spectral unmixing, and other methods to analyze hyperspectral images. The work developed, the routines, and final integration will be performed by the LARSIP integration team.

BIBLIOGRAPHY

- Adams, J.B. *Remote Sensing of Landscapes with Spectral Images: A Physical Modeling Approach*. Cambridge University Press, 2006.
- Arzuaga-Cruz, E., et al. "A MATLAB Toolbox for Hyperspectral Image analysis." *Proceedings of IEEE International Geoscience and Remote Sensing Symposium, IGARSS '04*, 2004: 4839-4842.
- Bárdossy, A., and L. Samaniego. "Fuzzy Rule - Based Classification of Remotely Sensed Imagery." *IEEE Transactions on Geoscience and Remote Sensing XL*, no. 2 (February 2002).
- Bastin, L., P. F. Fisher, and J. Wood. "Visualizing Uncertainty in Multispectral Remotely Sensed Imagery." *Computer & Geosciences* (Elsevier Science), 2002: 337-350.
- Bezdek, J.C., R. Ehrlich, and W. Full. "FCM: the Fuzzy C-Means Clustering Algorithm." *Computers and Geosciences X* (1984): 191-203.
- Biehl, L., and D. Landgrebe. "Multispec - a tool for multispectral - hyperspectral image data analysis." *Computers & Geosciences* (Elsevier Science), 2002: 1153-1159.
- Binaghi, E. "Soft Thematic Mapping from Remotely Sensed Data: Production, Interpretation and Accuracy Assessment." *Image and Signal Processing for Remote Sensing VI* (Proceedings of SPIE) 4170 (August 2001): 167-181.
- Binaghi, E., P.A. Brivio, P. Ghezzi, and A. Rampini. "A Fuzzy Set-Based Accuracy Assessment of Soft Classification." *Pattern Recognition Letters* (Elsevier Science), 1999: 935-948.
- Boardman, J.W. "Automating Spectral Unmixing of AVIRIS Data using Convex Geometry Concepts." *In Proceedings of JPL Airborne Earth Science Workshop*. Pasadena,CA, 1993.
- Boardman, J.W., F.A. Kruse, and R.O. Green. "Mapping Target Signatures Via Partial Unmixing of AVIRIS Data." *In Proceedings of JPL Airborne Earth Science Workshop*. Pasadena,CA, 1995.
- Chavez, P.S. "Image-Based Atmospheric Corrections - Revisited and Improved." *Photogrammetric Engineering & Remote Sensing* 62, no. 9 (September 1996): 1025-1036.
- Deer, P. J., and P. W. Eklund. "Selecting Parameter Values for Mahalanobis Distance Fuzzy Classifier." *The 10th IEEE International Conference on Fuzzy Systems*. 2001. 541-544.
- Deer, P. J., P. W. Eklund, and B. D. Norman. "A Mahalanobis Distance Fuzzy Classifier." *IEEE Australian and New Zealand Conference on Intelligent Information Systems*. 1996. 220-223.
- Dial, G., H. Bowen, F. Gerlach, J. Grodecki, and R. Oleszczuk. "IKONOS satellite, imagery, and products." *Remote Sensing of Environment* (Elsevier Science), August 2003: 23-36.
- Du, Q., and S. Chakravarthy. "Unsupervised Hyperspectral Image Classification Using Blind Source Separation." *IEEE International Conference on Acoustics, Speech, and Signal Processing*. 2003. 437-440.
- Duda, R. O., P. E. Hart, and D. G. Stork. *Pattern Classification*. 2nd Ed. John Wiley & Sons, Inc., 2001.

- Folkman, M. A., J. Pearlman, L. B. Liao, and P. J. Jarecke. "EO-1 Hyperion Hyperspectral Imager Design, Development, Characterizations, and Calibration." *Hyperspectral Remote Sensing of the Land and Atmosphere*. Proceedings of SPIE, 2001. 40-51.
- Foody, G.M. "Approaches for the Production and Evaluation of Fuzzy Land Cover Classifications from Remotely-Sensed Data." *International Journal of Remote Sensing* 17, no. 7 (1996): 1317-1340.
- Foody, G.M. "Cross-Entropy for the Evaluation of the Accuracy of a Fuzzy Land Cover Classification with Fuzzy Ground Data." *ISPRS Journal of Photogrammetry and Remote Sensing* (Elsevier Science) L, no. 5 (1995): 2-12.
- Foody, G.M. "Relating the Land Cover Composition of Mixed Pixels to Artificial Neural Network Classification Output." *Photogrammetric Engineering & Remote Sensing* 62, no. 5 (May 1996): 491-499.
- Foody, G.M. "Soft Classification for the Mapping of Land Cover from Remotely Sensed Data." *Applications and Science of Neural Networks, Fuzzy Systems, and Evolutionary Computation* (Proceedings SPIE) 3455 (July 1998): 23-34.
- Foody, G.M. "Status of Land Cover Classification Accuracy Assessment." *Remote Sensing of Environment* (Elsevier Science), 2002: 185-201.
- Foody, G.M., and D.P. Cox. "Sub-pixel Land Cover Composition Estimation Using Linear Mixture Model and Fuzzy Membership Functions." *International Journal of Remote Sensing* XV, no. 3 (1994): 619-631.
- Gu, Y., Y. Liu, and Y. Zhang. "A Soft Classification Algorithm based on Spectral-Spatial Kernels in Hyperspectral Images." *IEEE Second International Conference on Innovative Computing, Information, and Control*. 2007. 548-551.
- Haykin, S. *Communication Systems*. 4th Edition. John Wiley & Sons, 2001.
- Helmer, E. H., O. Ramos, T. Del M. López, M. Quiñones, and W. Díaz. "Mapping the Forest type and Land Cover of Puerto Rico, a Component of the Caribbean Biodiversity Hotspot." *In Caribbean Journal of Science* 38, no. 3-4 (2002): 165-183.
- Hollinger, A., et al. "Recent Developments in the Hyperspectral Environment and Resource Observer (HERO) Mission." *IEEE International Conference on Geoscience and Remote Sensing Symposium, IGARSS*, August 2006: 1620-1623.
- Huang, C., J.R.G. Townshend, S. Liang, and S.N.V. Kalluri. "Impact of Sensor's Point Spread Function on Land Cover Characterization: Assessment and Deconvolution." *Remote Sensing of Environment* (Elsevier) LXXX (2002): 203-212.
- ITT Visual Information Solutions. *Solutions for Extracting Information from Geospatial Imagery ENVI*. 2007. <http://rsinc.com/envi/> (accessed 2008).
- Jiménez-Rodríguez, L.O., E. Arzuaga-Cruz, and M. Vélez-Reyes. "Unsupervised Linear Feature - Extraction Methods and Their Effects in the Classification of High - Dimensional Data." *IEEE Transactions on Geoscience and Remote Sensing* XLV, no. 2 (February 2007): 469-483.

- Kaufmann, K., et al. "EnMAP - A Hyperspectral Sensor for Environmental Mapping and Analysis." *IEEE International Conference on Geoscience and Remote Sensing Symposium, IGARSS*, August 2006: 1617 - 1619.
- Kendall, M. S., et al. "Methods Used to Map the Benthic Habitats of Puerto Rico and the U.S. Virgin Islands." NOAA National Ocean Service, Biogeography Team. 2001. <http://biogeo.nos.noaa.gov/projects/mapping/caribbean/startup.htm>.
- Keshava, N. "A Survey of Spectral Unmixing Algorithms." *Lincoln Laboratory Journal XIV*, no. 1 (2003).
- Keshava, N., and J.F. Mustard. "Spectral Unmixing." *IEEE Signal Processing Magazine*, January 2002.
- Landgrebe, D. "Hyperspectral Image Data Analysis." *IEEE Signal Processing Magazine*, January 2002.
- Landgrebe, D.. *Signal Theory Methods in Multispectral Remote Sensing*. Wiley-Interscience, 2003.
- Landgrebe, D., and L. Biehl. *Purdue/LARS Multispec*. 1994-2008. <http://cobweb.ecn.purdue.edu/~biehl/MultiSpec/> (accessed 2008).
- Lockwood, R. B., et al. "Advanced Responsive Tactically Effective Military Imaging Spectrometer (ARTEMIS): System Overview and Objectives." *Imaging Spectrometry XII* (Proceedings of SPIE) 6661 (September 2007).
- Lu, D., and Q. Weng. "A Survey of Image Classification Methods and Techniques for Improving Classification Performance." *International Journal of Remote Sensing XXVIII*, no. 5 (March 2007): 823-870.
- Lucieer, A. "Uncertainties in Segmentation and their Visualization." PhD Thesis, Universiteit Utrecht, The Netherlands, 2004.
- Lucieer, A. "Visualization for Exploration of Uncertainty Related to Fuzzy Classification." *IEEE International Conference on Geoscience and Remote Sensing Symposium, IGARSS 2006*, 2006: 903-906.
- Masalmah, Y., and M. Vélez-Reyes. "Unsupervised Unmixing of Hyperspectral Unmixing Using the Constrained Positive Matrix Factorization." PhD Thesis, Computing and Information Science and Engineering, University of Puerto Rico - Mayaguez Campus, 2007.
- Melgani, F., B.A.R Al Hashemy, and S.M.R. Taha. "An Explicit Fuzzy Supervised Classification Method for multispectral Remote Sensing Images." *IEEE Transactions on Geoscience and Remote Sensing XXXVIII*, no. 1 (2000): 287-295.
- Mendel, J.M. "Fuzzy Logic Systems for Engineering: A Tutorial." *Proceedings of the IEEE*. 1995.
- NASA. *Landsat 7 Science Data Users Handbook*. January 10, 2008. <http://landsathandbook.gsfc.nasa.gov/handbook.html> (accessed June 2008).
- Nauck, D., and R. Kruse. "A Neuro-Fuzzy Method to Learn Fuzzy Classification Rules from Data." *In Fuzzy Sets and System* (Elsevier Science), 1997: 277-288.

- Plaza, A., P. Martínez, R. Pérez, and J. Plaza. "A Quantitative and Comparative Analysis of Endmember Extraction Algorithms from Hyperspectral Data." *IEEE Transactions on Geoscience and Remote Sensing* XLII, no. 3 (March 2004): 650-663.
- Plaza, A., P. Martínez, R. Pérez, and J. Plaza. "A Quantitative and Comparative Analysis of Endmember Extraction Algorithms from Hyperspectral Data." *IEEE Transactions on Geoscience and Remote Sensing* XLII, no. 3 (March 2004): 650-663.
- Richards, J.A. *Remote Sensing Digital Image Analysis: An Introduction*. 2nd Ed. Springer - Verlag , 1995.
- Rivera-Borrero, C., and S. Hunt. "The Development of Ground Truth Data and Accuracy Assessment of Hyperspectral Image Classification and Spectral Unmixing." MS Thesis, Electrical and Computer Engineering, University of Puerto Rico - Mayaguez Campus, 2007.
- Rosario-Torres, S. "Iterative Algorithms for Abundance Estimation on Unmixing of Hyperspectral Imagery." MS Thesis, Electrical and Computer Engineering, University of Puerto Rico-Mayaguez Campus, 2004.
- Rosario-Torres, S., E. Arzuaga-Cruz, and M. Vélez-Reyes. "An Update on the MATLAB Hyperspectral Image Analysis Toolbox." Edited by Proceedings SPIE. *Algorithms and Technologies for Multispectral, Hyperspectral, and Ultraspectral Imagery XI* 5806 (April 2005).
- Schouten, T.E. "Fuzzy Classification of Pixels using Neural Networks." *In Image and Signal Processing for Remote Sensing V* (Proceedings of SPIE) 3871 (September 1999): 205-215.
- Schowengerdt, R.A. *Remote Sensing: Models and Methods for Image Processing*. 3rd Ed. Elsevier, Inc., 2007.
- Townshend, J. R.G., C. Huang, S. N.V. Kalluri, R. S. Defries, and S. Liang. "Beware of Per-Pixel Characterization of Land Cover." *International Journal of Remote Sensing* (Taylor & Francis Ltd) 21, no. 4 (2000): 839-843.
- Tso, B., and P. M. Mather. *Classification Methods for Remotely Sensed Data*. Taylor & Francis, 2001.
- Tsoukalas, L.H. *Fuzzy and Neural Approaches in Engineering*. Wiley, 1997.
- Van Der Meer, F.D, and S.M. Jong. *Remote Sensing Analysis: Including the Spatial Domain*. Springer, 2006.
- Varshney, P.K., and M.K. Arora. *Advanced Image Processing Techniques for Remotely Sensed Hyperspectral Data*. Springer, 2004.
- Vélez-Reyes, M., and L. O. Jiménez-Rodríguez. "Subset Selection Analysis for the Reduction of Hyperspectral Imagery." *Proceedings of IEEE International Geoscience and Remote Sensing Symposium, IGARSS '98*, 1998: 1577-1581.
- Wang, F. "Fuzzy Supervised Classification of Remote Sensing Images." *IEEE Transactions on Geoscience and Remote Sensing* XXVIII, no. 2 (1990): 194-201.

Winter, M.E. "A Proof of the N-FINDR Algorithm for the Automated Detection of End-members in a Hyperspectral Image." *Algorithms and Technologies for Multispectral, Hyperspectral, and Ultraspectral Imagery X* (Proceedings of SPIE) 5424 (August 2004): 31-41.

Winter, M.E. "N-FINDR: an Algorithm for Fast autonomous Spectral End-Manner Determination in Hyperspectral Data." *Data Exploitation, Processing, and Compression I*. Proceedings of SPIE, 1999.

Zhang, J., and G.M. Foody. "Fully-Fuzzy Supervised Classification of Sub-Urban Land Cover from Remotely Sensed Imagery: Statistical and Artificial Neural Network Approaches." *International Journal of Remote Sensing* XXII, no. 4 (2001): 615-628.

APPENDICES

A. Description of .m functions that will be included into the HIAT (SSCT) by the LARSIP integration team

A.1 Soft Classification Module

Fuzzy Supervised Classification System (FSCS) (Melgani et al., 2000)

[FSCSMemMap,MajVote,MajVoteLabel,ThMap,t]=FSCSsc(XImg,RadRes,ClassName,C1,C2,C3,C4,C5)

Description	Input Variables	Output Variables
<p>This function generates the FSCS membership maps and a single classification map based on highest degree of membership.</p> <p>* This function calls “Rescal” and “Defuzzy” functions into the body of the function</p>	<p>XImg - Multi/Hyperspectral image (row x column x bands)</p> <p>ClassName - cell array with class names</p> <p>C1 - training samples of class 1</p> <p>C2 - training samples of class 2</p> <p>C3 - training samples of class 3</p> <p>C4 - training samples of class 4</p> <p>C5 - training samples of class 5</p> <p>* It is necessary an optimization of body function to use more than or less than 5 classes.</p>	<p>FSCSMemMap – Membership maps derived by FSCS . (row x column x classes)</p> <p>MajVote - higher degree of membership for each pixel in the scene. (N x 1)</p> <p>MajVoteLabel - class label with the higher degree of membership for each pixel in the scene. (N x 1)</p> <p>ThMap - Classification map derived by a FSCS hardening step</p> <p>t – execution time</p>

Fuzzy Maximum Likelihood (Wang 1990)

[FML_MemMap,ThMap,t]= **FMLsc** (XImg,ClassName,C1,C2,C3,C4,C5, C1Indx, C2Indx, C3Indx,C4Indx,C5Indx)

Description	Input Variables	Output Variables
<p>This function generates the FML membership maps and a single classification map based on highest degree of membership. At initial stage the degree of membership associated to each class is set at 1 or 0. ("pure pixels") in order to obtain the soft training parameters associated to each class iteratively. Training samples should be comprised from at least two classes.</p>	<p>XImg - Multi/Hyperspectral image (row x column x bands)</p> <p>ClassName - cell array with class names</p> <p>C1 - training samples of class 1</p> <p>C2 - training samples of class 2</p> <p>C3 - training samples of class 3</p> <p>C4 - training samples of class 4</p> <p>C5 - training samples of class 5</p> <p>* It is necessary an optimization of code function to use more than or less than 5 classes.</p>	<p>FML_MemMap – Membership maps derived by FML (row x column x classes)</p> <p>ThMap - Classification map derived by a FML hardening step</p> <p>t – execution time</p>

Fuzzy Maximum Likelihood – using LMM abundances to generate soft training parameters

[FML_MemMap,ThMap,t] = **FML_LMMsc** (LMMMemMap, XImg, ClassName, C1, C2,C3, C4, C5,C1Indx, C2Indx, C3Indx,C4Indx,C5Indx)

Description	Input Variables	Output Variables
<p>This function generates the FML membership maps and a single classification map based on highest degree of membership. LMM abundances are used as the proportion coverage associated to each class in order to generate the soft training parameters.</p>	<p>LMMMemMap – Membership maps derived by LMM</p> <p>XImg - Multi/Hyperspectral image (row x column x bands)</p> <p>ClassName - cell array with class names</p> <p>C1 - training samples of class 1</p> <p>C2 - training samples of class 2</p> <p>C3 - training samples of class 3</p> <p>C4 - training samples of class 4</p> <p>C5 - training samples of class 5</p>	<p>FML_MemMap – Membership maps derived by FML using LMM abundances in order to obtain the soft training parameters. (row x column x classes)</p> <p>ThMap - Classification map derived by a FML hardening step</p> <p>t – execution time</p>
	<p>* It is necessary an optimization of code function to use more than or less than 5 classes.</p>	

Fuzzy Maximum Likelihood – Initialized with LMM abundances

[FML_MemMap,ThMap,t] = **FML_LMMscInit** (LMMMemMap, XImg, ClassName, C1, C2,C3, C4, C5,C1Indx, C2Indx, C3Indx,C4Indx,C5Indx)

Description	Input Variables	Output Variables
<p>FML_LMMscInit function generates the FML membership maps and a single classification map based on highest degree of membership. LMM abundances are used as the proportion coverage associated to each class in order to determine iteratively the soft training parameters.</p>	<p>LMMMemMap – Membership maps derived by LMM</p> <p>XImg - Multi/Hyperspectral image (row x column x bands)</p> <p>ClassName - cell array with class names</p> <p>C1 - training samples of class 1</p> <p>C2 - training samples of class 2</p> <p>C3 - training samples of class 3</p> <p>C4 - training samples of class 4</p> <p>C5 - training samples of class 5</p> <p>* It is necessary an optimization of code function to use more than or less than 5 classes.</p>	<p>FML_MemMap – Membership maps derived by FML using LMM abundances in order to obtain the soft training parameters. (row x column x classes)</p> <p>ThMap - Classification map derived by a FML hardening step</p> <p>t – execution time</p>

Linear Mixing Model - Classification Map

[LMMMemMap, MajVote, MajVoteLabel, ThMap, t] = LMMsc (MemMaps_Img, ClassName)

Description	Input Variables	Output Variables
<p>This function generates a single classification map derived by LMM membership maps based on highest degree of membership.</p> <p>* This function calls “Rescal” and “Defuzzy” functions into the body of the function</p>	<p>MemMaps_Img - membership maps derived by Linear Mixing Model algorithm (row x column x classes)</p> <p>ClassName - cell array with class names</p>	<p>LMMMemMap –degree of memberships (0-1) associated to each class (row x column x classes)</p> <p>MajVote - higher degree of membership for each pixel in the scene. (N x 1)</p> <p>MajVoteLabel - class label with the higher degree of membership for each pixel in the scene. (N x 1)</p> <p>ThMap - Classification map derived by a LMM hardening step</p> <p>t – execution time</p>

A.1.1 Complementary functions

Rescaling

[DegMem_NNnom, t] = Rescal (DegMem_NN, number_of_classes)

Description	Input Variables	Output Variables
<p>This function normalizes the degree of membership to sum up to one.</p>	<p>DegMem_NN - Degree of memberships associated to each class (N x M)</p> <p>N – number of pixels</p> <p>M – number of classes.</p> <p>number_of_classes</p>	<p>DegMem_NNnom – degree of memberships associated to each class (normalize) (N x M)</p> <p>N – number of pixels</p> <p>M – number of classes.</p> <p>t – execution time</p>

Defuzzification (Hardening Step)

[DegMem, MajVote, MajVoteLabel, ThMap, t] = **Defuzzy** (MemMaps_Img, ClassName)

Description	Input Variables	Output Variables
This function generates a single classification map derived from membership maps produced by soft classification algorithms assigning the pixel to the class with the higher degree of membership.	MemMaps_Img - membership maps derived by soft classification algorithms (row x column x classes) ClassName - cell array with class names	DegMem – Degree of memberships associated to each class (N x M) N – number of pixels M – number of classes. MajVote - higher degree of membership for each pixel in the scene. (N x 1) MajVoteLabel - class label with the higher degree of membership for each pixel in the scene. (N x 1) ThMap - Classification map derived by a hardening step t – execution time

A.2 Accuracy Assessment Module

Entropy Image

[Entropy_XImg, Mn_Entropy_X, Mx_Entropy_X, u_Entropy_X, t] = **Entropy_Img** (MemMaps_Img)

Description	Input Variables	Output Variables
This function generates an entropy image based on the membership maps derived by soft classification algorithms.	MemMaps_Img - membership maps derived by soft classification algorithms (row x column x classes)	<p>Entropy_XImg – entropy image</p> <p>Mn_Entropy_X -value of minimum entropy in whole scene</p> <p>Mx_Entropy_X - value of maximum entropy in whole scene</p> <p>u_Entropy_X - an average of entropy values in whole image</p> <p>t – execution time</p>

Fuzzy Error Matrix (Binaghi et al., 1999)(Binaghi et al., 2000)

[OA, PA, UA, FEMmatrix, t] = **FEM** (TestingMemMaps, TestingSoftRef)

Description	Input Variables	Output Variables
This function calculates the fuzzy error matrix to evaluate the performance of soft classification algorithms using fuzzy sets. Soft-ground-truth data is required.	<p>TestingMemMaps –testing samples selected from membership maps derived by soft classification algorithms</p> <p>TestingSoftRef - testing samples selected from Soft-Ground -Truth Data for the same spatial coordinate (x,y) of TestingMemMaps samples.</p>	<p>OA – overall accuracy</p> <p>PA – producer accuracy</p> <p>UA – user accuracy</p> <p>FEMmatrix - Fuzzy Error Matrix (n+1) x (n+1) where <i>n</i> is the number of classes. (n+1) row and column corresponds to “Total Grades” for "soft reference" (row) and degree of membership outputs (column) respectively</p> <p>t – execution time</p>

Euclidean Distance

[EdImg, u_EdVect, t] = **EucDist** (MemMaps_Img, SoftRef_Img)

Description	Input Variables	Output Variables
This function estimates the separation of the degree of membership derived by soft classification algorithms and soft reference data based on the proportion coverage associated to each class in the pixel. Soft ground truth data is required.	<p>MemMaps_Img - membership maps derived by soft classification algorithms (row x column x classes)</p> <p>SoftRef_Img – soft reference data (row x column x classes)</p>	<p>EdImg - Euclidean Distance image.</p> <p>u_EdVect - an average of the ED computation per pixel.</p> <p>t – execution time</p>

Correlation Coefficient

[CorrMatrix R, t] = **CorrCoefAnalysis** (ClassName, MemMaps_Img, SoftRef_Img)

Description	Input Variables	Output Variables
This function generates scatter plots between degree of membership derived by soft classification algorithms and soft-ground-truth data and compute the correlation coefficient associated to each informational class.	<p>ClassName - cell array with class names</p> <p>MemMaps_Img - membership maps derived by soft classification algorithms (row x column x classes)</p> <p>SoftRef_Img – soft reference data (row x column x classes)</p>	<p>CorrMatrix - correlation matrix (between membership maps and soft reference data)</p> <p>R - correlation coefficient associated to class</p> <p>t – execution time</p> <p>* Scatter plots associated to each class</p>

A.3 Visualization Module

Fractional Maps

[rgbImg, RedCl, GreenCl, BlueCl, t] = **FracMaps** (MemMaps_Img, ClassName)

Description	Input Variables	Output Variables
This function generates RGB composite from three membership maps assigned to Red, Green, and Blue channels in order to explore the mixing among three informational classes.	<p>MemMaps_Img - membership maps derived by soft classification algorithms (row x column x classes)</p> <p>ClassName - cell array with class names</p>	<p>rgbImg – RGB composite derived by three membership maps assigned to RGB channels</p> <p>RedCl – class assigned to red channel</p> <p>GreenCl – class assigned to green channel</p> <p>BlueCl- class assigned to blue channel</p> <p>t – execution time</p>

Classification Map with Unclassified Class

[ThMap_UncCl, t] = **ThMapThr** (MajVote, MajVoteLabel, number_of_rows, number_of_columns, number_of_classes, ClassName)

Description	Input Variables	Output Variables
This function generates a single classification map with an unclassified class using a user defined threshold (between 0.01-0.99).	<p>MajVote - higher degree of membership for each pixel in the scene. (N x 1)</p> <p>MajVoteLabel - class label with the higher degree of membership for each pixel in the scene. (N x 1)</p> <p>number_of_rows</p> <p>number_of_columns</p> <p>number_of_classes</p> <p>ClassName - cell array with class names</p>	<p>ThMap_UncCl – classification map with unclassified class (user defined threshold)</p> <p>t – execution time</p>

Membership Maps – Binary Thresholds

[MemMapThr85, MemMapThr70, MemMapThr50, MemMapThr20, t] = **MemMapBinThr**
(MemMaps_Img)

Description	Input Variables	Output Variables
This function generates a binary maps using thresholds of 0.85, 0.7, 0.5, and 0.20 to visualize the spatial extent of a particular membership map	MemMaps_Img - membership maps derived by soft classification algorithms (row x column x classes)	MemMapThr85 – Membership binary map using a user defined threshold of 0.85 MemMapThr70 – Membership binary map using a user defined thresholds of 0.70 and 0.85 MemMapThr50 – Membership binary map using a user defined thresholds of 0.50, 0.7, and 0.85 MemMapThr20 – Membership binary map using a user defined thresholds of 0.2, 0.5, 0.7, and 0.85 t – execution time